Martino Figoni

Experimental and Numerical investigations on the Laser Shock Peening applied to thick components

Tesi di Laurea Specialistica

Università di PISA

Ottobre 2012

UNIVERSITÀ DI PISA

Corso di Laurea Specialistica in INGEGNERIA AEROSPAZIALE

Experimental and Numerical investigations on the Laser Shock Peening applied to thick components

Tesi di Laurea

CANDIDATO:
  Martino FIGONI

  ....

RELATORE:
  Prof. Ing. Luigi LAZZERI

  ....

RELATORE:
  Dott. Ing. Daniele FANTERIA

  ....

Anno Accademico 2011/2012

Sessione di Laurea 9 Ottobre 2012

A chi ha creduto in me...

...e anche a chi non lo ha fatto...

Abstract

In aeronautical constructions, fatigue is an issue of great concern.

Laser Shock Peening is an innovative technology which promises considerable improvements to the development of a residual stress field capable of mitigative fatigue induced failures. The process has been successfully used in military applications for compressor and fan blades and for primary structures and is being introduced in the commercial aviation.

The physical principles of the Laser Shock Peening, such as the Plasma Generation and the Shock Waves propagation, are reviewed and the cost/benefits of the technology are discussed. In order to investigate the influence of Laser Shock Peening on fatigue life of thick components, a test campaign was carried out by the author within EADS - Innovation Works Deutschland; the test campaign brought out that the Laser Shock Peening is capable of sensitive fatigue strength enhancements.

Some unexpected failures occurred during the experimental activities. In order to investigate this unforeseen behavior, numerical simulations by means of the finite element method were carried out by the author at the Department of Aerospace Engineering of University of Pisa regarding the specimens involved in the test campaign. The simulations highlighted a modification of the stress field in Laser Shock Peened specimens which explains the unexpected failures.

Acknowledgments

Ringraziamenti

Oggi è una tappa molto importante di un percorso mi sta portando molto lontano. Naturalmente, in questo percorso non sono stato solo: una miriade di uomini e donne mi sono stati vicini in questo quarto di secolo, arricchendomi delle loro idee, dei loro modi di pensare, della loro esperienza e del loro amore nei miei confronti.

I primi a dover essere ringraziati sono mio padre, mia madre e mio fratello: la mia Famiglia. Mi hanno dato tutto quello di cui ho avuto bisogno, ma ciò per cui più li voglio ringraziare in questa sede sono due cose: la grande stima e fiducia che hanno sempre nutrito nei miei confronti e la possibilità di studiare all'università senza problemi. Queste due cose sono state per me i mattoni e il cemento con cui costruirmi il futuro che voglio. Un grazie di cuore va a tutte le zie e gli zii che mi hanno sempre trattato come un figlio. Grazie anche ai millemila cugini.

Adesso devo ringraziare una persona speciale, una persona che si è seduta accanto a me il primo giorno di lezione, e da quel giorno molte altre volte è stata al mio fianco. Parlo della mia compagna di viaggio Erika: molti viaggi abbiamo fatto insieme e molti altri ne faremo. Insieme.

Come non ringraziare di cuore i miei cari amici, il cui elenco completo sarebbe troppo lungo. Sono tutte persone straordinarie che hanno trascorso con me gran parte del loro tempo, sorbendosi i miei scleri e le mie esuberanze. Diciamolo però, talvolta erano ben ripagate da un pranzo succulento! Per la cronaca: non vi state liberando di me!

Grazie a tutti gli insegnanti che ho avuto, di qualunque scuola e disciplina. Mi hanno insegnato la cosa più difficile: mi hanno insegnato a pensare.

In generale ringrazio chiunque stia leggendo queste righe (che presumibilmente sarà tutto ciò che leggerà di questa tesi). Lo ringrazio volutamente in fondo, perché se è arrivato a leggere fino a questo punto deve volermi davvero tanto bene!

Infine vorrei ringraziare me stesso. In fondo, credo di meritarmi alla fine un momento di autocompiacimento!

Contents

Part I

Introduction

In order to improve the performance of the mechanical components, in all the branches of industrial engineering and specially in aeronautical engineering, there is a need for a surface protection against premature failure and operative life enhancements.

There are several causes for those premature failures initiating from the surface: for instance, components during operation are frequently subject to forces resulting into fatigue phenomena and early component failure. Moreover, the surface does not have the physical and chemical stability of the bulk crystalline material (due to reduced inter-atomic forces and to increased chemical reactivity).

The surface region therefore is much more sensitive to mechanical and thermal loads than the bulk material and prone to cracks propagation from the surface into the bulk material. This can result into fatigue induced premature failure of a component.

The introduction of residual compression stresses into critical surfaces is a proper measure to prevent crack nucleation and propagation. For this reason, the residual stresses introduction is one of the most widely used way to protect components against early failure and thus increase their operative life.

The introduction of residual stresses into metal surfaces is a very old way to improve the operational performance of metallic components. Hammering (peening) and various forms of heat treatment have been the methods used for many years. The basic principles are still valid today, but have been improved technically and scaled up to industrial levels in all areas of metallic processing.

Within the aeronautical industry, Shot Peening (SP) is the most important technology used nowadays to introduce residual stresses in a controlled manner. SP is a cold-working process and is widely used for the fatigue life improvement of aircraft components. Other used methods for residual stress introduction are related to the mechanical strain hardening (i.e., finish rolling, cold hole expanding. . .).

A development of the peening technologies can improve the protection against premature failures induced by static and dynamic loads, vibration and corrosion, or combinations of these effects. Furthermore engineered residual stresses can be used to form integrated structures or aerodynamic profiles enhancing performances. In addition to this improvement of manufacturing methods, which would improve

quality and reduce costs, it will be beneficial to further develop peening technologies with a view to reducing operational costs. For example, enhancing structural performance would lead to an extension of maintenance intervals. Moreover, the society keep demanding for more efficient, safer and environmentally friendly air transport.

Although the maintenance and repair business is usually associated with the carriers (e.g., airlines), rather than the aircraft manufacturers, it is evident that maintenance and "repair-friendly" aircraft will provide the carriers with a considerable marketing advantage compared to conventionally designed products. Laser Shock Peening is a shock wave based peening method and it is a novel alternative surface processing technology to conventional stress field induction techniques (mainly shot peening), which promises considerable improvement in the development of residual stress fields in aircraft construction.

Laser Shock Peening is an innovative surface enhancement process based on the generation of compressive residual stresses. The process promises considerable improvements to the development of a residual stress field in aircraft (and not only) construction, the residual stress field being capable of mitigative fatigue induced failures. It has been successfully used in military applications for aircraft gas turbine engine compressor and fan blades to increase their resistance to foreign object damage (FOD) and improve high cycle fatigue (HCF) life of the primary structures (Peyre et al. 1996; Liu 2008; Tenaglia and Lahrman 2003).

This work is divided into three parts. In the first part, the state-of-the-art in the field of residual stress introduction processes and the physical and technological aspects of the Laser Shock Peening (LSP) are presented. In the second part it is shown an experimental campaign on LSP treated coupons aiming at improving the application of this technology to aluminum thick components. The third part is devoted to numerical simulations and analysis of the specimens used during the test campaign, carried out by means of the software Abaqus.

Chapter 1

Conventional technologies for residual stress introduction

1.1 Conventional shot peening

Shot Peening treatments are widely used in mechanical and aeronautical engineering to improve the fatigue lives of components. The process is normally associated with harder metals such as steels, nickel and titanium alloys. Although this is generally the case, simply configured aluminum alloy components have for many years been peened.
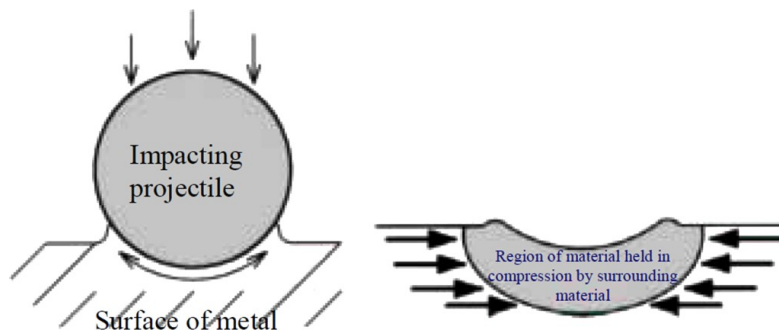
Figure 1.1: *The process of deforming the surface as the result of the impact of a projectile produces residual strain which is more commonly referred to as residual compressive stress.*

Shot Peening is a cold working process in which the surface of a part is bombarded with small spherical media, such as steel or glass balls. When such spherical

projectiles impact the target surface, the contact region is deformed against the resistance of the surrounding material. In so doing, a complex sub-surface residual stress distribution is generated in which, generally, the material just below and to the sides of the impact are in elastic compression as shown in figure 1.1, produced by the enlarged surface layer. To balance this compression zone an elastic tension zone surrounds the compression zone. The transition to this tension zone can be rapid. For the case where the surface has been covered by impacts the zones may be considered to be in layers receding from the surface so that the surface is generally in compression followed by a layer of tension which, on moving deeper decays to zero as shown in figure 1.2.
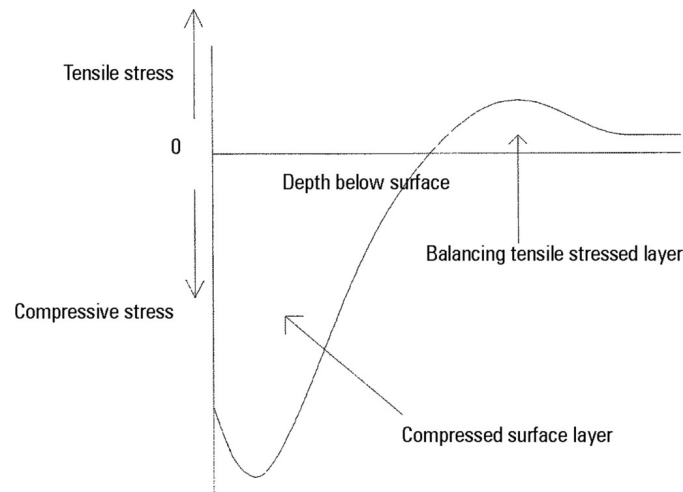
Figure 1.2: *Schematic of residual stress distribution below a peened surface. With traditional bead peening techniques this compressive layer generally extends 0.2-0.4mm below the surface*

.

The compressive residual stresses keep the crack closed when a far field tensile stress is applied to a component, to a level related to the magnitude of the compressive residual stresses, reducing the amount of crack tip opening. This reduction in crack opening, and therefore crack tip stress intensity range (ΔK) retards the crack growth. The retardation caused by these compressive stresses still operates when the crack tip has grown into the tensile stress field at deeper depths, where the crack tip is held open by the tensile residual stresses since the crack behind the tip (wake) is still clamped closed by the compressive residual stresses. Therefore

the effect of the residual stresses produced by peening is always to retard the crack growth by raising the far field stress required to open the crack from its far field unloaded state.

In reality peening does not produce a consistent surface condition since the resultant residual stresses are the product of many individual impacts by the peening media. These impacts are not distributed evenly over a surface, so the result is a variation in the final residual stress field. An example of a peened 7050T7451 surface as imaged by backscattered electron channelling diffraction pattern mapping methods in the scanning electron microscope (SEM) is shown in figure 1.3. Here the variation in color shows the variation in the intensity of the residual strains.
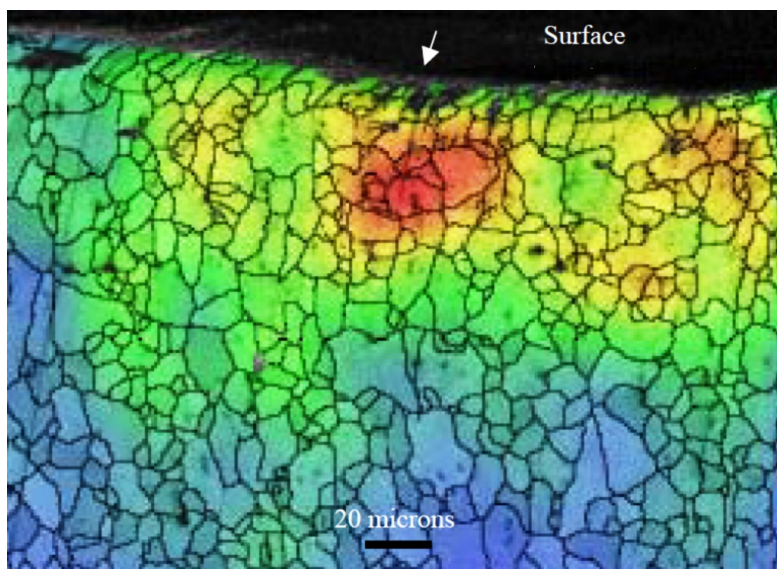
Figure 1.3: *Example of strain variation in a peened section of 7050 T7451 aluminum alloy as shown by backscattered electron channelling diffraction pattern mapping. The strain appears to be highest directly below the centre of a peening dent (arrow). The lines indicate the sub-grain boundaries. (Note that the image does not show the full extent of the peening, just the variation in strain)*

Along with the above local variations, the residual stress field is reliant on the constraint that is maintained by the material surrounding the deformed material. Such constraint are no at a free surface, thus the magnitude of the residual stresses can be reduced at external radii (re-entrant radii usually have excellent constraint). This leads to the most favorable region for crack propagation being at external corners of peened components. Since the surface is unconstrained the compressive

residual stress usually drops very close to the surface and, because the surface is not smooth, may contain regions of residual tension. This allows surface flaws to initiate fatigue cracks more favorably than internal flaws.

The application of Shot Peening to soft materials has resulted in reports of extensive variation in the fatigue life results for these high strength aluminum alloy peened components and, in some cases, a decrease in fatigue life was observed. Such variability naturally raises concern that the peening process developed for use with hard materials such as steels might not always be suitable for peening high-strength aluminum alloys which are much softer. In detail, the optimum peening parameters for steels are generally different from the ones for aluminum alloys.

An extensive amount of literature dating back to early in the twentieth century examining the effects of peening on steels and other hard alloys exists. An excellent review of this literature may be found in Company 2001.

It is an effective process, which increases the fatigue limit of alloys and prevents the occurrence of tensile and corrosion cracks in structural parts. However, the surface can be severely damaged by the shot peening process and the subsequent increase in surface roughness is a very important factor in relation to crack initiation. Therefore, additional and costly finishing operations have to be performed in order to re-smooth the surface. The shot peening procedures, which are serially applied nowadays, have additional disadvantages in that they need a relatively big effort and voluminous tools for the handling of the treated parts. In addition, the method has its limitations, with respect to the residual stress depth profiles that can be achieved, and consequently improved validated technologies will be required to meet the future standards in, for example, life-cycle extensions and/or improved utilization of light metal alloys.

Figure 1.4 shows a comparison of the stress fields, induced by conventional shot peening and LSP at variable process conditions (nomenclature: LSP 2-18-2 means $2GW/cm^2$ power density - 18 nm pulse width- 2 layers LSP treatment). These experiments were performed by Metal Improvement Company (UK). Such stress distribution are measured with Incremental Hole Drilling method.

Figure 1.5 shows an example of residual stresses induced in the high temperature resistant Ni- alloy Inconel 718, a material e.g. used in jet engine manufacturing (high pressure turbine blades, nozzle rings). Experiments were performed by
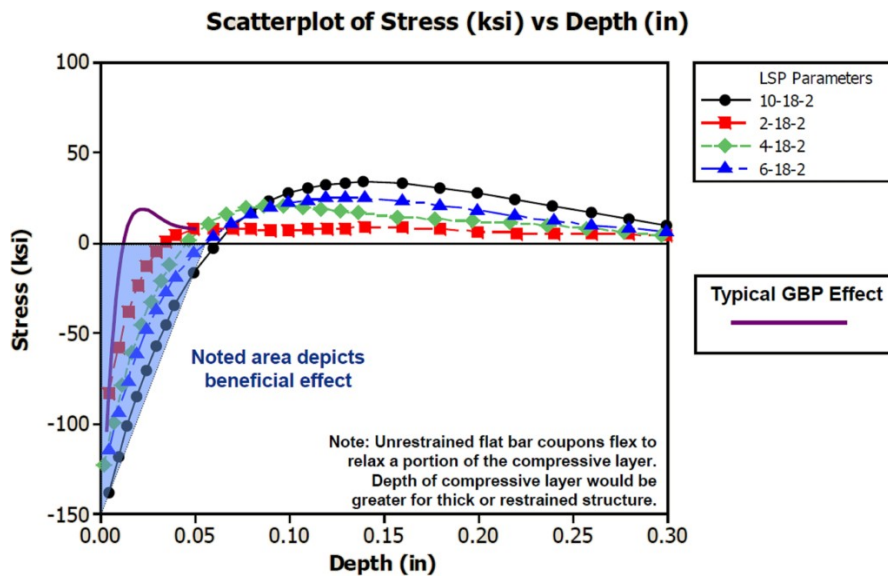
Figure 1.4: *Shot Peening and Laser Shock Peening residual stress profiles. (Jensen 2010)*

Metal Improvement Company (UK)
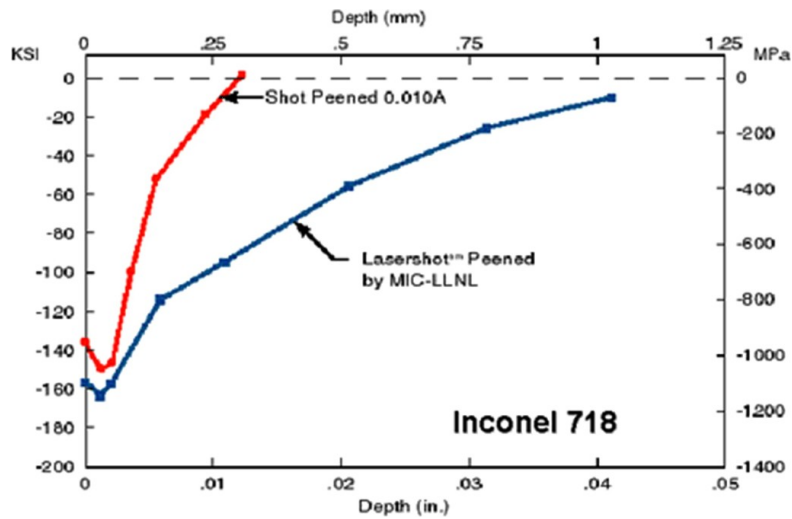
Figure 1.5: *Shot Peening and Laser Shock Peening residual stress profiles in Inconel 718. (MIC)*

It can be seen that the LSP treatment of both Ti6Al4V and Inconel 718 leads to a much deeper and intense residual stress distribution compared with conventional shot peening. In addition, the surface roughness after conventional shot peening

is much worse than is the case for LSP. Consequently, the following are clear disadvantages of conventional shot peening:

- The rough surface promotes increased fatigue crack initiation;

- In most practical cases, the roughness must be eliminated, which requires an additional manufacturing step and associated additional costs. Moreover, re-machining of a shot peened material can lead to disturbances in the induced residual stress field, which would have a negative impact on fatigue life.

1.2 Ultrasonic Shot Peening

The Ultrasonic Shot Peening (USP) is another example for a cold working process. USP is based on producing ultrasonic waves via an electro-mechanical transducer, and delivering those waves into the workpiece. An acoustically tuned body is brought to resonance by energizing an ultrasonic transducer. The energy generated by these high frequency impulses is imparted to the treated surface through the contact of specially designed steel pins or even metallic or ceramic balls which hit the surface on the workpiece. These transfer pins are free to move axially between the resonant body and the treated surface. When the tool, made up of the ultrasonic transducer, pins and other components, comes into contact with the work piece it acoustically couples with the work piece, creating harmonic resonance. This harmonic resonance takes place at a carefully calibrated frequency (the resonance frequency), resulting in compressive residual stress, stress relief and grain structure improvements. The energy transferred to the workpiece as each piece of shot hits the surface is small. The required surface strain is achieved through continuous peening for a set time.

1.3 Cold Hole Expansion

The Cold Expansion of Holes ("cold working") is a fatigue enhancement technique, which is used extensively on metallic aircraft components to enhance fatigue

performance of a structural assembly. Conventional processes pull an oversize tapered mandrel through a fastener hole. The hole increases in size, plastically deforming surrounding material, which results in high compressive residual stresses around the hole. The zone of compressive residual stresses is a barrier to both crack formation and growth. Fatigue life enhancement is generally increased by a factor between two and seven. Although the current processes provide reasonable results in fatigue enhancement, they exhibit disadvantages such as inhomogeneous strain distribution around the hole, risk of crack formation - in particular with high-strength Aluminum alloys, occasional tool seizure, and - for the so called split sleeve process - a large number of sleeves, which are costly to dispose.

Part II

The Laser Shock Peening process

Chapter 2

General aspects and process principles

The Laser Shock Peening (LSP) process is based on the production of shock waves using a high-power pulsed laser. When the laser beam is focused onto a solid, a high-temperature plasma is generated. The blow-off of the high-pressure plasma generated at the target surface can induce a mechanical impulse to the solid. In consequence of this mechanical impulse at the surface, a shock wave penetrates inside the material. This mode is called "direct ablation"; in this case the irradiated target is in vacuum and the plasma freely expands. In this regime, it has been shown that pressures ranging from a few kilobars to more than 50 megabars can be obtained mainly by varying the incident plasma intensity from about $10^8 - 10^9$ to $\sim 10^{15}$ W/cm^2. Moreover, in this regime, due to the rapid cooling of the generated plasma by its adiabatic expansion in vacuum, the time duration of the applied pressure is roughly equal to the laser pulse duration.

There is another interesting mode of laser-material interaction, called "confined ablation" (which is currently the most widely used), where the expansion of the generated plasma is delayed by confining it, fig. 2.1. The confinement is obtained when the irradiated surface is in close contact with a transparent overlay, such as water or glass. In this case, the laser beam passes through the transparent overlay and strikes the opaque target, which vaporizes. This vapor then absorbs the incoming laser energy by *inverse bremsstrahlung*, a process in which the particles

absorb radiating energy gaining kinematic energy. The consequent ionization of the paint vapor results in the formation of the high pressure (up to tens of MPa) and high temperature (over 10 000 K) plasma. The rapidly expanding plasma is then confined by the water overlay such that, for a short time, very high local pressures are induced; this pressure delivers an impulse momentum to the target (Devaux et al. 1993; Masse and Barreau 1995). The total impulse momentum transmitted to the target in the "confined" mode is roughly 4 times higher than in the "direct" mode.

The plasma pressure is transmitted into the target through shock waves that plastically deform the target surface. Once the dynamic stresses induced by the shock waves exceed the dynamic yield strength, the uniaxial compression driven by the plasma expansion generates tensile stretching on the surface layers, so an opposite reaction of the surrounding zones (beside and below) induces the compressive residual stress field, see figure 2.2 (Peyre et al. 1998)
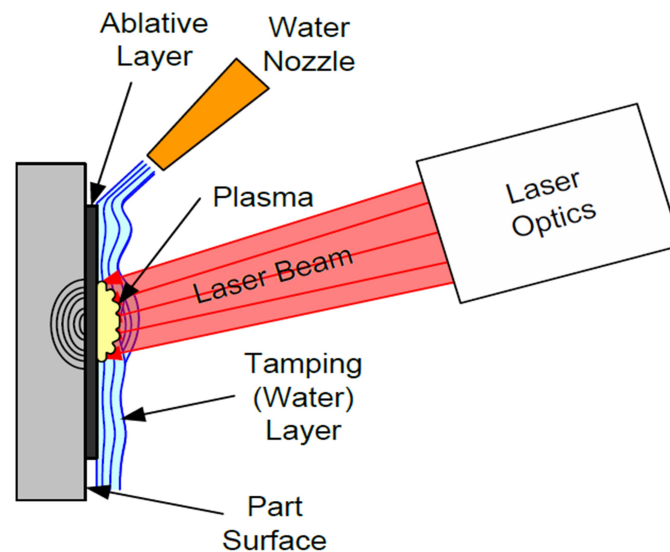
Figure 2.1: *Schematic of LSP in the confined ablation mode. (MIC website)*

The pulsed laser beam may be used either to impact directly the target surface or an opaque coating overlay. The direct impact method is unusual since the absence of the opaque overlay results in melting and subsequent damage of the target surface: in this configuration, it has been shown by Peyre et al. (1998) (see figure 2.3) that very high tensile residual stress values can be reached in the surface
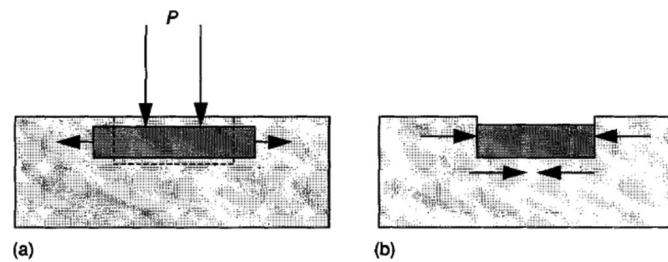
Figure 2.2: *Principle of the generation of compressive residual stresses with laser shock treatment (with an overlay), during the interaction (a) and after the interaction (b).(Peyre and Fabbro 1995)*

of the material, which may lead to premature failures.
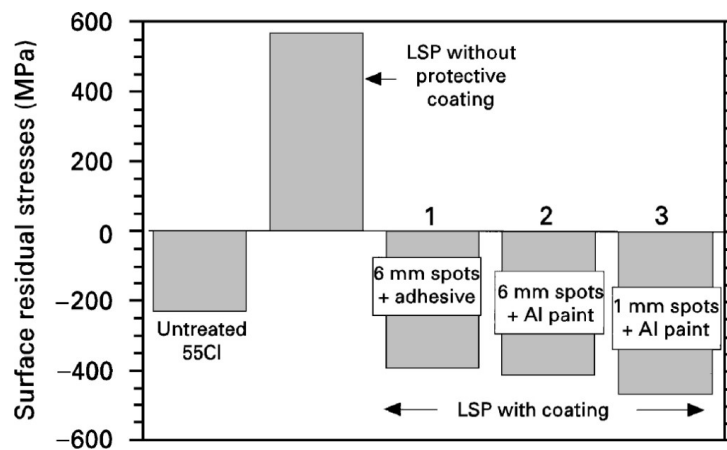
Figure 2.3: *Average residual stress values determined at the surface of notched fatigue samples with different LSP conditions at 5 GW/cm² in the water-confining regime: (1) 6 mm impacts+aluminum adhesive, (2) 6 mm impacts+aluminum paint, (3) 1 mm impacts+aluminum paint. (Peyre et al. 1998)*

The opaque overlay acts in two ways:

- as a sacrificial layer that is vaporized by the laser pulse preventing surface melting from direct contact with the laser-induced plasma;

- as an energy absorbing layer that increases the efficiency of the energy transfer to the confining layer above.

For these reasons, coatings are involved in almost all LSP treatments. The opaque coating overlay may be in form of dry or wet paint, black tape, metal foils or adhesive-backed metal foils.

2.1 Physical study of the laser-produced plasma in confined ablation mode

The impulse momentum necessary for the plastic deformation of the material is delivered by the blow-off of the high-temperature plasma generated at the target surface. This expansion has been described by Fabbro et al. (1990) and divided in three steps as follows.

1. During the laser pulse duration, the pressure generated by the plasma induces two shock waves which propagates into the target and the confining material respectively.

2. When the laser is switched off, the plasma still maintains a pressure which decreases during the expansion due to its cooling. The cooling can be assumed as adiabatic because of the short time duration of the process. During these two steps, the target receives an impulse momentum due to the induced shock wave. This additional momentum is the responsible of the enhanced peening conditions in the confined ablation mode compared to the direct ablation one.

3. Finally, for longer times, after the complete recombination of the plasma, the "cannon-ball-like" expansion of the heated gas inside the interface adds more momentum to the target, but during this period the exerted pressure is not sufficient to realize a plastic deformation of the material, thus this phase will be neglected in this analysis.

It is considered only a monodimensional solution of this problem.[1] The laser energy is deposited over a typical thickness of solid material of few atomic distances, at the surface between the solid material (in figure 2.4 indicated as 1) and the transparent layer (2). This volume is then heated, vaporized and ionized. Its blow-off being impeded by the transparent medium, the pressure increases and has the effect to open the interface.

---

[1]Only the monodimensional solution will be taken into account because high magnitude waves (e.g. $P > 1$GPa) often "shock up", because at high pressures solids become less compressible as external electron shells interact, steeping the wave, thus the shock wave can be studied as a 1D planar shock wave (Prime 2008)
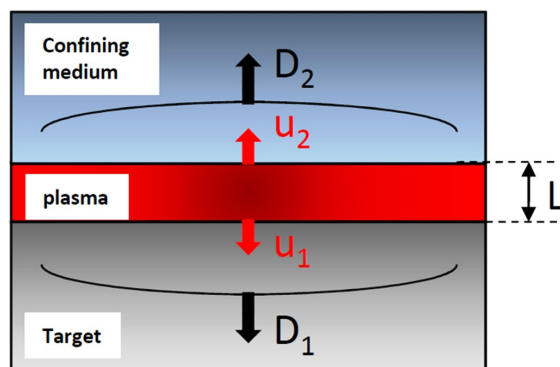
Figure 2.4: *Schematic of the monodimensional problem for the plasma confined expansion. (Peyre, Berthe, and Fabbro 2011)*

Supposing that this pressure is strong enough for generating two shock waves in the two media, the interface wall displacement will result only from the fluid motion behind the two shock waves which are propagating inside the two materials. Let us call $L(t)$ the thickness of the interface at time t; then it is

$$L(t) = \int_0^t \left[u_1(t) + u_2(t) \right] \mathrm{d}t \tag{2.1.1}$$

In order to calculate the fluids velocities u_i $(i = 1, 2)$ it is possible to relief in the shock wave relations as obtained by Zel'dovich and Raizer (1966) for a normal shock wave in a monodirectional flux:

$$\rho_b D u = P_a - P_b$$

where, in this case, ρ_b is the density of the material before the shock, D is the shock wave velocity, u is the velocity of the particles after the shock (for sake of simplicity, the initial velocity has been supposed null) and P_b and P_a are the absolute pressures before and after the shock. The value of v D can be obtained by tables, but there is a semiempiric relation between the the shock velocity and the bulk elastic sound speed (Ballard 1991; Devaux et al. 1993):

$$D = C_0 + \sum_{i=1}^{n} S_i u^i$$

where the S_i are material constants (usually a linear relation is observed, thus only the S_1 is used, some materials are non-linear and have higher order terms) and C_0 is the bulk elastic sound speed computable as follows

$$C_0 \simeq \sqrt{\frac{B}{\rho}} \quad \text{with} \quad B = \frac{E}{3(1 - 2\nu)}$$

It is possible to arrange this equation introducing the definitions of plasma's relative pressure P ($P_b \simeq P\text{atm}$) and of shock impedance $Z_i = \rho_i D_i$ (ρ_i being the base density of the material i and D_i the shock wave velocity in it) obtaining

$$P = Z_i u_i \quad \Rightarrow \quad u_i = \frac{P}{Z_i}$$

Using this relation and using it in the (2.1.1) it is possible to state

$$\frac{\mathrm{d}L(t)}{\mathrm{d}t} = \left(\frac{1}{Z_1} + \frac{1}{Z_2} \right) P(t) = \frac{2}{Z} P(t)$$

2.1.1   Heating phase

In the heating phase, the absorbed laser energy is used to increase the internal specific energy of the plasma inside the interface and as work to open it. During the time interval $\mathrm{d}t$, this plasma thickness increases by $\mathrm{d}L$. The energy per unit surface which is deposited by the laser $I(t)\,\mathrm{d}t$ is then used to increase the internal specific energy $e_i(t)$ by $\mathrm{d}[e_i(t)L]$ and as work of the pressure forces $P(t)\,\mathrm{d}L$. Therefore it is proven that

$$I(t)\,\mathrm{d}t = P(t)\,\mathrm{d}L(t) + \mathrm{d}\left[e_i(t)L(t) \right] \tag{2.1.2}$$

It is legit to assume that only a constant fraction α of the internal energy $e_i(t)$ represents the thermal specific energy $e_t(t)$, the fraction $(1 - \alpha)$ being used for the ionization of the gas.

It is possible to find a correlation between the plasma pressure and the thermal specific energy proceeding from the definition of thermal energy E_t:

$$E_t = \frac{1}{2} N f k_B T$$

where N is the number of particles of the system in analysis, k_B is the Boltzmann constant and T is the absolute temperature. For gaseous systems, the factor f, the number of degrees of freedom, commonly has the value 3 in the case of the monatomic gas, 5 for many diatomic gases, and 7 for larger molecules at ambient temperatures For this analysis will be assumed that the high temperature plasma behaves as a perfect monoatomic gas, so $f = 3$. Developing the calculations it is possible to write

$$P(t) = \frac{2}{3}e_t(t) = \frac{2}{3}\alpha e_i(t)$$

This allows to manipulate the (2.1.2) obtaining

$$I(t) = P(t)\frac{\mathrm{d}L(t)}{\mathrm{d}t} + \frac{3}{2\alpha}\frac{\mathrm{d}}{\mathrm{d}t}\left[P(t)L(t)\right]$$

For a constant laser intensity I_0, a pulse duration τ and an initial gap between target and confining medium $L(0) = 0$, the pressure of the plasma is constant during the laser pulse and it is

$$P = A\sqrt{\frac{\alpha}{2\alpha + 3}}\sqrt{ZI_0} \tag{2.1.3}$$

where A is a constant and it is $A = 0.01$ if P is measured in kbar, Z in g/cm^2 s and I_0 in GW/cm^2 and

$$L(\tau) = 2 \times 10^4 \frac{\tau P}{Z}$$

if L is measured in μm and P and Z as before.

2.1.2   Adiabatic cooling

The laser is now switched off at time $t = \tau$. For simplicity's sake it is possible to neglect the heat conduction losses of the plasma toward the walls off the interface, because of the short time duration of the process. Therefore, the plasma will experience an adiabatic cooling for $t \geq \tau$ described by the following relation (Fabbro et al. 1990):

$$P(t) = P(\tau) \left(\frac{L(\tau)}{L(t)} \right)^{\gamma}$$

where the evolution of $L(t)$ for $t \geq \tau$ will be

$$L(t) = L(\tau) \left(1 + \frac{\gamma + 1}{\tau}(t - \tau) \right)^{\frac{1}{\gamma+1}}$$

where $\gamma = \frac{5}{3}$. The pressure decreases to $P(\tau)/2$ for $t = 1.8\tau$ whereas in the direct ablation mode the pressure would nullify quite instantly after the laser switching-off. The pressure is applied over a much longer period than the laser-pulse duration. The result of this effect is to increase the impulse momentum $\mathcal{I}_0$ delivered to the shock wave. For example, in the case of a constant laser intensity irradiating a target during the time interval $t \in [0, \tau]$, the total impulse momentum in the shock wave is

$$\mathcal{I}_0(t) = \int_0^t P(t)\,\mathrm{d}t =$$
$$= Z\frac{L(t)}{2} =$$
$$= \frac{L(t)}{L(\tau)}P(\tau)\tau =$$
$$= \beta(t)[P(\tau)\tau] =$$
$$= \beta(t)\mathcal{I}_0(\tau)$$

At time $t = t_1 = 16.7\tau$, the pressure has decreased by one order of magnitude and the plasma thickness is 4 times greater than its thickness at $t = \tau$ (so $\beta = L(t)/L(\tau) = 4$), so the total impulse momentum is 4 times greater than the one obtainable in the first phase (which is roughly the one obtainable in the direct ablation mode). It has been shown (Fabbro et al. 1990) that the thickness of the material which is plastically strained by the shock wave is directly proportional to the impulse. Therefore, this impulse momentum is the parameter in this process to maximize.

Unfortunately, there is an upper limit to the laser intensity due to the dielec-

trical breakdown of the confining medium. When the laser power density exceeds a certain limit, the dielectric becomes opaque to the laser beam because a plasma is created inside the dielectric volume. The laser energy is no longer absorbed at the interface but in the plasma inside the dielectric volume, over the target. This phenomenon drives to saturation or reduction of the peak pressure (Fabbro et al. 1990).
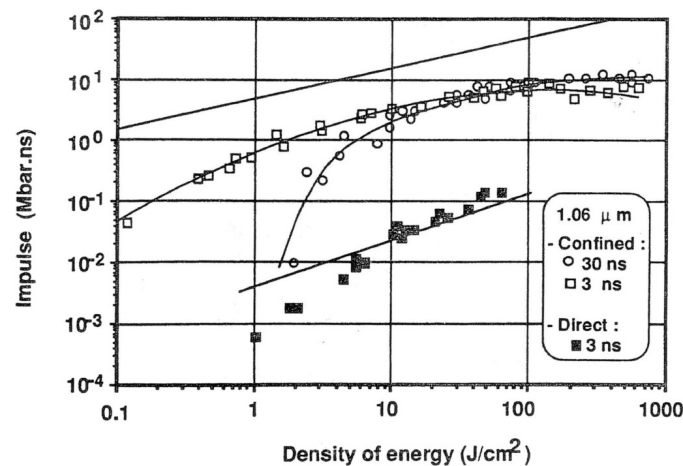
Figure 2.5: *For direct or confined regime, variation of the impulse momentum $\mathcal{I}$ as a function of the incident energy per unit area. (Fabbro et al. 1990)*

The laser induced breakdown appears as an irreversible (and, in case of solid confining medium, destructive) alteration of the dielectric due to an intense laser light wave. The dielectric materials, transparent to laser radiation, have low absorption coefficients (10^{-5} $-$ 10^{-1}cm^{-1}). One might think that the impurities absorption could lead to the dielectric breakdown; but, it has been shown (Fabbro et al. 1990) that if the size of impurities does not exceed 0.1μm, the breakdown is independent of the impurities density. The physical mechanism responsible for the breakdown has been identified as avalanche electron ionization. In Devaux et al. (1993) it is shown that the only way to put more energy near the target interface and to obtain high pressure is to use the shortest possible rise-time laser pulse in order to limit the expansion of the ionization wave far from the target surface.

2.2   Generation of residual stresses due to the shock waves

The shock wave generated by the blow-off of the plasma bubble propagates into the target, causing plastic deformation to a depth at which the peak stress no longer exceeds the Hugoniot Elastic Limit (HEL) of the material (also called dynamic yield strength or yield strength at high strain rate, this is equivalent to the yield strength under shock conditions) and generating the residual stresses. The Hugoniot Elastic Limit is defined as follows

$$HEL = \left(1 + \frac{\lambda}{2\mu}\right)\sigma_y = \left(\frac{1 - \nu}{1 - 2\nu}\right)\sigma_y$$

The elastic-plastic model proposed by Peyre et al. (1996) and Ballard (1991) is able to predict the amount of plastic strain and residual stress induced by any fast impact considered as a pure uniaxial deformation. This model is based on the calculation of the elastic-perfectly plastic response of a material to longitudinal and planar shock wave systems. The following assumptions are used in this model:

- the shock-induced deformation is uniaxial and planar;

- the pressure pulse is uniform in space;

- materials obey a von Mises plasticity criterion.

The plasma pressure P acting at the surface rises during the heating phase up to a maximum given by eq. (2.1.3) and then decreases in the adiabatic cooling phase . Treating the elastic and plastic loading and unloading phases separately, the model comes to the following definite conclusions:

1. no plastic deformation is possible for $P < HEL$;

2. plastic deformation increases linearly for $HEL < P < 2HEL$;

3. above $2HEL$, plastic deformation reaches a maximum limit;

4. above $2.5HEL$, surface release waves focus and amplify from the edges of the impacts thus modifying the RS field, regardless of the impact shape (circular or square).

Ballard (1991) states that the plastic deformation field induced by the treatment is

$$\underline{\varepsilon_p} = \begin{pmatrix} -\frac{\varepsilon_p}{2} & 0 & 0 \\ 0 & -\frac{\varepsilon_p}{2} & 0 \\ 0 & 0 & \varepsilon_p \end{pmatrix}$$

The relation between the plastic deformation ε_p at the surface and the plasma pressure P, only valid for $HEL < P < 2HEL$, is given by

$$\varepsilon_p = -\frac{2HEL(1 - 2\nu)}{E}\left(\frac{P}{HEL} - 1\right)$$

which indicates a linear dependence of ε_p and the P/HEL ratio. As a consequence, according to the model, the optimal peak pressure corresponds to $2 - 2.5HEL$ (fig. 2.6).
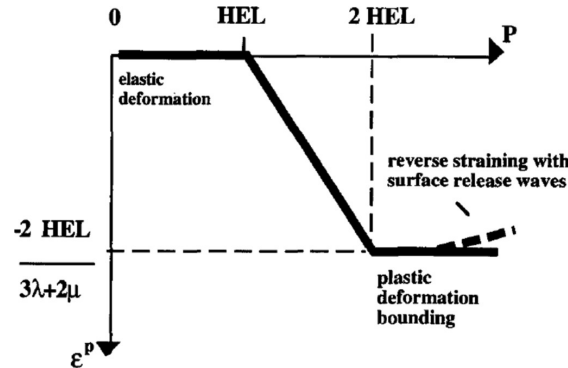
Figure 2.6: *Plastic deformation induced by LSP as a function of peak pressure. (Peyre et al. 1996)*

Once chosen the optimal pressure as the one that drives to a saturation of ε_p it is possible to predict the plastically affected depths $\mathcal{L}$ and the maximum surface stresses σ_{surf} with the following relations:

$$\mathcal{L} = \frac{P - HEL}{2HEL}\left(\frac{C_{\text{el}}C_{\text{pl}}\tau}{C_{\text{el}} - C_{\text{pl}}}\right) \tag{2.2.1}$$

$$\sigma_{\text{surf}} = -\left(\frac{P}{HEL} - 1\right)\frac{1+\nu}{1-\nu}\left[1 - \frac{4\sqrt{2}}{\pi}(1+\nu)\frac{\mathcal{L}}{a}\right]\sigma_y \tag{2.2.2}$$

where τ is the pressure pulse duration, a the edge of the laser spot (mm) and C_{el} and C_{pl} are elastic and plastic waves velocities (Ballard 1991)

$$C_{\text{el}} = \sqrt{\frac{E(1-\nu)}{\rho(1-2\nu)(1+\nu)}} \qquad\qquad C_{\text{pl}} = \sqrt{\frac{E}{3\rho(1-2\nu)}}$$

2.3   Laser Shock Parameters

The LSP parameters that play a very important role in the process include laser power density, laser spot size and geometry, pulse duration, wavelength, repetition rate and number of shots per point.

2.3.1   Laser Power Density

The Laser Power Density (or Fluency) is defined as laser beam energy per unit area, thus increasing the laser power or reducing the laser spot size will lead to an increase in laser power density, which results in an increase in peak plasma pressure. The relationship between the laser power density and the peak plasma pressure can be expressed by the (2.1.3):

$$P = 0.01\sqrt{\frac{\alpha}{2\alpha + 3}}\sqrt{ZI_0} \tag{2.3.1}$$

where P is the peak plasma pressure, α is the fraction of the internal energy devoted to the thermal energy (typically, $\alpha \simeq 0.11^2$), I_0 is the incident power density, Z is the reduced shock impedance between the target and confining medium, defined (for the modern sets-up) by the relation:

$$\frac{2}{Z} = \frac{1}{Z_{\text{confin}}} + \frac{1}{Z_{\text{target}}} \tag{2.3.2}$$

where Z_{confin} and Z_{target} are the shock impedance of the confining medium and the target, respectively. $Z_{\mathrm{water}} = 0.165 \times 10^6$ g/s cm^2 for water[2] and $Z_{\mathrm{target}} = 1.5 \times 10^6$ g/s cm^2 for the aluminum target. Using these values, equation (2.3.1) can be simplified to

$$P = B\sqrt{I_0} \qquad\qquad (2.3.3)$$

where B is a constant and, if P is measured in kbar and I in GW/cm^2, it is $B = 21$ if the confining medium is glass and $B = 10.2$ for water. From the above equation, it can be seen that increasing the laser power density (I_0) results in an increase in the peak plasma pressure (P) within the limitations due to the dielectric breakdown.

Figure 2.7 shows residual stress profiles for a 12.7 mm thick titanium alloy plate (Ti-6Al-4V) under different LSP intensity levels. The minimum yield stress of this material is about 828 MPa (120 ksi). Lower intensity shock peening produces both a lower surface compressive stress and a shallower depth. An intermediate intensity shock peening creates a higher surface compressive stress. After a higher intensity peening, the compressive stresses extend down to about 0.75 to 1 mm (0.03 to 0.04 in). The residual stresses after LSP generally lie in the range of -689 to -827 MPa (-100 to -120 ksi) for this alloy, although higher compressive stresses at the surface have been observed.

2.3.2   Repeated rate and multiple shots

As discussed in Clauer (1996), the compressive residual stresses can be driven deeper below the surface by using multiple or successive laser shots. This is illustrated in figure 2.8 for a 0.55% carbon steel. As the number of shots on the surface increases from one to three, the depth of the compressive residual stress increases from $0.9mm$ to $1.8mm$. This same trend has been observed in other alloy systems, including titanium and aluminum alloys.

In thin sections, increasing the layers of laser peening will not necessarily in-

---

[2]The shock impedance of the glass is about ten times the one of the water, but the use of the glass is inhibited for actual components because the water is more adaptable to complex geometries.
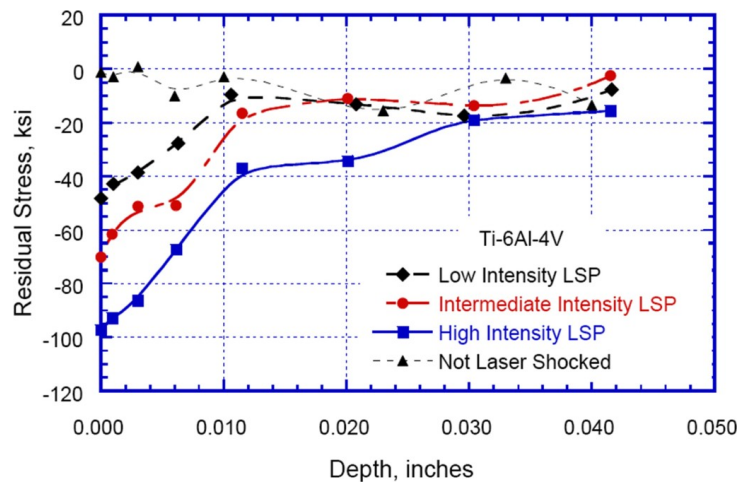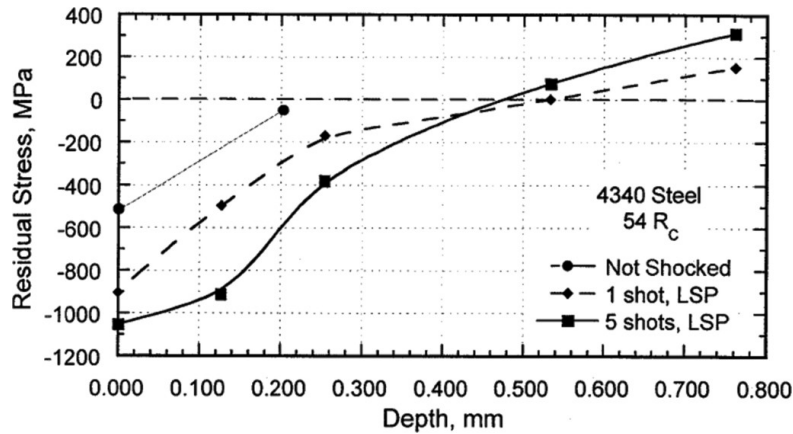
Figure 2.7: *Residual Stress profiles in depth in Ti-6Al-4V at three different laser shock peening intensity levels. (Liu 2008)*
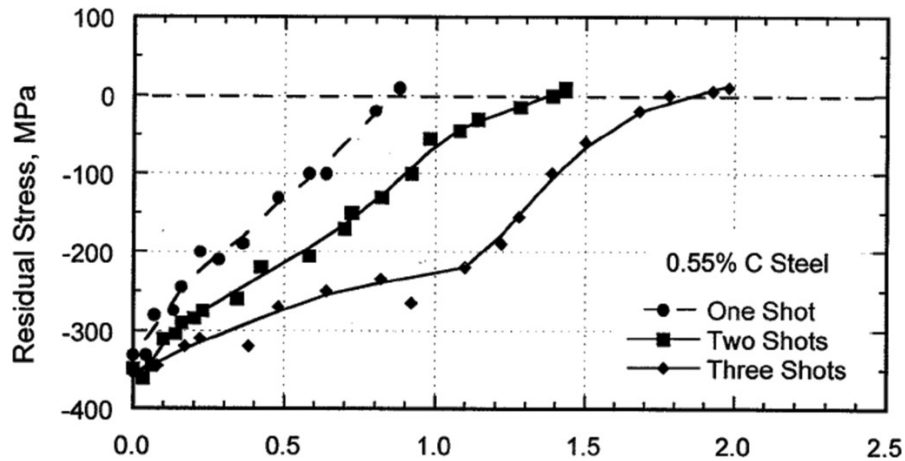
Figure 2.8: *The effect of increasing laser peening intensity on the in-depth residual stresses in a 0.55% carbon steel. (Clauer 1996)*

crease the depth of the compressive stresses, but it will increase the magnitude of the stresses in-depth. This is shown in figure 2.9. This 1.5 mm-thick 4340 steel sheet was heat treated to 54 R_c hardness before laser shock peening. It was then peened with one and five shots from both sides simultaneously, and the residual stresses measured. The depth of the compressive stress is nominally $0.5mm$ for both peening conditions, but the magnitude of the compressive stresses is higher after five shots. In addition, the tensile residual stress at the mid-thickness ($0.75mm$) of the sheet is higher after five shots. When doing thin sections, the processing

conditions have to be carefully selected to avoid or minimize a high tensile residual stress at the mid-thickness of the section.


Figure 2.9: *Residual stress profiles in thin, 4340 steel sheet after different laser peening intensities. The mid-thickness of the sheet is at 0.75 mm. (Clauer 1996)*

2.3.3   Spot size and Geometry

Laser spot size affects the residual stress profile, particularly for surface residual stresses. Peyre et al. (1998) investigated laser-induced residual stresses in 55C1 steel (medium carbon steel) as a function of changes in laser spot size. The laser spot sizes used for the LSP process were 1 mm and 6 mm in diameter, respectively. The Metal Improvement Company carried out similar experiments on Ti 6-4 blocks using square spots of different sizes (1, 2 and 3 mm edge) using the same fluency. The results indicated that a large spot size produced a residual stress profile much deeper beneath the treated surface compared with a small one (figure 2.10.1). However, the magnitude of surface compressive residual stresses was not increased by reducing the laser spot size, as shown in figure 2.10.2. In other words, the distribution of in-depth residual stresses is almost steady if the fluency is not modified (figure 2.11).

The magnitude of residual stresses is usually highest at the surface and gradually decreases as depth below the surface increases. However, as shown in Masse and Barreau (1995), for a circular laser spot, there is a lack of residual stresses at the center of the treated zone after laser interaction. It is attributed to the
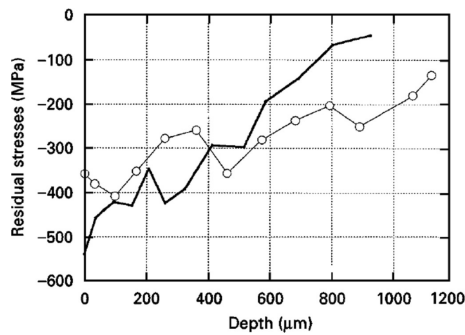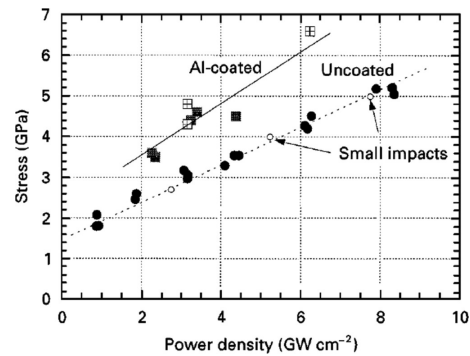
2.10.1   2.10.2

Figure 2.10:
*On the left: In-depth residual stresses on 55C1-LSP 5 GW/cm². Influence of impact
sizes on the affected depths: solid line for 1 mm, dots for 6 mm impacts.
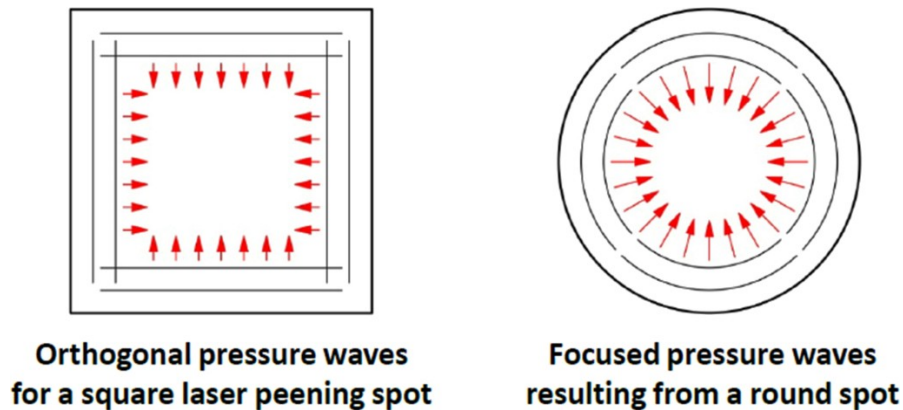On the right: Internal stress curve: influence of the coatings on the stress amplitude
values. All measurements made with 3-4 mm impacts except three stress determinations
made with 1 mm diameter spots. Empty circle and full circle for base materials
(aluminum or steels), full square for 316L+140 μm aluminum paint, crossed square for
316L+ aluminum adhesive.(Peyre et al. 1998)*
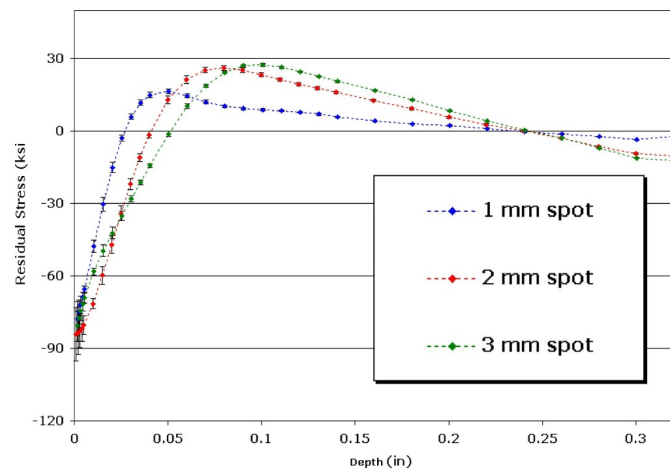
Figure 2.11: *The spot dimension doesn't influence much the stress profile for equal
power density. (Dane et al. 2011a)*

simultaneous focusing of the waves emitted from the edges of the area under im-
pact and leads to a non uniform surface stress, a poor surface quality (presenting
peaked structures at the spot centers) and a possible bulk spalling damage. This
phenomenon can be artificially minimized by using convenient coverage ratios, or

by eliminating the circular symmetry (fig. 2.12), so by changing the geometry of the laser spot, i.e. using a square or ovoid shape. The elastic pressure release after the peening pulse can generate a circular wave with a tight focus for a round laser spot, a well-known phenomenon in high energy laser optics. A square spot replaces the focused waves with quasi-orthogonal plane waves which can reduce the pressure concentration at the center of the spot.

Orthogonal pressure waves for a square laser peening spot

Focused pressure waves resulting from a round spot

Figure 2.12: *The shape of the spot can influence the pressure concentration at the center of the spot. (Dane et al. 2011a)*

Figure 2.13.1 shows how the Toshiba has been able to obtain a square spot. Also Metal Improvement Company (a subsidiary of Curtiss-Wright) is able to obtain square spots. In figure 2.13.2 are shown two surface residual stress profiles along treated zones, for two impact shapes with the same treatment conditions (water-confined mode; fluence, 5 GW/cm^2).

Moreover, the square spots provide an efficient and more uniform coverage in a single treatment layer; this is clearly visible by the comparison between fig. 2.14.1 and fig. 2.14.2.

2.3.4   Confining media and ablative layers

During the laser exposure, the heated zone is vaporized and then absorbs the incoming laser energy reaching temperatures in excess of 10 000°C, and due to the ionization is transformed into a plasma. The latter continues to absorb the laser energy until the end of the deposition time. The pressure of the plasma is
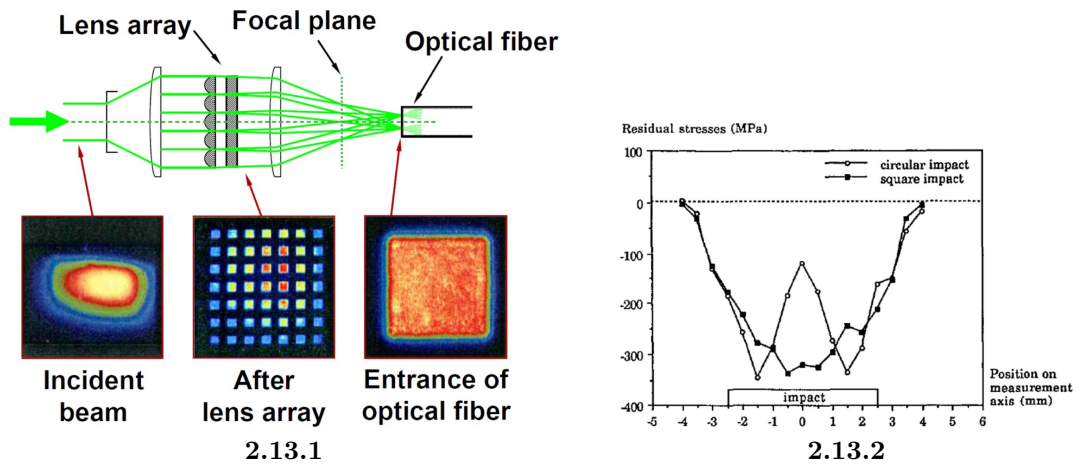
Figure 2.13:
2.13.1: How Toshiba achieved a square shape of the spot (Sano et al. 2010);
2.13.2: Superficiall residual stress profiles after circular and square laser shocks. (Masse and Barreau 1995)
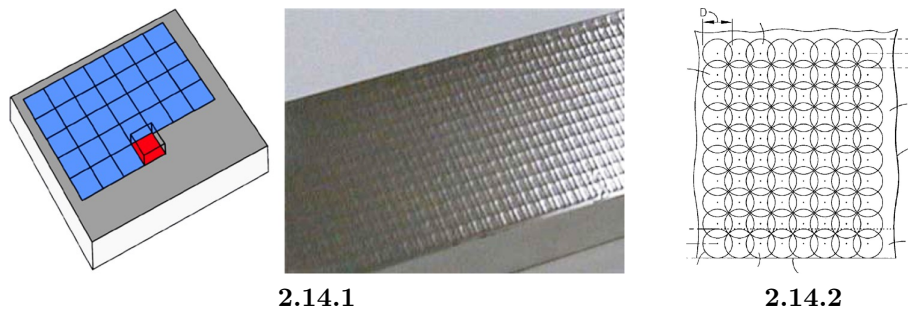

Figure 2.14: *Surface aspect after Laser Shot Peening.*
2.14.1: square spot (Dane et al. 2011a);
*2.14.2: round spot. (*Lower fluence boundary laser shock peening*)*

transmitted to the sample through a shock wave. This type of interaction is called "direct ablation" and pressures of only some tenths of a gigapascal are achieved.

To obtain higher shock pressures, it is necessary to delay the plasma expansion. For this purpose, it is necessary to coat the sample surface with a material opaque to laser light (black paint or aluminum foil) and then with a material transparent to the laser radiation (typically distilled water or BK7 glass). The laser beam crosses the transparent overlay and is absorbed by the opaque overlay, partly vaporizing the latter.

The transparent overlay traps the thermally expanding vapor and plasma against the surface of the workpiece. The hydrodynamic expansion of the heated plasma in the confined region between the sample and the transparent overlay creates a high amplitude high pressure pulse required for laser shock surface treatment. The shock pressures are magnified by a factor of 10 compared with a "direct ablation" configuration, reaching 10-60 kbar.

Water, applied using an appropriately placed nozzle, has been found to be the simplest and most cost effective method for producing the transparent overlay (Tenaglia and Lahrman 2003).

Nevertheless, there is a limiting effect due to the amount of energy absorbed by the confining material: beyond a certain fluence, no energy is able to reach the opaque overlay. Any plasma created at an earlier stage is suddenly released by breaking up of the confining matter. This effect is explained by an electron avalanche caused by initiating the electrons existing in glass and, in the case of water used as confining material, the presence of impurities producing hot spots leading to quick vaporization (Masse and Barreau 1995).

Using glass instead of water as confining material allows to achieve higher plasma pressures. This discrepancy is due to the difference in the acoustic impedance between glass and water. The larger value is for glass (about 10 times the value for water) which is the reason why higher pressures are achieved when using glass as a confining material.

During the laser interaction with an uncovered sample surface, the treated zone is dilated by the thermal effect and then compressed by the surrounding matter, creating a compressive stress field. After the deposition time, the treated zone is restored by mechanical action of the untreated matter, inducing a tensile stress field (see figure 2.3).

If the sample surface is first covered with a material opaque to laser light, the thermal effect only affects the protective coating. The opaque overlay can be in a variety of forms such as dry or wet paint, black tape, metal foils and adhesive-backed metal foils Shock waves alone penetrate into the sample, creating a tensile stress field. The surrounding matter reacts to this volume expansion by inducing a compressive stress field.

The first atomic layers of the coating not only protect the surface from thermal

rise but also from the plasma in itself, indicating that they can play a fundamental role on the plasma properties and particularly the plasma pressure. Most of all, differences of acoustic properties, Z, at the interface between the surface coating and the underlying substrate can modify the stress loading by type mismatch impedance effects: if $Z_1 < Z_2$, the peak stress increases when the shock wave comes from material 1 to material 2.

Chapter 3

Benefits of the technology

LSP has a number of advantages over conventional shot peening. It can create a residual compressive stress zone up to 1 mm or greater in depth in aluminum alloys, whereas conventional shot peening methods only produce compressive residual stress to approximately 250 μm deep below the treated surface. Moreover, the laser radiation is highly controllable and the process is readily amenable to automation. In addition, there is little or no modification of the original surface profile. Even very thin sections can be laser processed without deformation of the part, eventually with back-up supports or treating both surfaces with two laser beams of equal intensity; these beams strike the part on opposite surfaces simultaneously. In some component geometries containing holes and slots, it is very difficult for conventional technologies - such as shot peening - to be used due to limited accessibility, whereas LSP can easily reach these areas by using an optical fiber as the delivery system.

The benefits of LSP are already proving to be considerable, for example, in turbine engine applications. After LSP treatment, the turbine engines blades had longer life and reduced maintenance costs (Tenaglia and Lahrman 2003). Consequently, LSP technology is becoming an important method for increasing fatigue life of components in modern aircraft engines. LSP has also been successfully used to enhance the performance of other materials and structures resulting in increased fatigue life, reduced fretting fatigue damage, improved resistance to corrosion and increased resistance to foreign object damage (FOD) (**lauer06**; Tenaglia

and Lahrman 2003; Liu 2008)

3.1   Residual stresses depth

Figure 3.1 shows an example of the deep compressive stress profiles achieved using LSP in AA7075 compared with the shallower profile when conventional mechanical shot peening was used (Peyre et al. 1996). Consequently, it may be hypothesized that if a fatigue crack nucleates at or near the surface in an LSP treated component, its growth would be retarded and fatigue life substantially increased due to the deeper compressive residual stress.
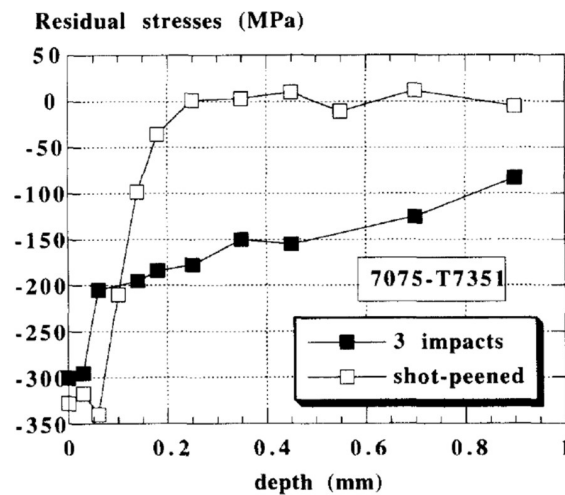
Figure 3.1: *Mechanical effects induced by LSP and SP: comparison of the residual stress fields induced in 7075 (LSP: 3 impacts, 4 GW/cm^2). (Peyre et al. 1996)*

In addition, the magnitude and depth of the residual stresses increase with laser power density. For example, for Ti-6Al-4V, three different laser power densities were applied to one surface of a 19 mm thick specimen. The compressive stress on the surface increased with increasing laser power density from about -100 MPa for the low intensity to about -650 MPa for the high density (fig. 3.2). The lowest power density produced compressive residual stresses near the surface only, whereas at higher densities, the residual stresses extended deeper below the surface and the magnitude of the stress increased as well. The deepest compressive stresses were achieved at the highest laser power density (Liu 2008).
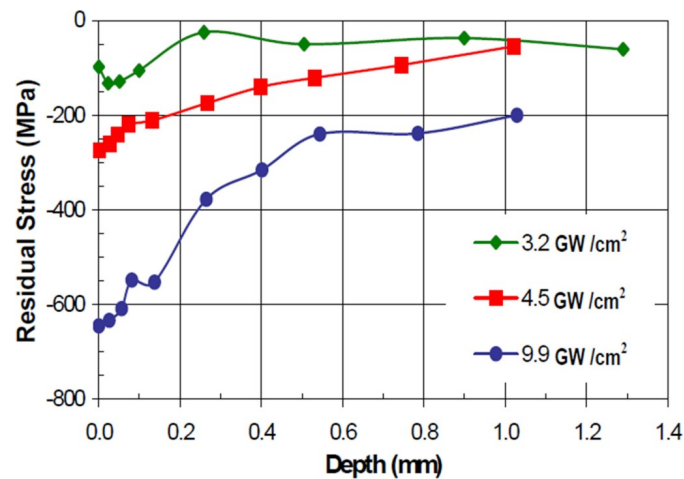
Figure 3.2: *Residual stress profiles as a function of depth for different laser power densities in Ti-6Al-4V. (Liu 2008)*

3.2   Thermal stability of the residual stresses

One of benefits is that LSP provides improved stability of residual stresses at elevated temperatures due to its lower cold work impact compared to conventional shot peening. Figure 3-3 shows the thermal effect on the relaxation of residual stresses by LSP for titanium alloy Ti-8Al-1V-1Mo (Lykins, Prevey, and Mason 1995). After four hours exposure, no relaxation of the residual stress was observed. Similar results were also obtained for other types of materials, such as INCONEL 718 and Ti-6Al-4V.
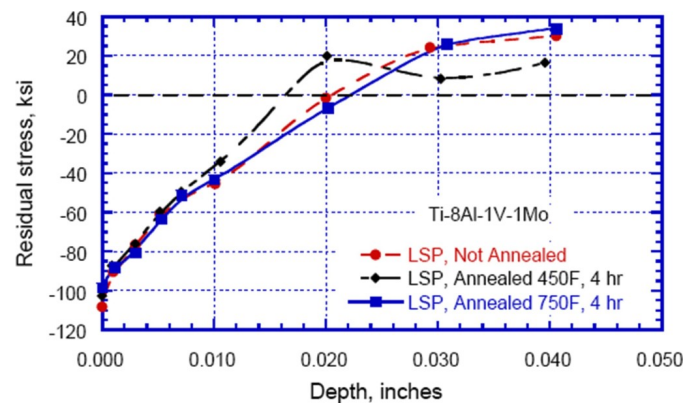

Figure 3.3: *Thermal relaxation of in-depth residual stress profiles after annealing Ti-8Al-1V-1Mo for 4 hours at elevated temperature. (Lykins, Prevey, and Mason 1995)*

3.3   Fatigue life extension

As mentioned above and as will be widely discussed in the following parts, LSP induces significantly deeper residual compressive stresses compared to conventional SP. This additional depth provides increased protection against surface-related damage such as fatigue cracks and corrosion. In other words, the surface of a material treated by LSP shows better fatigue performance than the same material treated using conventional SP. Figure 3.4 compares the fatigue properties of AA7075-T7351 specimens subject to LSP and SP treatment with those of unpeened specimens (Liu 2008). The notched fatigue specimens were tested in 3-point bending, using test conditions of $R = 0.1$ and $K_t = 1.68$. The experimental results show that the typical fatigue life of LSP parts were about $30 - 50\%$ longer than the one of untreated cases.
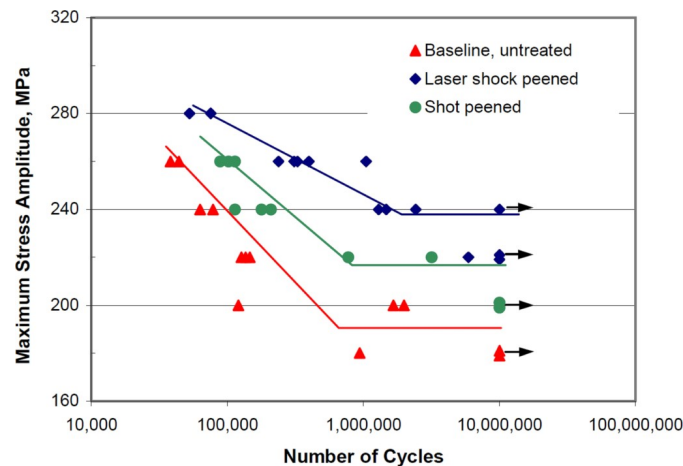
Figure 3.4: *Comparison of fatigue properties for AA7075-T7351 untreated, LSP and SP specimens using the 3-point bending method, R=0.1, $K_t = 1.68$, 3.8 GW/cm² (data points with arrows indicate tests halted with no failure). (Peyre et al. 1996)*

LSP has also been shown to be very effective in reducing foreign object damage (FOD), which occurs in engine turbine blades. In an investigation on F101 aircraft engine fan blades, LSP and different SP treatments were applied on the blades. The fatigue results are shown in fig. 3.5. The baseline, undamaged blade failed at 552 MPa (80 ksi) after 10^6 cycles. The electric discharge machine (EDM) notched, untreated blades failed at 138 MPa (20 ksi) to 207 MPa (30 ksi). The average failure stress for the EDM notched, dual intensity shot peened blades was

242 MPa (35 ksi), and for the (notched) high intensity peened blades, 311 MPa (45 ksi). By comparison, the failure stress of the chisel notched, laser shock peened blades averaged about 690 MPa (100 ksi), and well above the failure stress of the undamaged blades with dual intensity shot peened treatment. The failure stress of the laser shock peened blades containing an EDM notch was at about the same level as the undamaged blades.
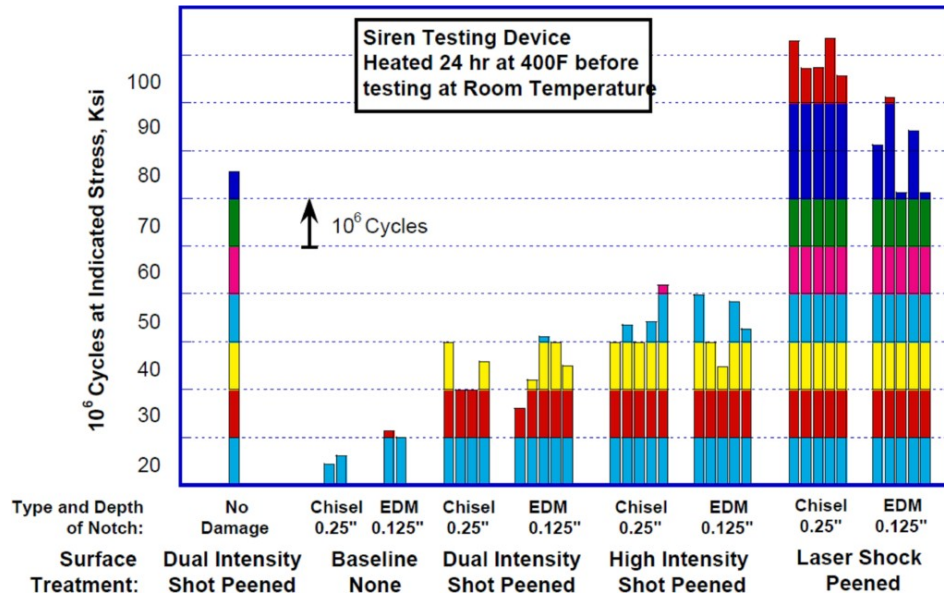

Figure 3.5: *Effects of laser peen and shot peen processing on the leading edge of F101-GE-102 fan blades. (Liu 2008)*

3.4   Corrosion resistance

Although there are only limited studies available, some LSP treated materials have shown increased resistance to corrosion and stress corrosion cracking (SCC). The results of corrosion tests on AA2024-T351 aluminum alloy showed anodic current density shifts after LSP, indicating enhancement of pitting resistance for both initiation and propagation (Peyre et al. 2000). The results also showed a reduction of passive current density on the LSP treated surface, indicating an increase in corrosion resistance. In the same test campaign, the LSP treated AISI 316 steel samples have been immersed 24 hours in $MgCl_2$ 44% boiling solution

at 153°C. Metallographic observations showed that LSP completely inhibits SCC and prevents macrocracking, except on very local zones where small surface crack develop.

Another group, conducted by Shepard ("Applications and future trends in US Air Force Service"), reported that LSP substantially increased the resistance to SCC of one inch thick welded 316 stainless steel as measured in a bath of 40% solution of $MgCl_2$ at 160°C. No cracks were observed at the LSP treated area after a week of exposure, but cracks occurred in the non-LSP treated area after only 24 hours of exposure, as shown in figure 3.6.
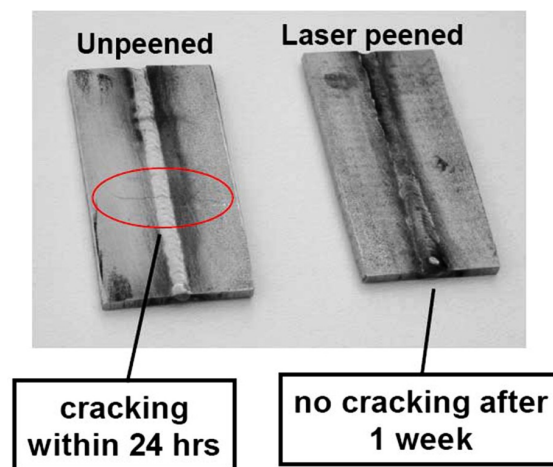

Figure 3.6: *Comparison of un-peened and LSP treated, 316 stainless specimens containing welds. (Liu 2008)*
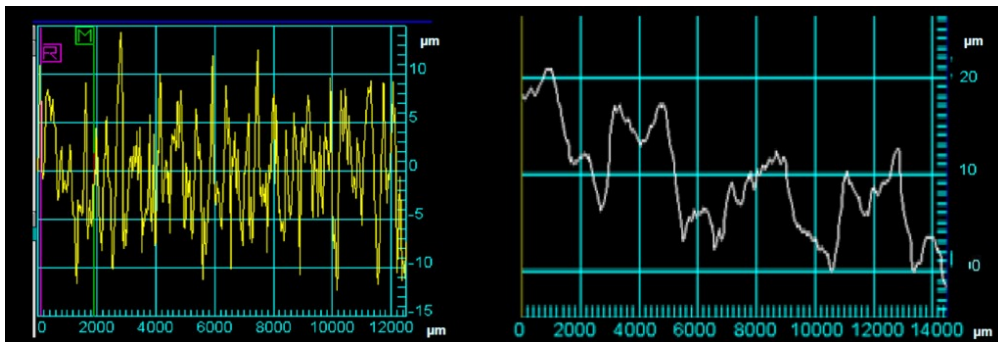
3.5 Surface finish

LSP normally causes very little indentation damage to the treated surface. The depth of any indentation decreases with laser power density. Typically, for soft materials such as aluminum alloys, the depth of any damage is about $10 - 25$ μm; on machined surfaces of harder alloys (such as steels) it is difficult to see where the surface was laser shocked, thus the damage is negligible.

Studies carried out in EADS - Innovation Works on Al 7050 samples reveal that roughness profiles of LSP treated surfaces are rather wavy, no sharp edges
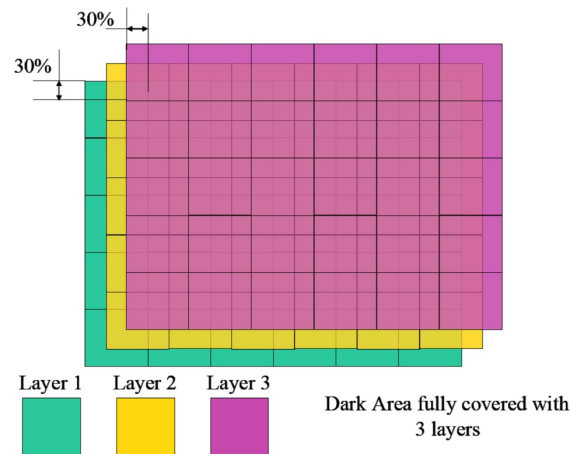
Figure 3.7: *LSP patterns with 30% offset in both directions studied by EADS.*

are generated which create a notch effect . The maximum roughness of a shot peened surface is comparable with the roughness of the LSP specimen, but the shot peened surface appears as a rather sharp profile. The comparison of the new LSP pattern with a 30% diagonal offset (see fig. 3.7) to the initial pattern with 50% horizontal offset reveals an improved surface quality. In fig. 3.8 is shown a comparison between the surface roughness of a conventional shot peening treated surface and an LSP treated surface.

Figure 3.8: *Comparison of the surface finish after Shot Peening and Laser Shot Peening. (Heckenberger et al. 2010)*

3.6   Complex geometries and accessibility

LSP is able to treat mechanical parts even when access to the treated surface is limited or impossible with conventional mechanical treatments (e.g., shot peening). This is allowed by different beam delivery strategies available for the laser peening application (Dane et al. 2011b).
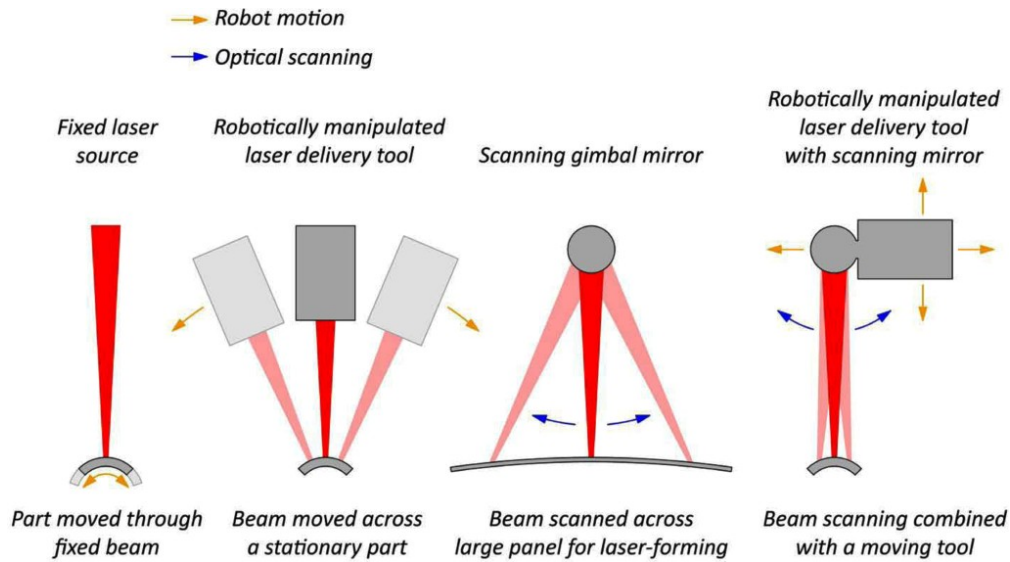
Figure 3.9: *Beam delivery strategy must be matched to the laser peening application. (Dane et al. 2011b)*

With LSP, treating just the fatigue critical area(s) (or more generally specific areas) on a part without masking the area around it is easily accomplished. This enables localized treatment around holes, and in and along notches, keyways, fillets, splines, welds and other highly stressed regions.

Moreover, LSP can accomplish to particular geometries (e.g., notches) thanks to the correction of the single spots for size, rotation and aspect (fig. 3.10).
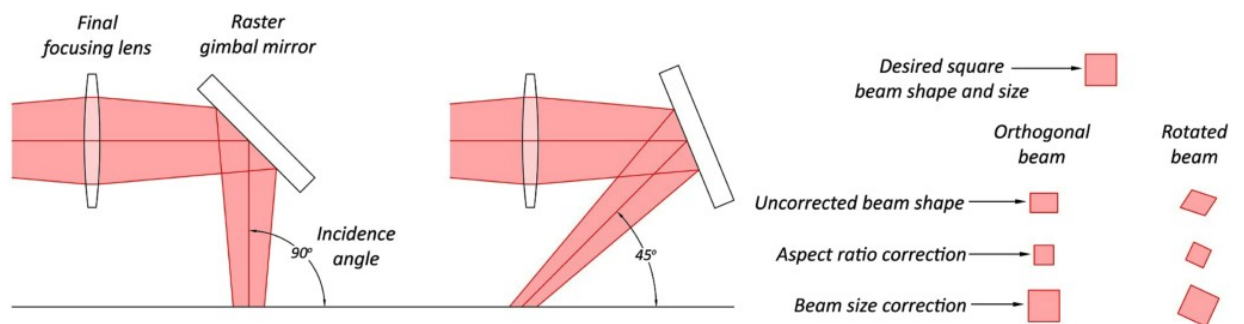
Figure 3.10: *MIC technology: each pulse is individually corrected for size, rotation, and aspect. (Dane et al. 2011b)*

Chapter 4

Limitations of the technology

Although LSP has been used successfully on conventional titanium alloys, Ni-based super-alloys, steels and aluminum alloys, the high cost of laser facilities and their operation, combined with the relatively slow repeat rate of the process and immobile nature of the application facility prevent its wide application in practice. For example, the laser pulse repeat rate is normally only 0.25 to $0.5Hz$ for currently available laser peening systems. Consequently, part treatment costs are relatively high.

Recently, this situation has been greatly improved, with robust, production-ready laser peening systems with higher efficiency becoming available. One example is the Lawrence Livermore National Laboratory (LLNL) and Metal Improvement Company (MIC) developed Lasershot$^{\text{sm}}$ Peening system. This system can produce laser pulses at a rate of 10 $\sim$ 20 times faster ($\sim$ 5 Hz) than previously available laser systems. LSP Technologies in the USA has also developed similar a laser system with a high repeat rate known as the LaserPeen® system. Advances in processing technology for automating the application of LSP and removal of process overlay coatings (such as RapidCoater$^{\text{TM}}$ system) have also reduced the cost of using the technology (LSP Technologies; Tenaglia and Lahrman 2003).

An LSP facility requires a relatively large working space, typically 1.5 by 2 m (Dane et al. 2000), making it difficult to carry out either on-site or in-situ treatments. This shortcoming has been overcome by a mobile laser peening system at MIC for large stationary parts, allowing application of LSP on site, as shown
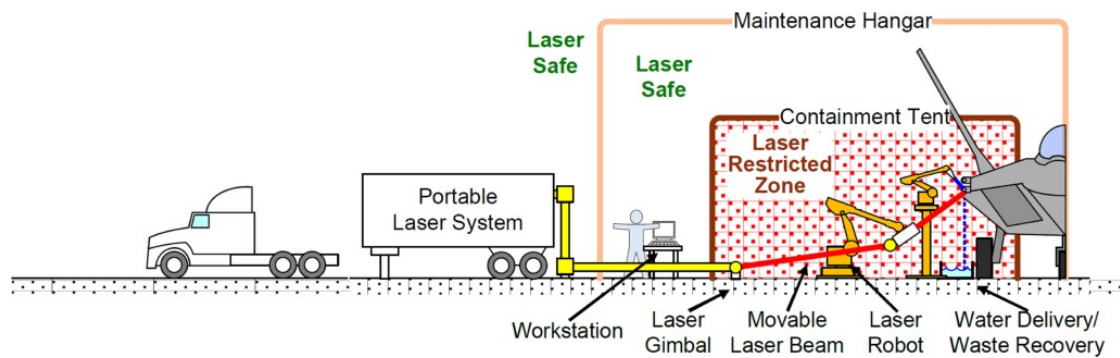
Figure 4.1: *Schematic of the mobile LSP device. (Jensen 2010)*

in figure 4.1.

Moreover, being the pressure related to the square root of the laser intensity, the compressive residual stresses induced by the LSP are limited by the dielectric breakdown of the confining medium, which imposes a laser intensity threshold beyond the latter no more energy can be transfered from the laser to the surface.

Chapter 5

Suitable applications

LSP potentially has broad applications for Defense, aerospace or related industries such as for the treatment of turbine blades and disks, rotating shafts and gears. This technology can also be used on airframe structures including skins and fastener holes.

5.1 Life enhancement of engine blades

Implementation of LSP on components such as turbine engine airfoils significantly reduced maintenance costs, improved the reliability of aircraft engines, and improved the operational availability of combat aircraft. In addition, aircraft crew safety and mission readiness have been vastly enhanced. For the US Air Force (USAF), the application of laser peening to the engine blades of the B-1B Lancer, F-16 Falcon, and F-22 Raptor has already avoided over $US59 million in costs through reduced turbine engine airfoil failures, blade replacement costs, and reduced secondary damage repair costs.

The production implementation of LSP and resultant savings to the USAF represent only the initial benefits of this technology. LSP is being evaluated for a number of other US Department of Defense (DoD) weapons system applications such as transmission gears in the CH-47 helicopter, turbine engine blades in tanks and other ground vehicles, and aircraft landing gear components.

The application of LSP to resolve the FOD tolerance problem on F119 4th

stage integrally bladed rotors (IBR) will avoid a redesign effort, while preventing a potential delay in the introduction of a full flight envelope qualified F119 engine to the fleet (F/A-22 Raptor) - a major benefit to the combat aircraft. Figure 5.1 shows that the fatigue life of F119 IBR airfoils after LSP treatment is greatly increased. Compared to the previous state-of-the-art, reductions in processing costs associated with this program will result in savings of more than \$US 10M dollars for the 4th stage IBR alone, over the entire F-22 engine delivery program (738 engines). LSP surface treatment will also reduce the maintenance cost per flight hour and increase mission readiness for the F/A-22 Raptor by decreasing the frequency of required maintenance inspections on this IBR by 30 to 50 percent. Overall, the potential savings using LSP have been estimated to approach US\$1 billion when calculating the impact over all engines in the Air Force inventory (Tenaglia and Lahrman 2003).
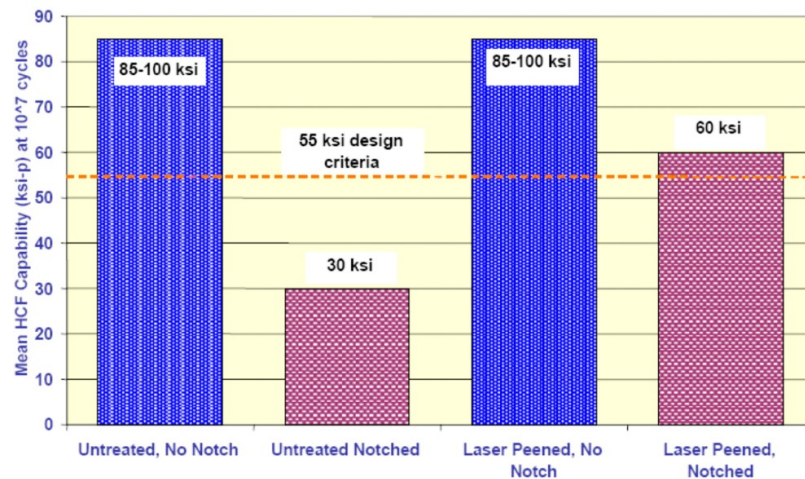
Figure 5.1: *Effect of laser peening on F119 IBR fatigue lives at both notched and unnotched cases*

5.2 Enhancement of resistance to FOD

Components treated by LSP have been shown to have higher resistance to FOD. An investigation by GE Aircraft Engines (GEAE) showed significant improvements in high cycle fatigue performance. For example, FOD damage to F101-GE-102

aircraft gas turbine engine fan blades could reduce the fatigue strength from about 517 MPa to less than 138 MPa, which was less than half the design requirement. However, LSP treatment restored blade fatigue strength to between 517 MPa and 690 MPa. In addition, the sensitivity to FOD defects up to 6.35 mm in F101 blades was virtually eliminated (Tenaglia and Lahrman 2003). Consequently, GEAE and the USAF see LSP as a potential solution to increase the durability of titanium fan blades and decreasing sensitivity to FOD.

5.3   High cycle fatigue life extension

When the areas around holes in sheet materials are laser shock peened with a solid spot around a hole, the crack tends to initiate on the hole surface at mid-thickness, and then tunnels down the mid-thickness of the sheet between the compressive surface layers before it breaks through to the surface beyond the laser shocked region. While the crack propagation rate is slowed considerably by this behavior, (fig. 5.2, solid spot), and fatigue life is significantly increased, the crack itself is not easily detected. This is sometimes a concern in failure-sensitive applications. (Clauer 1996)
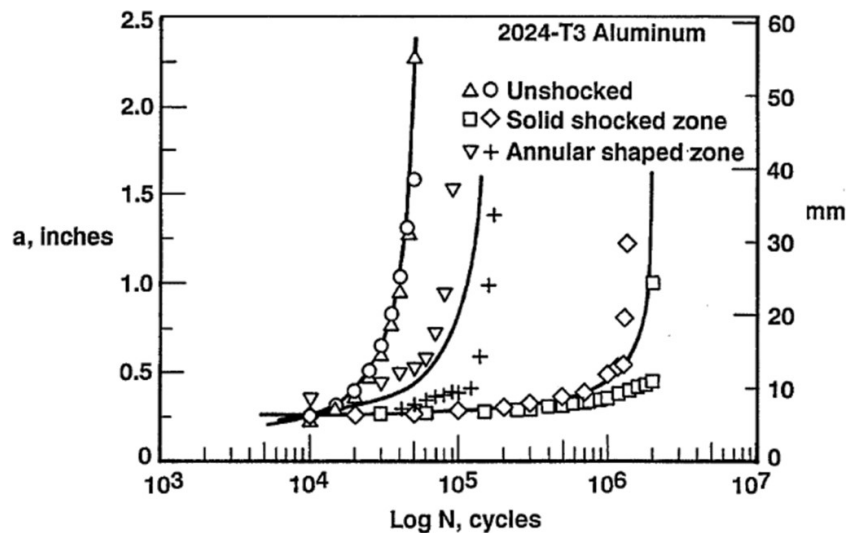

Figure 5.2: *Fatigue crack propagation in non-shocked and laser shock peened 2024-T351 aluminum at a stress amplitude of 103 MPa. The crack length a is shown vs. the number of cycles N. (Clauer 1996)*

The annular spot was chosen to demonstrate that a crack could be initiated and detected at a fastener hole, and then be significantly slowed when it reaches the laser shocked region. This would allow ample time for the detection and monitoring of cracks originating from holes before failure.

LSP is also effective in arresting pre-existing cracks. Large 2024-T351 aluminum specimens similar to that described above were pre-fatigued to create cracks 0.5 mm long, coming out each side of the fastener hole. The region ahead of each crack was then laser shock peened, and the specimens re-tested in tensile fatigue, $R = 0.1$, at 103 MPa maximum stress amplitude. The results are shown in fig. 5.3.1. The unshocked condition had a fatigue life of about 145 000 cycles, and the laser shocked condition without a pre-crack had lives of 700 000 to 1 000 000 cycles. After pre-cracking and laser shocking, the fatigue lives were in the same range as those of the laser shocked material tested without a pre-crack.

The fatigue life of weldments can also be extended by LSP. Plates of 5456 aluminum alloy 6.3 mm thick were butt-welded together, the weld bead machined off and the weld and heat-affected-zones laser shocked with overlapping spots. Test specimens machined from this plate were then tested in tensile fatigue, $R = 0$, in both the as-welded and laser shock peened conditions (fig. 5.3.2). At a stress amplitude of 138 MPa, the fatigue life was increased by at least an order of magnitude. More significantly, at 158 MPa the fatigue life was increased from less than 50 000 cycles to more than 3 to 6 million cycles without failure after LSP. The fatigue strength, in the non-shocked condition was about 116 MPa.

Laser shock peening is also effective against fretting fatigue. Dog-bone specimens and pads of 7075-T6 aluminum were laser treated around a simulated fastener hole in each piece, then fastened together through the hole with a manufactured (CSK) fastener. This combination was then fatigue tested in tension at $R = 0.1$. The stress differential between the larger cross-section of the pad and the smaller cross-section of the dog-bone created an elongation differential between the two pieces during each cycle, leading to fretting around the fastener hole. The results are shown in fig. 5.4. The tests were initially conducted at 96 MPa. When a long life was reached, the stress was raised in 10% increments until failure occurred within few hundred thousand cycles. Even at 113 MPa, the fretting fatigue life is increased by LSP.
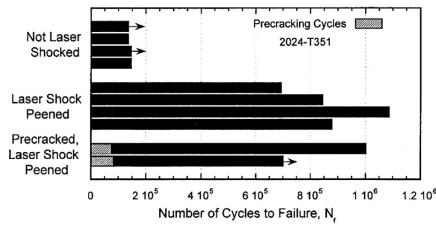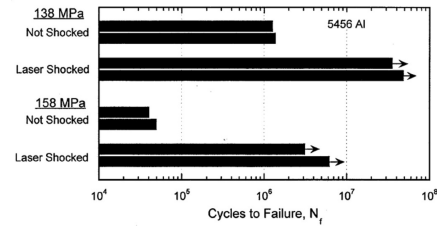
5.3.1   **5.3.2**

Figure 5.3:
*5.3.1: The effect of laser shock peening on fatigue life of precracked specimens of
2024-T351 aluminum tested at a stress amplitude of 103 MPa.
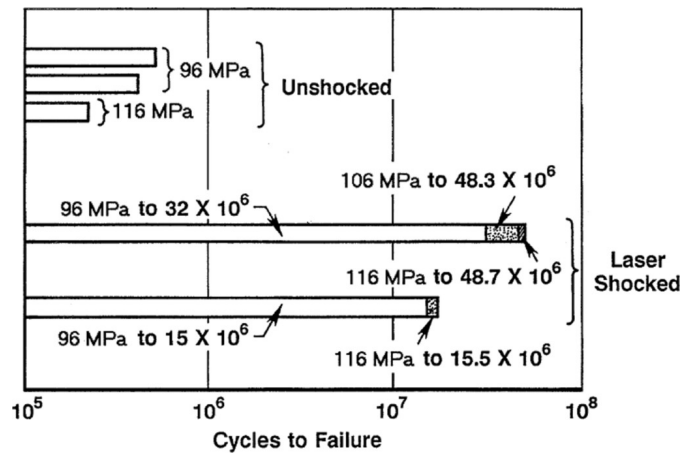5.3.2: Fatigue life increased in welded 5456 aluminum after laser shock peening.
(Clauer 1996)*

Figure 5.4: *Increased resistance to fretting fatigue around fastener holes after laser
shock peening 7075-T6 aluminum. (Clauer 1996)*

# 5.4   Other potential and emerging applications

Much progress has been made at decreasing the cost and increasing the through-
put of laser peening, making the process affordable for many new applications.
Further progress is expected as production applications of laser peening expand.
Numerous applications are under development or are good candidates for improve-
ment using this technology. In addition to engine components for the Air Force, nu-
merous applications for airframe structures exist, including (Tenaglia and Lahrman
2003):

- fatigue-critical components such as F-16 bulkheads, wing attachments, flight control mechanisms, wheels, brakes, landing gear;

- welded titanium and aluminum components for improved reliability;

- welded aging aircraft parts for improved reliability;

- fasteners and fastener holes to combat fatigue, fretting fatigue and stress corrosion cracking;

- cost-effective, high reliability castings to replace forgings;

- mobile laser peening for deployment at repair depots for treatment of large structures and detection of exfoliation corrosion.

In addition to the application of LSP in military aircraft discussed above, the technique can be used to improve SCC and crevice corrosion resistance in submarine and surface vessels. Other candidates include fatigue prone catapult and tail-hook arrest mechanisms on aircraft carriers (Liu 2008).

LSP is generally envisaged for high-cost, fully localized mechanical parts, whereas SP can be used on larger parts with a smaller cost. In this context, preliminary studies were performed to investigate the combination of the two treatments. Figure 5.5 shows that laser shocking a pre-shot-peened zone combines and enhances the advantages of the two treatments with both in-depth and superficial RS increases. Therefore SP beneficial effects are preserved (hardening) or increased (RS field) by LSP treatment. Further fatigue studies should provide interesting information on the mechanical improvements generated by SP+LSP treatment which seems to be a very promising process.

In addition to laser shock peening, there are potential uses in a variety of applications having nothing to do with fatigue, but instead based on the localized strain hardening or shock impact characteristics of the process. For example, localized surface plastic strain induced by shock impact could enhance diffusion bonding of small components, or similarly, a coating. The shock wave may be used to locally densify porous coatings, or to compact powders in unique situations. It may also be useful in unique metal forming operations or connector attachments (Clauer 1996).
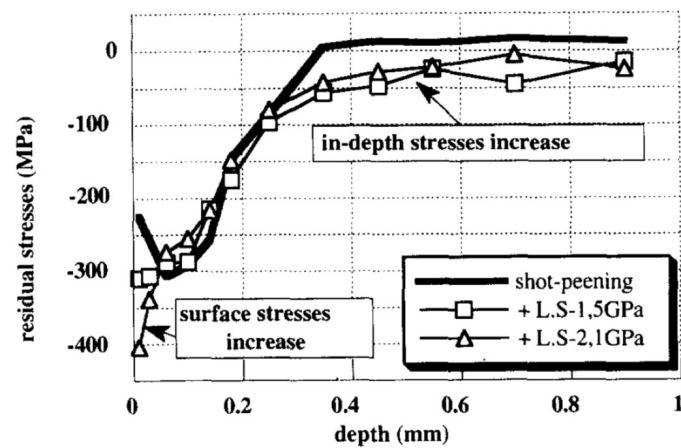
Figure 5.5: *Residual stresses induced by a combination of shot peening and laser shock treatment on 7075 alloy. (Peyre et al. 1996)*

5.4.1   Eligible materials

Many metallic materials has been successfully LSP treated: steels, aluminum alloys (especially from 2xxx and 7xxx series), titanium alloys, nickel-base superalloys, cast irons and powder metallurgy iron alloy.

Chapter 6

Cost/Benefits of the Laser Shock Peening technology

The key benefit in application of LSP is the potential for significant increase in fatigue life of the treated aircraft components. Consequently, LSP technology can be applied in fatigue, fretting or FOD prone locations, or surfaces to improve material performance in service. Worldwide experience shows that the laser shock peening process is a reliable and effective technology for life extension and enhancement of engine components such as turbine blades and other aircraft components. DSTO research has also showed that LSP is an effective life extension/enhancement technology for airframe materials such as AA7xxx series aluminum alloys, provided the process parameters are optimized. However, some technology-related risks were also identified in this research program.

The assessment of the cost/benefit of life extension using LSP is complex and should be performed on a case-by-case basis. Generally, the cost benefit analysis must take into account:

- the life extension achieved;

- the performance improvement obtained;

- the cost of repair, compared with the cost and the availability of a new part;

- the capital investment in equipment; and,

- the training of personnel.

However, due to lack of specific cost information for LSP processing (including capital and running costs) from open literature and other sources, a comprehensive analysis of the cost benefits using LSP cannot be carried out. Therefore, in this section, only the preliminary study of the cost benefit of LSP technology for application to aircraft components is considered.

6.1   Main cost drivers

6.1.1   Capital investment

There is no direct information concerning the cost of LSP equipment available from accessible public sources. The cost of that equipment was estimated by Liu (2008) to be about AUD\$ 250 000. The repeat rate and laser power were very low and the equipment was more than 10 years old. Currently, the cost for a typical LSP treatment plant is estimated to be more than 1 million US dollars as in the case of LSP Technologies, USA.

6.1.2   Running costs

No information is available concerning running costs from public sources. The operating cost would probably be around AUD \$ 30 000 $\sim$ 50 000 per annum, which includes optics, flash-lamps, electricity, etc.

6.1.3   Training cost

Skills and safety training of the operator of the LSP equipment would be mandatory to meet the ANSI laser safety standards and operator training requirements. The cost of the training might only be a small percentage of the total cost of the facility. Once training is completed, it may no longer be needed for a particular laser facility, unless new equipment or technology is acquired, or new staff is engaged.

6.1.4   Process optimization

As for other peening procedures, LSP process must be optimized for each application. For example, the laser intensity must be optimized for each material and the number of layers must be selected according to the geometry and material. Before each new application, several tests must be carried on in order to compare the influences of the laser parameters on the residual stress field in the component.[1]

6.1.5   Additional costs

In addition to capital costs, on-going maintenance and repair will be required to the facility and equipment. That may require parts or components to transport off-site, or, for on-site repairs, parts, equipment and personnel would need to be transported to the site. These costs will depend on proximity of the LSP facility to repair facilitators.

6.1.6   Local technology availability

Local accessibility can certainly greatly affect the cost benefit. Currently, LSP facilities are limited in number: only few companies (e.g. LSP technologies, MIC, USA) or agencies (LLNL, USA) have such facilities at their disposal. Inaccessibility of the technology locally is a major barrier to cost-effective implementation. The MIC laser facilities around the world are shown in figure 6.1

6.2   Potential cost savings

6.2.1   New LSP systems

In order to increase the throughput and reduce the cost of the process, several new technologies were developed and implemented into production by major organisations specializing in LSP technology. A laser machine with high efficiency

---

[1]Before the test campaign exposed in part III, a previous test campaign aimed to state the best laser parameters combination for the specific application.
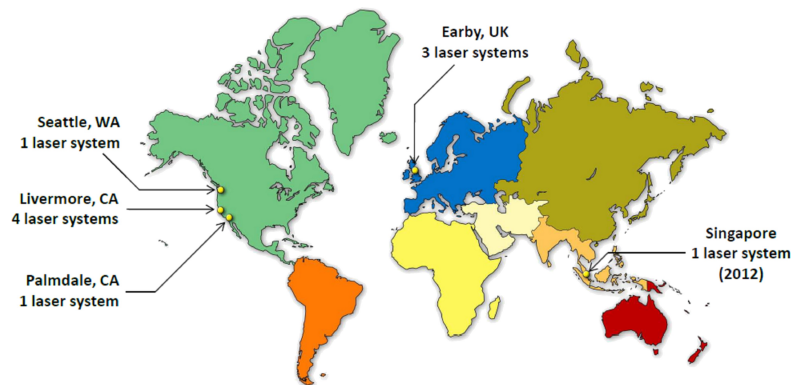
Figure 6.1: *MIC Laser facilities around the world. (Dane et al. 2011a)*

and repetition rate (e.g.: high frequency) will generally reduce the total cost of LSP processing. The Lawrence Livermore National Laboratory (LLNL), USA, has developed a new laser system, which can produce pulses at a rate of $10 \sim 20$ times faster (5 Hz) than comparable systems. The system can peen about one square meter of metal per hour. LSP Technologies has also developed a new system (LaserPeen®), which uses a four-beam laser arrangement. While having a nominally similar capital investment, the higher repetition rate of these new systems means a reduction in cost-per-part treated.

Another new system, called the RapidCoater$^{\text{TM}}$ system, was developed by LSPT Technologies, which allows continuous processing of the overlay coating. As mentioned, in traditional laser peening, the black paint used as an opaque overlay coating needs to be applied to a part before laser peening. Normally, the overlay coating has to be re-applied manually many times during processing of the part. This is labour-intensive, particularly for complex parts, reducing the cost effectiveness of the process. The RapidCoater$^{\text{TM}}$ system can greatly increase the efficiency of the process. It is claimed that use of this system can reduce the cost of laser peening by $30 \sim 40\%$ and increase the process throughput by $4 \sim 6$ times compared to conventional laser peening, as shown in table 6.1.

6.2.2   Laser Shock Peening Manufacturing Cell - LSPMC

LSP Technologies has commissioned the ManTech Laser Shock Peening Manufacturing Cell (LSPMC) for the USAF. The LSPMC uses the latest generation of

Technologies	Increase of throughput[1]	Cost Reduction	Developed by
RapidCoater™	$4 \sim 6$ times	$30 \sim 40\%$	LSPT[3]
LSPMC[2] with RapidCoater™	$6 \sim 9$ times	$50 \sim 75\%$	LSPT[3]
LaserPeen[sm]	~ 10 times (5Hz)	N/A	MIC[4] & LLNL[5]

Table 6.1: *Technologies for increasing the throughput and reducing the cost in LSP process.*
Notes:
(1) Compared to conventional laser peening;
(2) LSPMC stands for LSP manufacturing cell, which was commissioned to USAF;
(3) LST is LSP Technologies, Inc., USA;
(4) MIC is Metal Improvement Company, USA;
(5) LLNL is Lawrence Livermore National Laboratory.

laser peening system using a 125 Watt laser. It uses a laser beam spot diameter of 5.6 mm, which allows processing at a rate of 4 square inches per minute. The LSPMC combined with the RapidCoater™ system reduced the cost of laser peening by $50 \sim 75\%$ compared to conventional LSP systems. For example, for F119 integrally bladed rotors (IBRs), the process increased throughput by $6 \sim 9$ times (see table 6.1).

6.2.3   Lasershot[sm] peening

The Metal Improvement Company (MIC) and the LLNL have developed a new technique for improving the mechanical properties of metallic materials used in the aerospace industry. The technique, known as Lasershot[sm] peening, uses LLNL's solid state laser and can produce laser densities up to $\sim 200 \text{J/cm}^2$ at $0.25 \sim 10\text{Hz}$ with a pulse duration of $10 \sim 100$ ns. In 2002, a new version of this laser system was implemented with robotic parts handling. The rate of LSP coverage was higher than $100 \text{ in}^2/\text{h}$. It was found that jet engine fan blades treated by this system had their service life extended by a factor of three to five times. This laser shock peening system is currently in-service at a US Navy facility at the Kennedy Space Centre, Cape Canaveral, Florida and a second system is used at the USAF Phillips Laboratory, Albuquerque, New Mexico.

Part III

Experimental activities

During a six months internship by EADS - Innovation Works (Ottobrunn, Germany), the author carried out an experimental activity on Laser Shock Peening treated samples representative of actual components of an aircraft structure. This test campaign aimed to evaluate the Laser Shock Peening treatment applied on thick components, and in detail on some critical areas of the airframe structure.

In this part, the above mentioned test campaign will be presented. In the chapter 7 are summarized the experimental conditions, the specimens' geometry, the material, the surface treatments and the test apparatus and will be exposed the matrix of tests. In the chapter 8 will be presented the test results and the anomalous data will be remarked.

Chapter 7

Experimental conditions

During this campaign two different kinds of specimen have been used: the IW-MS DF19d (fig. 7.1.1) and the IW-MS DF20f (fig. 7.1.2). From now on, they will be called as the *Step* specimen and *Single Edge Notch* (SEN) specimen respectively. With both kinds of samples two kinds of test have been carried out: High Cycle Fatigue tests (HCF) and Crack Propagation tests (CP).

7.1.1   **7.1.2**
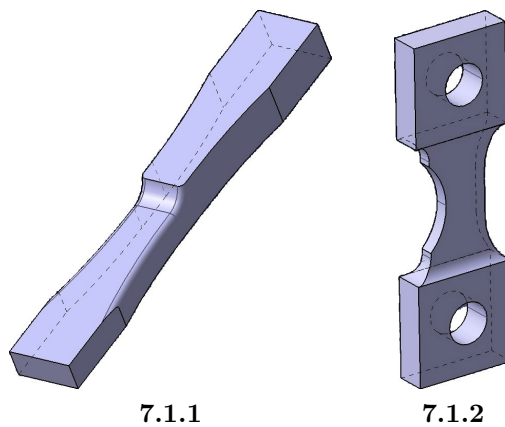
Figure 7.1: *The two specimens used during the test campaign: the IW-MS DF19d (Step specimen, 7.1.1) and the IW-MS DF20f (Single Edge Notch specimen, 7.1.2).*

7.1   Material

The specimens were manufactured from a 64 mm thick AA7050 T7451 plate produced by Alcan, according to aerospace specifications. The data about the chemical composition and the mechanical properties are provided by the supplier via inspection certificate and are summarized in tables 7.1 and 7.2. The data were not verified by EADS-IW measurements.

Si [%]	**Fe** [%]	**Cu** [%]	**Mn** [%]	**Mg** [%]	**Cr** [ppm]	**Ni** [ppm]	**Zn** [%]	**Ti** [%]	**Zr** [%]
0.04	0.09	2.1	0.01	2.2	60	53	6.2	0.02	0.11

Table 7.1: *Chemical composition of parent material.*

	Mechanical data			
	UTS [MPa]	**YTS [MPa]**	**A [%]**	K_{IC} **[MPa m$^{1/2}$]**
L	12	446	13	40.1
ST	506	445	7.6	28.8
LT	515	447	10	30.7

Table 7.2: *Mechanical data of parent material as delivered.*

In order to simulate a real/realistic application, the longitudinal lamination direction of the plate does not correspond to the load direction of the specimen: in fact the load direction of the specimen corresponds to the long transverse direction of the plate, the width of the specimens is in the thickness of the plate and the thickness of the specimens is in the longitudinal direction, see figure 7.2.

Figure 7.2: *Lamination directions in the specimens.*

7.2   Geometry

The Laser Shock Peening can be effectively applied in locations which might be highly stressed and/or difficult to reach for reparations . Both specimens involved in this test campaign are then representative of fatigue prone locations on aircraft box structures. The final geometries have been selected between several configurations, which have been analyzed by FEM analyses, by comparison with actual components of civil aircrafts. In order to simulate those components, the geometry of the specimen has been especially designed; in detail, for the Step specimen the similarity parameters were the normalized peak stress (or concentration factor, $K_t = 1.9$) and the stress gradient in a 10 mm thick layer underneath the notch and for the SEN specimen the $K_t = 2$ and the thickness. The testing machine limit capabilities (see sec. 7.4) were also held in account. The complete specimens' geometry is described in figure 7.3.

In both cases, the important feature that leads to this particular stress distribution is the secondary bending due to the load eccentricity. A first level analysis of the effects of the load eccentricity on the Step specimen is presented in the following section; regarding the SEN specimen, this kind of analysis is completely inadequate, thus it is not mentioned.

7.2.1   First level analysis of the Step specimen's geometry

In order to have a preliminary analysis of the stress field in the specimen, the de Saint-Venant's theory and the Euler-Bernoulli technical theory of beams will be used. *This analysis will provide information about the average moments exchanged by specimen and clamping device*, being inadequate to describe the stress field in the notch region.

If one ideally cuts the specimen just before and just after the notch, it is possible to notice that there is a difference of the bending moment in the two sections, as shown in figure 7.4. Regarding the latter, it is possible to state

$$M_A = M_B + F \cdot b \Rightarrow \Delta M = F \cdot b$$

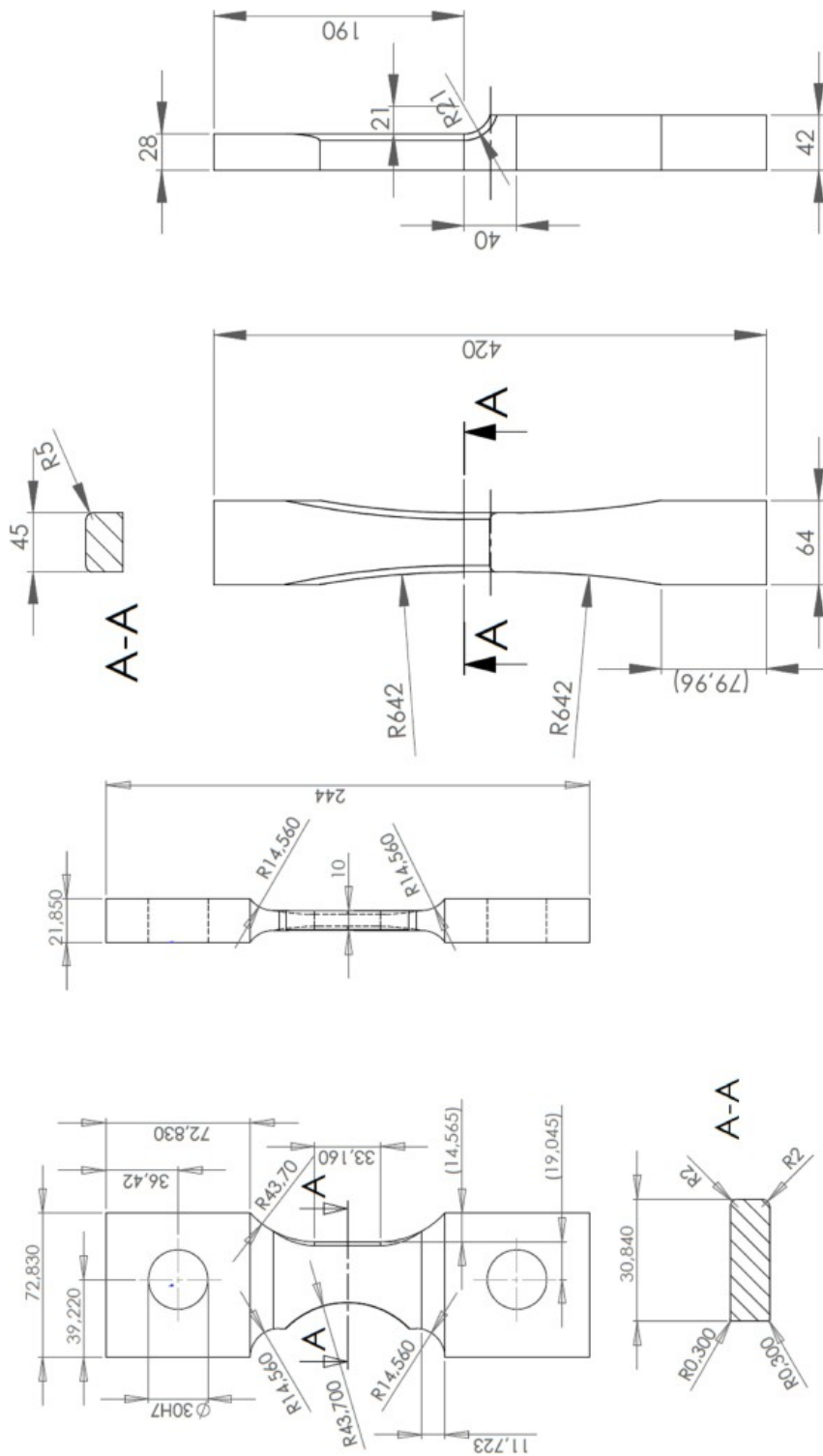According to the de Saint-Venant's principle, for the clamping areas this dif-

Figure 7.3: *Specimens' geometry: the SEN specimen on the left, the Step specimen on the right.*
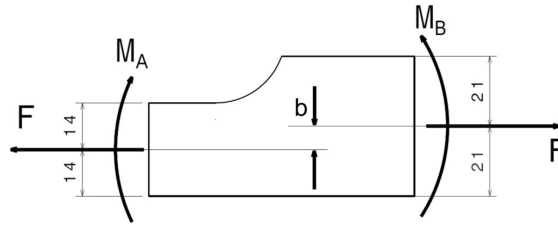
Figure 7.4: *Local equilibrium near the notch.*

ference in the bending moment is statically equivalent to a concentrated moment applied in the notch region. The system can be simplified by idealizing the extremity displacements and so the boundary conditions. The final system can be obtained by modifying the specimen and turning it into a 1D beam with two different flexural stiffnesses, EJ_A and EJ_B, as shown in figure 7.5. For the Step specimen's geometry it is proved that $EJ_A = 1.5^2 EJ_B$.
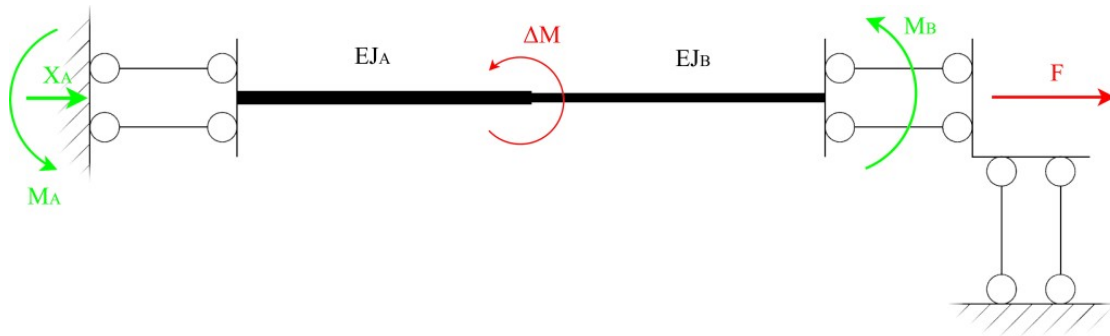
Figure 7.5: *Simplified system for a first degree stress analysis for the Step specimen.*

Splitting the problem into two sub-problems (figg. 7.6.1 and 7.6.2) and using the Superposition principle it is possible to affirm that

$$\mathcal{F}_e = \mathcal{F}_0 + x\mathcal{F}_1$$

where $\mathcal{F}_i$ is a dimension measured on the $i-$th system (e = actual, 0 = main, 1 = first auxiliary) and x is the elasticity constant defined by the Müller-Breslau's elasticity equation

$$\eta_1 = \eta_{10} + x\eta_{11}$$
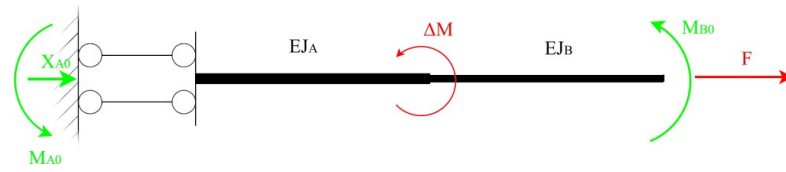
7.6.1: *Subsystems: main system*
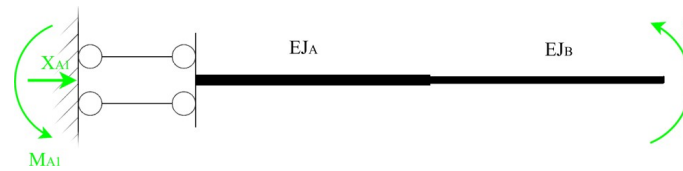
7.6.2: *Subsystems: first auxiliary system*

Carrying out the calculations one obtains

$$\eta_0 = 0$$

$$\eta_{10} = \frac{\Delta M l}{E J_A}$$

$$\eta_{11} = l \frac{E J_A + E J_B}{E J_A E J_B}$$

and solving for x one has

$$x = -\Delta M \frac{J_B}{J_A + J_B}$$

The bending moment in the two segments (A) and (B), representing the thick region and in the thin region respectively, can be now determined; it is plotted in figure 7.6.

$$M_A = \Delta M \frac{J_A}{J_A + J_B} \simeq 77\% F \cdot b$$

$$M_B = -\Delta M \frac{J_B}{J_A + J_B} \simeq 23\% F \cdot b$$

This way it is possible to state that the bending moment acts stretching the back side fibers in the thick segment. This is considered as one of the reasons of the unexpected failures occurred in the back side of the step specimens discussed in part IV.

As already said, this analysis is valid "far enough" from the notch, but this is a
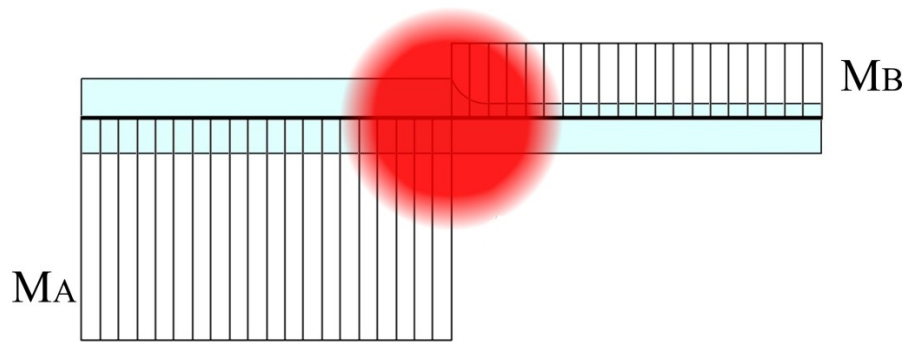
Figure 7.6: *Bending moment distribution along the specimen (first order approximation). In the red area the analysis is not accurate enough to describe the stress distribution.*

good estimation of the moment in the clamping devices. A FEM analyses is needed to know the stress field in proximity of the notch; such analyses are exposed in part IV.

7.3 Surface treatments

As will be exposed in detail in section 7.5, several surface conditions have been tested in order to compare the test results and have a general description of the influence of the surface treatments on the fatigue life. The surface treatments involved in this test campaign are summarized in the following paragraphs.

7.3.1 Chromic Acid Anodizing

The Chromic Acid Anodizing (CAA) is an electrolytic anodizing process in a chromic acid solution. The CAA process results in the electrochemical growth of an aluminum oxide/hydroxide layer by interaction of a clean aluminum surface with a chromic acid based immersion bath with an applied voltage between the parts and a suitable cathode. The oxide layer produced by the process has good corrosion resistance and wear resistance and provides better adhesion for paint primers and adhesives than bare aluminum does. Chromic acid anodizing produces thinner (0.5 μm to 18 μm), more opaque films that are softer, more ductile, and to a degree self-healing with respect to other anodizing methods. Still, the oxide film is far

brittler than the metal substrate.
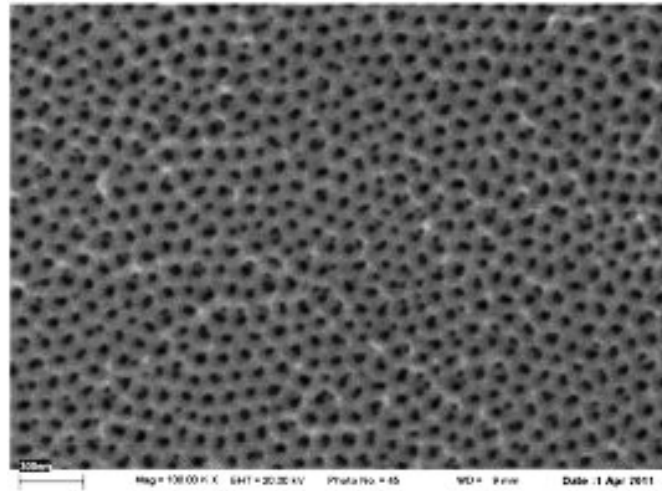
Figure 7.7: *SEM topographical image of the anodic aluminum oxide template obtained after the second anodization step, in a 0.3 M chromic acid for 3 h at 40 V and 298 K.* *(***meyre12***)*

As discussed in Lee, Jeong, and Kim 2012, anodizing has an intrinsically adverse effect on fatigue resistance, which is attributed directly to the brittle and porous nature of the oxide layer and tensile residual stress induced during the anodizing process. Because the anodizing layer is brittle compared with the aluminum substrate, it cracks easily under tensile cyclic stress, causing easy fatigue crack initiation. Moreover, the tensile residual stress developed internally on the anodizing surface reduces the resistance to fatigue by increasing the effective tensile stress.

Above all, the CAA in 7050 aluminum alloys give place to a pits formation caused by a "preferential etching" (a selective micro galvanic corrosion); those pits, formed during the exposure to pretreatment solution, usually form on grain boundaries. An example of these pits is shown in figure 7.8.

Previous studies carried out within EADS-IW confirm the results carried out by Lee, Jeong, and Kim (2012) and Camargo and Voorwald (2007): the CAA used in 7050 T7451 gives place to a pitting phenomenon due to the preferential etching on grain boundaries that results in multiple nucleation sites, dramatically reducing the fatigue life.
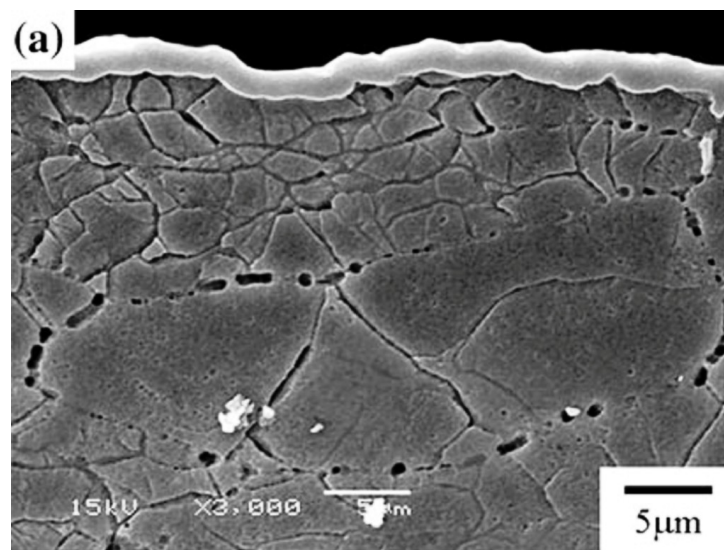
Figure 7.8: *SEM cross-sectional views of 7050-T7451 specimens with CAA anodized layer. (Lee, Jeong, and Kim 2012)*

For the specimens involved in this test campaign which have been CAA treated, the process has been carried out according to the Airbus specification AIPS 02-01-001 and all surfaces of both specimens have been anodized.

7.3.2   CAA removal

The CAA removal is the first step for every retrofit and repair procedure (cfr. section 7.5). The CAA removal is a surface grinding out that allows obtaining a virgin surface to rework (e.g., with peening). In the present case a 0.3 mm depth has been grinded out. Preceding analysis carried out by EADS-IW suggest that to be sure to remove all CAA generated pits a grinding out of about 100 μm would be required. There are evidences of the presence of these pits even after the 300 μm removal (cfr. section 8.3). The surfaces involved in this treatment are shown in figg. 7.9.1 and 7.9.2.[1]

---

[1]Indeed, all the following treatments on the SEN specimens have been applied in the surface shown in figure 7.9.2: Shot Peening, Laser Shock Peening, CAA removal and Alodine.
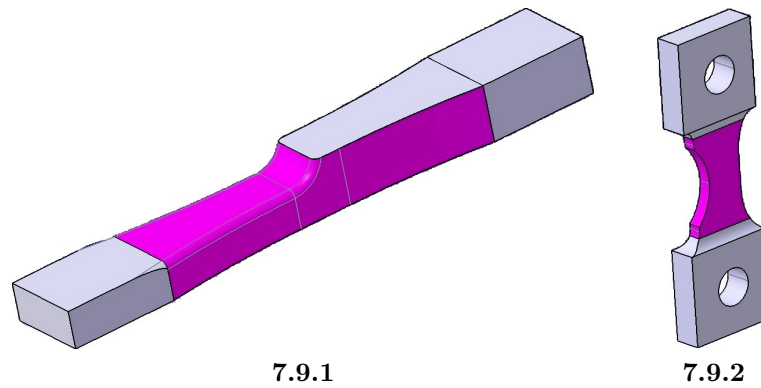
Figure 7.9: *Surface in which CAA removal has been applied.*

7.3.3   Shot Peening

The Shot Peening (SP) was carried out by the Metal Improvement Company (MIC), Unna. The MIC is a subsidiary of Curtiss-Wright Corporation. For the Step specimens the blasting agents were 0.6 mm diameter steel beads and the peening intensity was 0.2-0.24 mmA.[2] The specimens were peened all around except the clamping area, as shown in figure 7.10. For the SEN specimens, 6 mm in diameter hard steel beads were used and the peening intensity was equal to 0.254-0.3556 mmA.
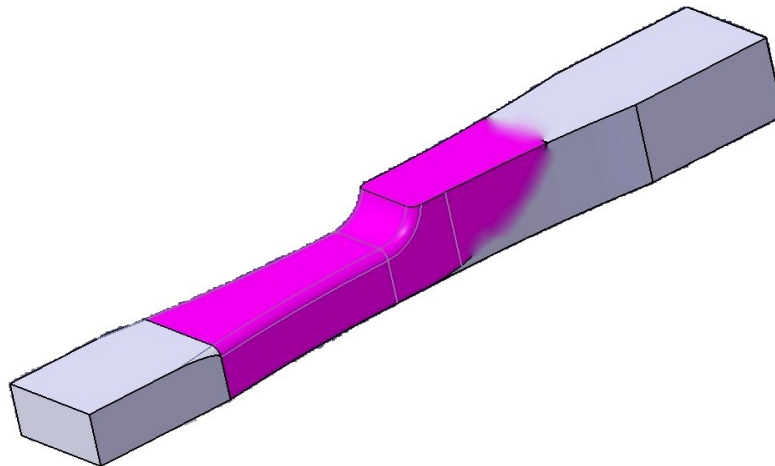
Figure 7.10: *Surfaces in which Shot Peening was applied.*

---

[2]The definition of the peening intensity is described in appendix B

7.3.4   Ultrasonic Shot Peening

For the specimens used in this campaign the specifications about the peening intensity were the same as for the Shot Peening, but 2-3 mm diameter ceramic beads were required. The USP treatment for the specimens in this test campaign was carried out by the SONATS Company located in Nantes. The USP treated surfaces are shown in figure 7.11.
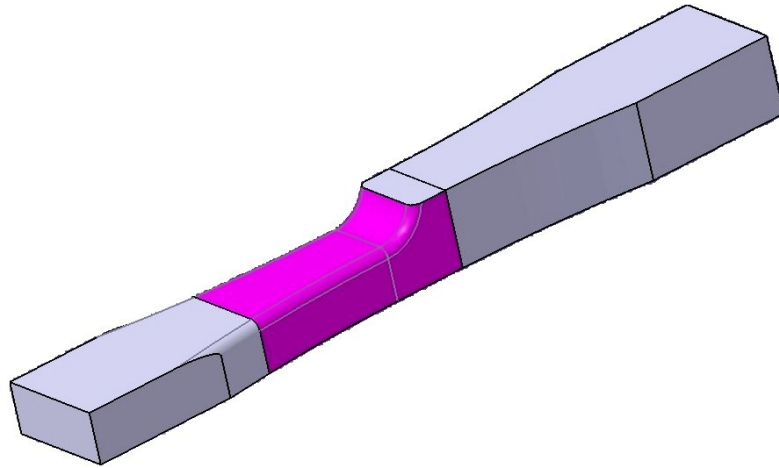
Figure 7.11: *Surfaces in which Ultrasonic Shot Peening was applied.*

7.3.5   Laser Shock Peening

The Laser Shock Peening was carried out by the Metal Improvement Company LLC. This company is the only one within Europe capable to introduce engineered laser shock induced residual stresses in metallic materials. The selected parameters are summarized in table 7.3

	Step specimen	SEN specimen
Power:	4 GW/cm²	2 GW/cm²
Pulse duration:	18 ns	18 ns
N. of layers:	3	4

Table 7.3: *Selected Laser Shock parameters.*

As mentioned, in order to obtain a treatment as homogeneous as possible, the
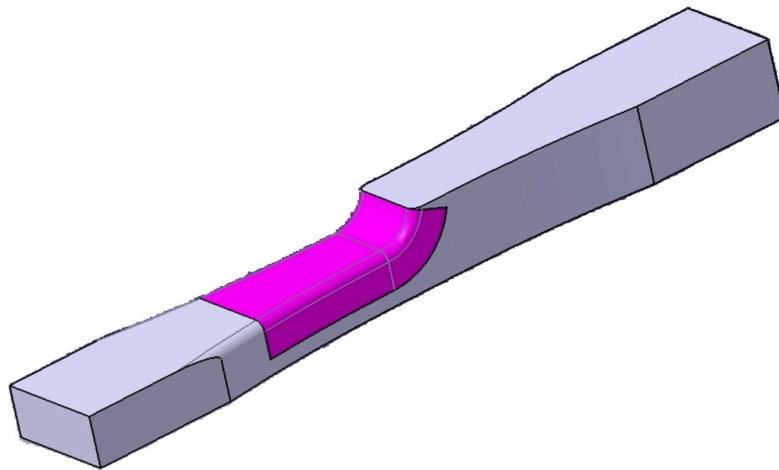
Figure 7.12: *Surfaces in which Laser Shock Peening was applied.*

layers were applied with a 30% offset for the spot diameter in both directions, as shown in figure 3.7. The treated portion of the surface is shown in figure 7.12 and the aspect of such surface is shown in figure 7.13. For the SEN specimens, the offset shots was optimized by the MIC as well as the shot sequence.
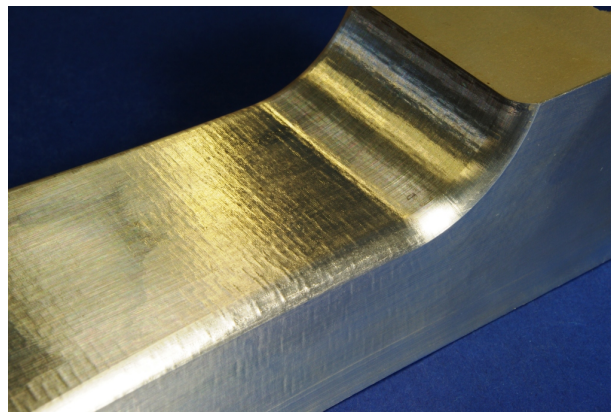
Figure 7.13: *Surface appearance of an LSP treated surface.*

7.3.6   Alodine

The specimens in the "Retro" conditions[3] were coated with Alodine®1132, which is an inorganic chromate based conversion coating and effectively phosphates most metals including aluminum. The Alodine can also offer a good adhesion to further paints.

7.3.7   Laser Notch

For all the Crack Propagation tests a Laser Notch (LN) was applied with the purpose of forcing the crack to start from a given point and from the begin of the test. In most cases, the Laser Notch was followed by a fatigue pre-cracking in order to obtain a "natural" crack shape.

7.4   Test apparatus

For logistical reasons the Step specimens were tested with two different machines: a part of them (the "Serial 2" and the "Retro 2" series, cfr sec.7.5) were tested with a Schenck 1000 kN servo-hydraulic testing machine with hydraulic clamping devices; the remaining ones were tested with a Schenck 400 kN servo-hydraulic testing machine with hydraulic clamping devices. In both cases, anti-bending devices were installed in order to protect the machine from extensive detrimental bending of the piston.

For the fatigue tests, the maximal eligible force is 80% of the maximal static force, thus for the Schenck 400 and for the Schenck PSB 250 the maximum loads available are 320 kN and 200 kN respectively.

For the Crack Propagation tests, the crack lengths were measured with a Wild M420 microscope.

All SEN specimens were tested with a Schenck PSB 250 kN servo hydraulic machine with *ad hoc* manufactured clamping devices. The crack lengths were measured with a SMZ 140 microscope.

---

[3]The specimens were divided in two groups: the "Retro" group refer to specimens in which retrofit procedures were applied (cfr. section 7.5).
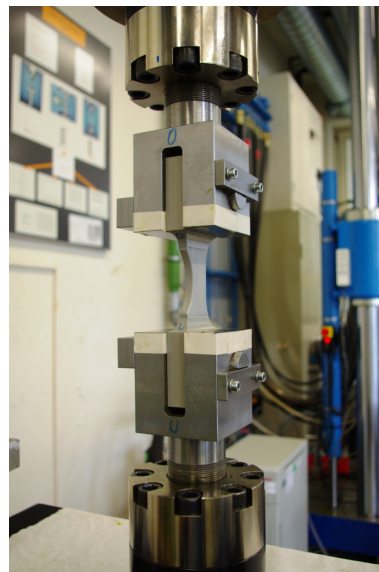
7.14.1: *Schenck 400 kN. The Schenck 1000 kN appears identical.*
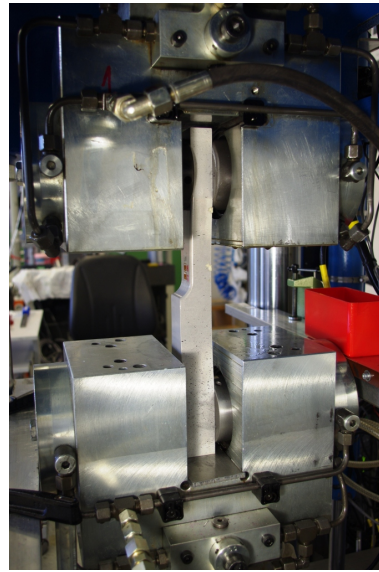
7.14.2: *Schenck 400 kN: the hydraulic clamping device.*

7.14.3: *Schenck PSB 250 kN.*

7.14.4: *Schenck PSB 250 kN: the clamping device.*

7.5 Test matrix

In order to investigate the influence of the different surface treatments on the fatigue life, High Cycle Fatigue (HCF) and Crack Propagation (CP) tests have been carried out on both specimens.

7.5.1 Step specimen

The complete matrix of the HCF tests on the Step specimen is summarized in table 7.4. The goal of these investigations is to show the behavior of LSP, SP and USP treatments in the "serial" and "retro" conditions. The "serial" conditions aim to simulate new components and the "retro" ones aim to simulate retrofit situations, so components already made produced different technologies and which might be critical and that need a precautionary rework (e.g., peening). Two stress rations were used during the fatigue tests: the $R = 0.1$ and the $R = -1.75$. The first one simulates the load history of details prone to tensile stress during the majority of their operative life (e.g., lower panels of fuselage and wings), the second one is a representative load case for highly compressed regions which may be tensed in particular conditions (e.g., upper panels of fuselage and wings).

Series	Description	R=0.1	R=-1.75	FbF
Reference	CAA	5	10	3
Basic	As machined	5	10	-
Serial 1	SP + CAA	10	10	-
Serial 2	LSP + CAA	10	10	-
Retro 1	CAA + CAA rem. + SP + Alodine	5	10	-
Retro 2	CAA + CAA rem. + LSP + Alodine	10	10	3
Retro 3	CAA + CAA rem. + USP + Alodine	5	8	1

Table 7.4: *Matrix of High Cycle Fatigue tests on Step specimens.*

For a better exposure of the phenomena and for an easier comparison between the different treatment parameters, the series were divided in two groups: the "Serial" group (which collects the "Basic", "Reference", "Serial 1" and "Serial 2" series) and the "Retro" group (which collects the "Reference", "Retro 1", "Retro 2" and "Retro 3" series). The "Serial" group shows different potential conditions

of new components whereas the "Retro" group shows how a potentially critical condition can be improved with further surface treatments.

In order to investigate the behavior of the samples with a realistic load sequence, a few specimens from 3 different groups were tested with a Flight-by-Flight spectrum, as shown in table 7.4 .The load sequence used for these tests, shown in figure 7.14, is totally defined when a reference load (e.g., the maximum load) is given. This load sequence is a simplified Ground-Air-Ground history for the compressed components in a wing box.
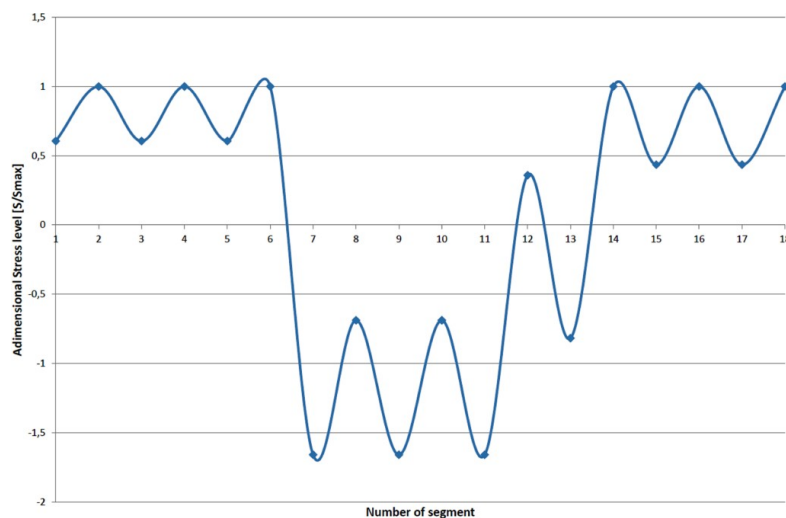
Figure 7.14: *Simulated flight for $R = -1.75$.*

In order to have more information about the crack growth in the virtually repaired or retrofitted components, several crack propagation tests were performed on differently treated Step samples. In detail, the involved specimens' conditions are briefly summarized in table 7.5

Series	Description	N. spec.
Reference	CAA + LN (+ pre-cracking)	3
Retro 1	CAA + CAA rem. + SP + LN (+ pre-cracking)	3
Retro 2	CAA + CAA rem. + LSP + LN (+ pre-cracking)	3
Retro 3	CAA + CAA rem. + USP + LN (+ pre-cracking)	1
Retro 2X	CAA + CAA rem. + LN + pre-cracking + LSP	3

Table 7.5: *Matrix of Crack Propagation tests on Step specimens.*

The "Reference" specimens should simulate the actual component's behavior, the "Retro 1", "Retro 2" and "Retro 3" specimens are representative of the behavior of the component after SP, LSP or USP retrofit procedures respectively. The retrofit procedures are intended to be applied on components without crack initiations. The "Retro 2X" specimens are representative of a repaired component in which a crack is already present and which is treated with LSP. This last condition is intended to prove the ability of LSP in slowing down already present cracks in case they have not been detected before application of LSP. All tests were carried out with $R = 0.1$.

All tests were carried out under force control with constant load amplitude and frequency, exception for the Flight by Flight tests, carried out with variable amplitude.

7.5.2   SEN specimen

As for the Step specimens, High Cycle Fatigue and Crack Propagation tests were performed for the SEN specimens. In order to reduce the amount of tests to perform and the amount of specimens to manufacture, preliminary tests were carried out on a limited number of specimens. The surface conditions analyzed during this preliminary analysis were four:

- CAA reference;
- CAA + CAA removal + Shot Peening + Alodine;
- CAA + CAA removal + Laser Shock Peening + Alodine;
- CAA + CAA removal + Laser Shock Peening + Shot Peening + Alodine.

The Shot Peening or the Laser Shock Peening, when applied after a 0.3 mm CAA removal, are both capable of remarkable fatigue life enhancement, but they were not able to give a sufficient performance improvement. At the same load level, the Shot Peening and the Laser Shock Peening can improve the fatigue life by the 560% and by the 580% respectively, but the combination of Laser Shock Peening and Shot Peening (applied in this order) can improve the fatigue life of the 1070%. The results are summarized in figure 7.15.

Thus, only two series were compared: the "Reference" and the "Retrofit"; the specimens involved in the High Cycle Fatigue and in the Crack Propagation tests
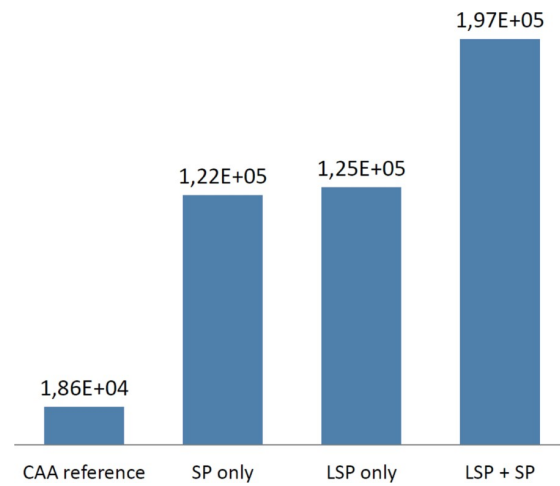
Figure 7.15: *Results of the preliminary tests on SEN specimens.*

Series	Description	HCF	CP
Reference	CAA reference (+LN)	10	3
Retrofit	CAA +CAA rem. + LSP + SP + Alodine (+LN)	10	3

Table 7.6: *Matrix of the tests performed on the SEN specimens. The Laser Notch was applied only in the Crack Propagation tests.*

are summarized in table 7.6: the "Retrofit" series is representative of a retrofitted component. In the CP samples, a 0.2 mm long laser notch were applied with the purpose of simulating a crack nucleation during the service. Both HCF and CP tests were performed under stress control with constant load amplitude and frequency; the stress ratio was $R = -1$. All the CP tests were carried out at the same stress level (180 MPa).

Chapter 8

Test results

The results of the test campaign are exposed below; the results are sorted by test type (High Cycle Fatigue first, then Crack Propagation) and again by specimen type. Follows a summary of the unexpected or anomalous failures and a discussion on the test results.

8.1   High Cycle Fatigue tests

In order to compare the test results, two analytical instruments will be used: the Life Improvement Factor (LIF) and the Fatigue Strength Enhancement (FSE).

The LIF can be defined as the ratio of the fatigue life of a given sample and an appropriate reference sample *at the same stress level*:

$$\text{LIF} = \frac{FL|_{\sigma=\bar{\sigma}}}{FL^{\text{ref}}|_{\sigma=\bar{\sigma}}}$$

where FL stands for Fatigue Life of the specimen considered, FL^{ref} is the Fatigue Life of a suitable reference specimen and $\bar{\sigma}$ is the stress level at which both specimens were tested. The LIF is a useful parameter for comparisons between different surface conditions at the same stress conditions (e.g., for the preliminary tests on the SEN specimens, pag. 73)

The FSE can be defined as the load increase necessary to have *the same fatigue life* for the sample under analysis and for an appropriate reference sample expressed in percentage:

$$\text{FSE} = \frac{\sigma|_{FL=\bar{FL}} - \sigma^{\text{ref}}|_{FL=\bar{FL}}}{\sigma^{\text{ref}}|_{FL=\bar{FL}}} \times 100[\%]$$

For a better understanding of these two definitions, an example is provided. Supposing the situation shown in fig. 8.1, one wants to calculate both LIF and FSE .
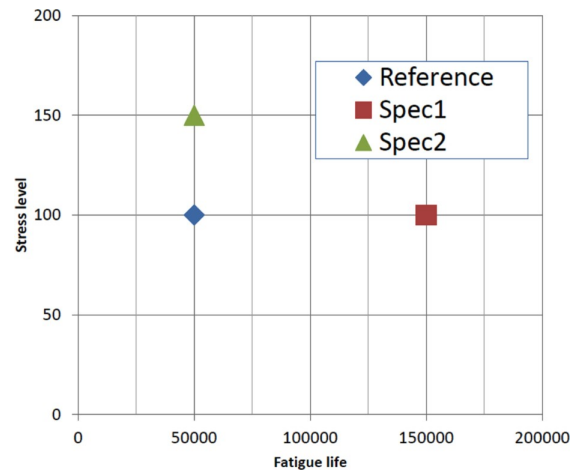
Figure 8.1: *Example: an hypothetical sample for LIF and FSE calculation.*

It is possible to calculate the LIF for the Spec1, which is

$$\text{LIF}_1 = \frac{150000}{50000} = 3.0$$

It is also possible to calculate the FSE for the Spec2, which is

$$\text{FSE}_2 = \frac{150 - 100}{150} \times 100\% = +50\%$$

8.1.1   Step specimen

The results are resumed in fig. 8.2.1 for $R = 0.1$ and in fig. 8.2.2 for $R = -1.75$.

It is shown that in both cases the CAA treatment leads to a significant decrease of the fatigue life and of the fatigue strength. Compared with the bare specimens, the CAA, when applied alone, leads to an FSE equal to -20% for $R = 0.1$ and up to -17% for $R = -1.75$.
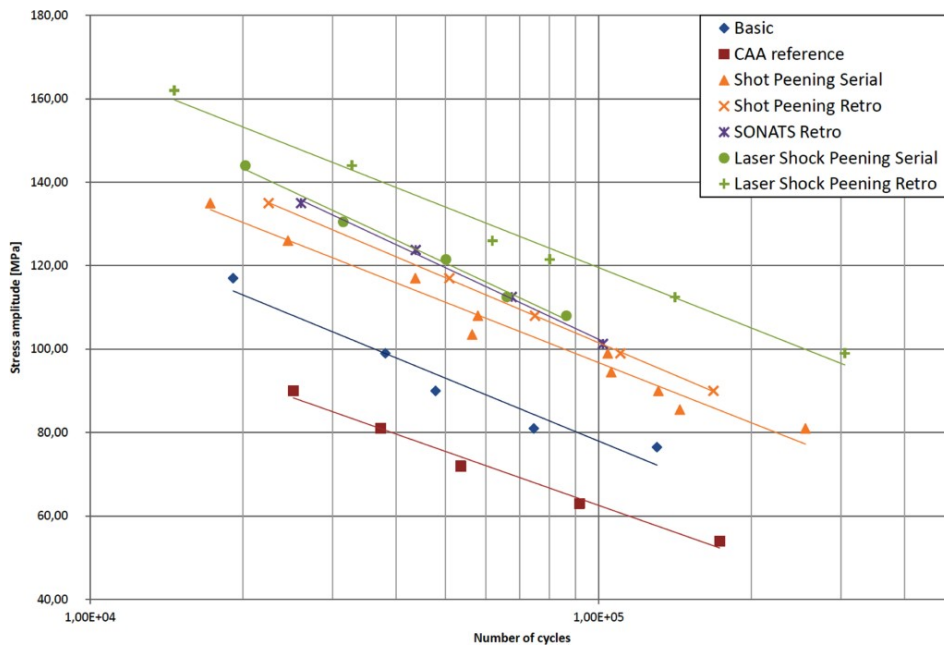
8.2.1: *Test results for HCF tests on Step specimens, $R = 0.1$.*
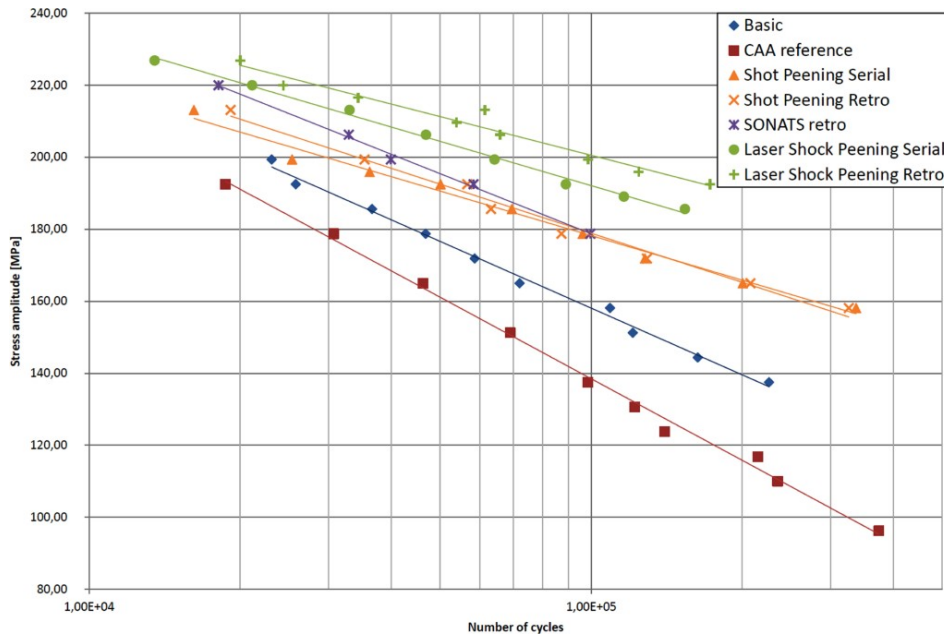
8.2.2: *Test results for HCF tests on Step specimens, $R = -1.75$.*

Applying Shot Peening before the CAA treatment leads to an enhancement of the fatigue strength. Compared with the bare specimens again, the related FSE is up to $+24\%$ for $R = 0.1$ and up to $+19\%$ for $R = -1.75$.

The best results for "serial" conditions are obtainable when LSP is applied before the CAA: in this case the FSE 's value is up to $+33\%$ for $R = 0.1$ and up to $+29\%$ for $R = -1.75$.

Regarding the retrofit solutions, removing the CAA layer and applying Shot Peening or Ultrasonic Shot Peening results in a remarkable improvement of the fatigue strength: the FSE reaches values up to $+64\%$ for $R = 0.1$ and up to $+42\%$ for $R = -1.75$. The results from the specimens treated with these procedures are fully comparable.

The best retrofit solution appears to be the one related to the LSP applied after the CAA removal. In this case the FSE rise up to $+91\%$ for $R = 0.1$ and up to $+64\%$ for $R = -1.75$.
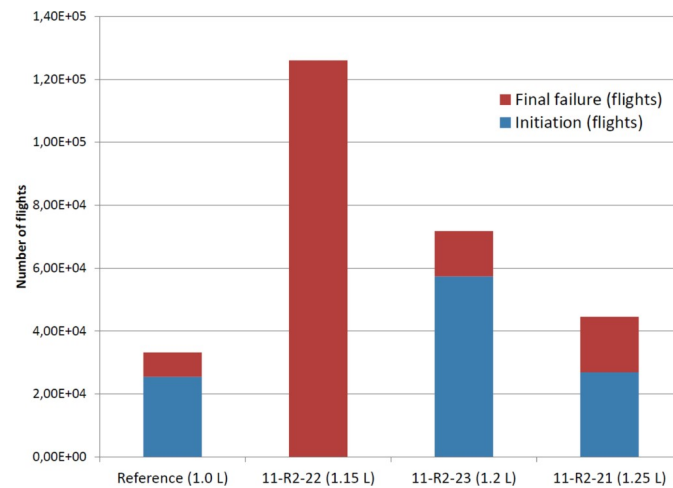
Figure 8.2: *Flight-by-Flight test results.*

Moreover, Flight-by-Flight tests were carried out; the results are shown in figure 8.2. These results show that even with a load increased by the $+15\%$, the fatigue life of an LSP treated specimen is about 4 times the one of a specimen treated with LSP only. For higher loads, the fatigue life decreases (as expected), but for a load increased by the $+25\%$, the fatigue life of an LSP treated specimen was about 1.4 times the one of the CAA reference.
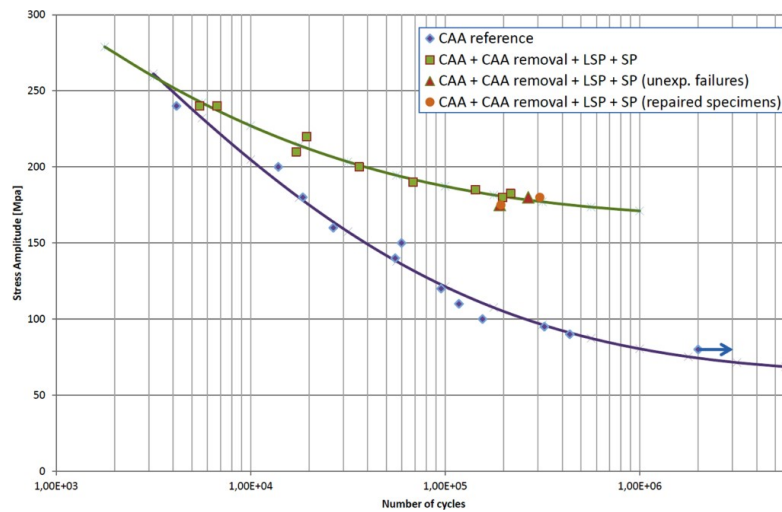
Figure 8.3: *Wöhler curves for High Cycle Fatigue tests on SEN specimens.*

8.1.2 SEN specimen

The results of the High Cycle Fatigue test performed on the SEN specimens are exposed in fig. 8.3; the results highlight that a retrofit solution obtained by removing the CAA layer and then applying Laser Shock Peening and Shot Peening can provide significant enhancements, up to and FSE of +87% under the lower loads. The specimen's $K_t = 2$, which means that for the high stress levels the tension exceeds the yield tension, thus it is proved that the notch region is prone to a cyclic massive plastic deformation. In this case it is possible to speak of "low cycle fatigue"; in this field the benefits given by the peening procedures are dramatically reduced.

8.2 Crack Propagation tests

The Crack Propagation tests were carried out in order to learn more about the behavior of a fatigue crack growing in a compressive residual stress field. Moreover, a comparison between the effects of different surface conditions can be carried out.

8.2.1   Step specimen

The test results are exposed in figg. 8.4.1 and 8.4.2. The results show that the crack propagation rate is much lower in LSP treated specimens than in other specimens despite the stress level is generally higher in LSP specimens. Data about long cracks in LSP specimens are not available due to the premature unexpected failures occurred not in the notch.

8.2.2   SEN specimen

The test results (figg. 8.5.1 and 8.5.2) confirm that the combination of LSP and SP can slow the crack down by over 10 times, especially in the first phases of the propagation, allowing much longer mean times between overahuls and, of course, providing a longer fatigue life. The longer the crack is, the lower the advantages are: for short cracks the crack growth ratio in the LSP treated specimens is a tenth than the one in the unpeened ones, whereas for longer cracks in the LSP treated specimens the cracks is 4 times slower than in the unpeened ones.
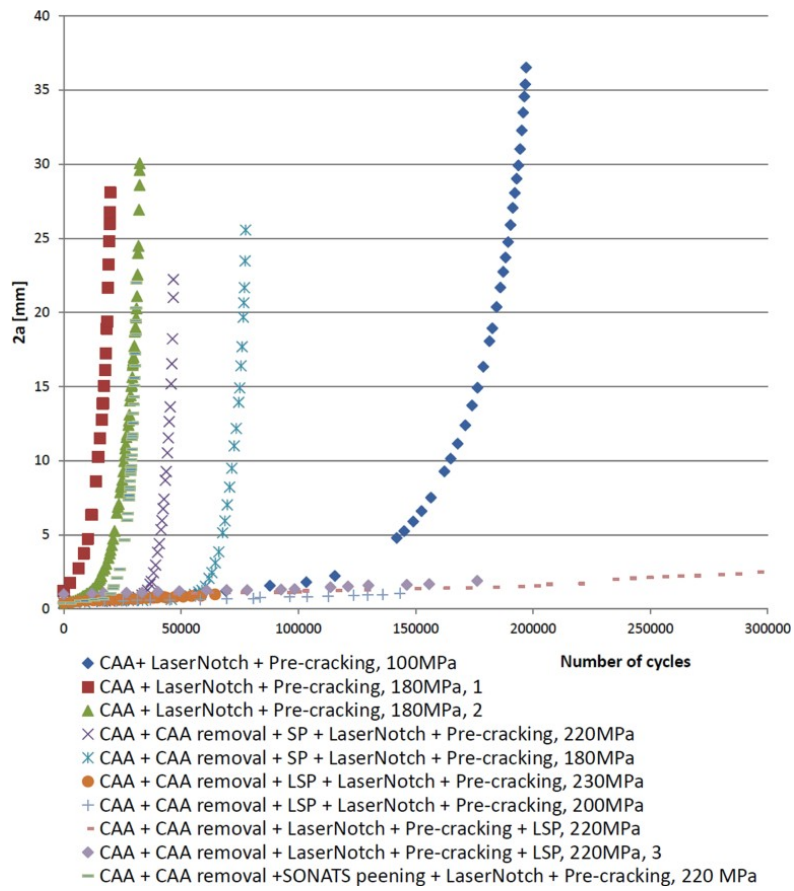
8.4.1
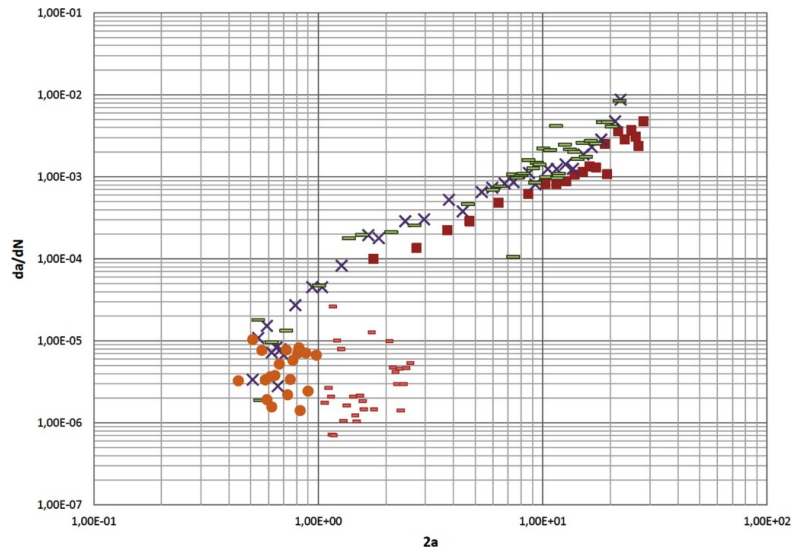
8.4.2

Figure 8.4: *Crack propagation tests on Step specimens.*

81 di 117
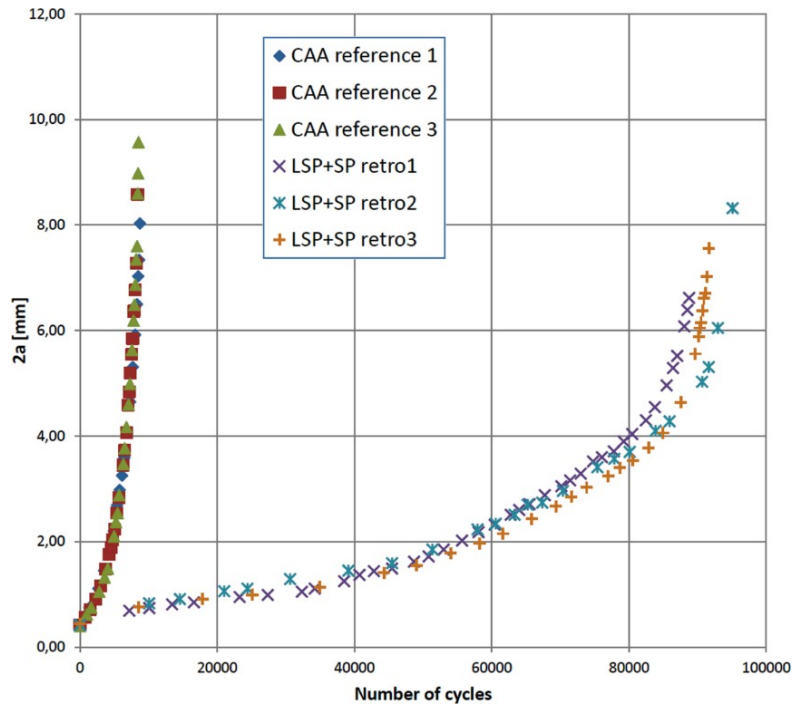
8.5.1
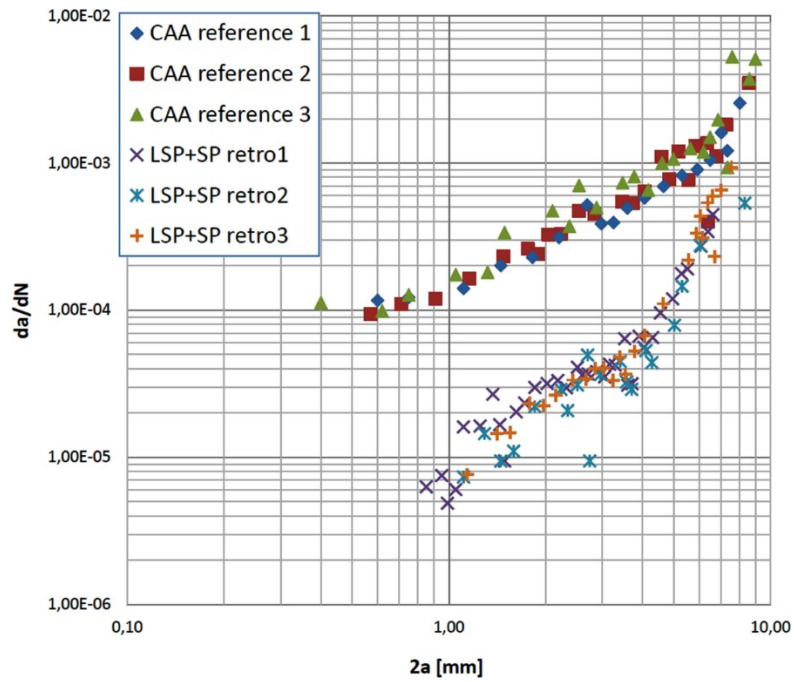
8.5.2

Figure 8.5: *Crack propagation tests on SEN specimens.*

8.3   Remarks
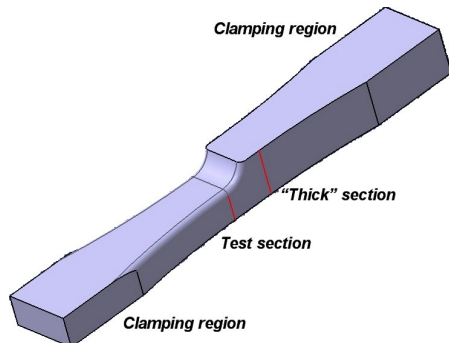
8.6.1: *Locations in the Step specimen.*
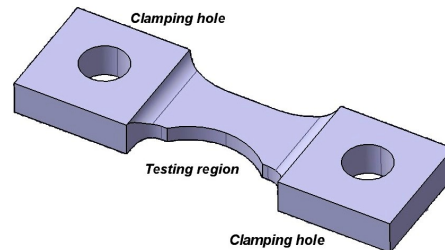

8.6.2: *Locations in the SEN specimen.*

Many specimens broke in unexpected ways: some of them broke near the clamping region (see figg. 8.6.1 and 8.6.2) whereas many Step specimens broke in the region marked as "thick" in fig. 8.6.1, which is the thick region just over the notch.

These cases are the most interesting because the failure started from the back side of the specimen (fig. 8.6); all of those failures occurred in LSP treated specimens, as shown in table 8.1. On the other hand, for LSP treated samples there is no unexpected failures for $R = -1.75$ whereas the SP treated coupons showed failures in the clamping regions.

	CAA ref.	Basic	Serial 1	Serial 2	Retro 1	Retro 2	Retro3	Retro2X
$R = 0.1$	-	-	-	5/10	-	1+4 /10	-	nd
$R = -1.75$	-	-	2/10	-	2/10	-	2/8	nd
CP	-	nd	nd	nd	-	2/3	-	2/3

Table 8.1: *Table of unexpected failures on Step specimens. The red color indicates those specimens which broke in the thick section whereas the LSP specimens' column are highlighted in cyan.*

The back side of the specimens has not been LSP treated. In order to counter at list the CAA effect, the back surface was milled, but this operation proved to be not sufficient to avoid failures from the thick section.
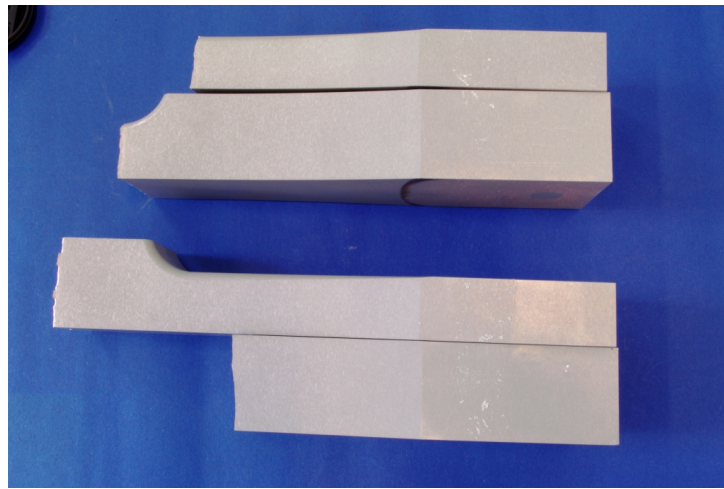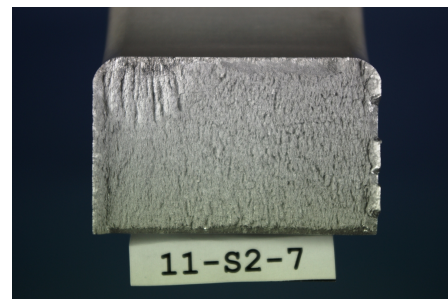
Figure 8.6: *A specimen broken in an unexpected region.*

There is a remarkable amount of failures on the edge radii, such as in figg. 8.7.1 and 8.7.2. The 10% of the SP treated specimens had such failure whereas the 30% of the LSP treated specimens shown a similar failure.
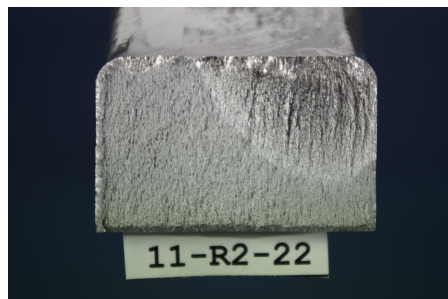

| 8.7.1 | 8.7.2 |

Figure 8.7: *Failures starting from the edge radius.*

A particularly interesting example of corner failure is given by a crack propagation specimens, in which there was a 0.4 mm laser notch grown up to a 1 mm pre-crack before the LSP treatment. In this sample, several secondary flaws (figg. 8.9.1 and 8.9.2) were detected and one of them, situated in the corner, caused the final failure. The crack surface is shown in fig. 8.8.
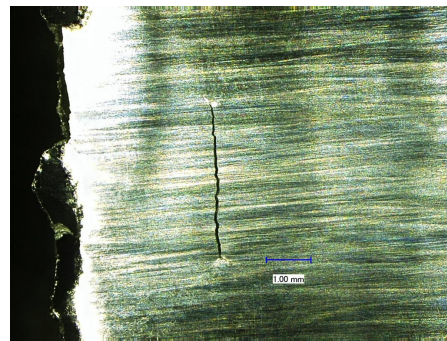
Also two SEN specimens broke in the clamping holes, as shown in fig. 8.10. Fretting marks were detected near the crack initiation point, which was in the
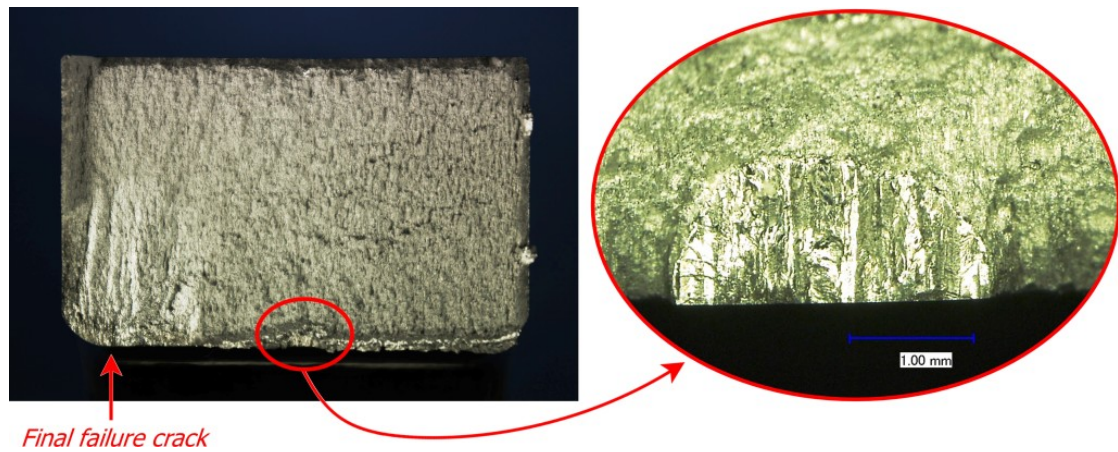
Figure 8.8: *Crack surface appearance: the crack starting from the laser notch (magnified on the right) did not grow whereas the corner crack grown breaking the specimen.*
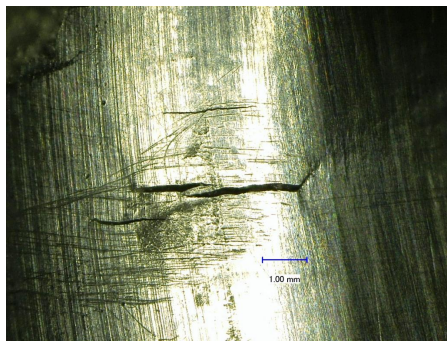

Figure 8.9: *Secondary flaws detected, the 8.9.1 in the corner and the 8.9.2 in the middle of the specimen.*

clamping hole edge. Given that $R = -1$ and that the specimen was free to rotate around the pins that clamped the specimens generating cyclic friction, it is impossible to eliminate the fretting. After some modifications to the clamping device (more precisely to the pins) the fretting problems were moved out from the critical area and all the failures appeared in the testing region. Both failures happened in LSP treated specimens. Those specimens were repaired with steel screws and the tests could go on, even if the failure occurred after a relatively low number of cycles.
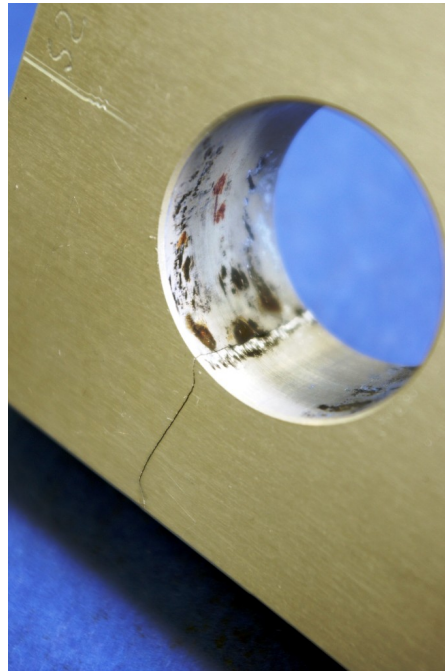
Figure 8.10: *Fretting marks in the surface of the clamping hole in a SEN specimen.*
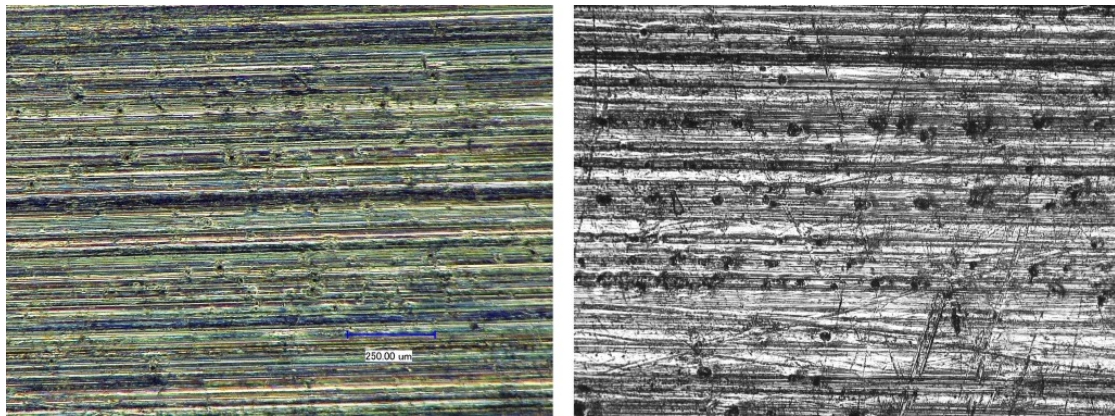
8.4 Optical analyses

Optical analyses were carried out with a Keyence VHX/VH digital microscope and with a Zeiss LEO 1430 Scanning Electron Microscope.

The first alarming information resulting from those investigations is that, despite the 0.3 mm grinding out, CAA pits were observed in the Step specimens (figg. 8.11 and 8.12). This can mean that several pits were deeper than 0.3 mm, so much deeper than previously expected. This can result in premature failures.

Previous studies carried out by EADS-IW stated that the maximum depth of the CAA pits was 60 μm, so a 100μm removal was considered to be enough to eliminate all risks associated to the CAA pits.

In some CAA reference Crack Propagation SEN specimens, secondary flaws were found. In those specimens a laser notch was made and the surface was mirror polished; despite this, several flaws were observed during and after the tests, especially near the edges, most probably starting from CAA pits that the polish has not been able to remove. The pictures 8.13.1 and 8.13.2 show some of those secondary flaws.

**Figure 8.11:** *CAA pits visible after the 0.3 mm CAA removal.*
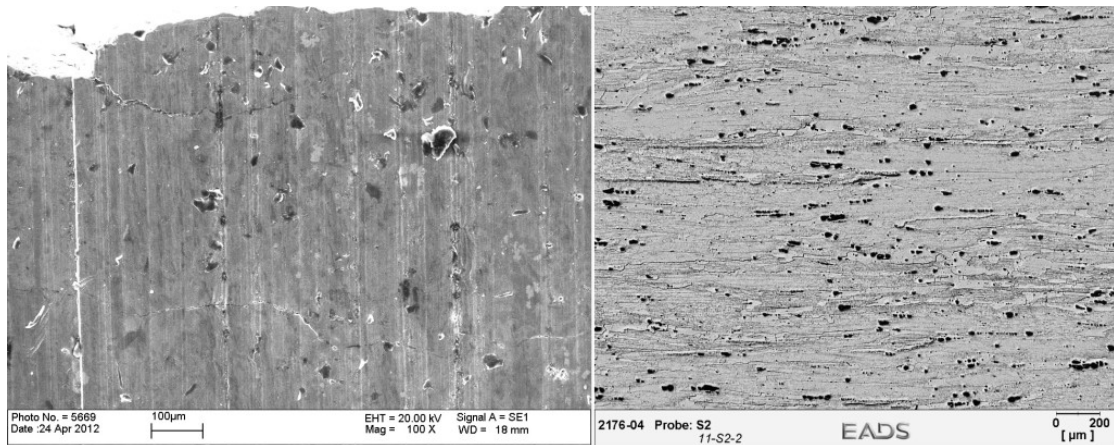
Figure 8.12: *CAA pits visible after the 0.3 mm CAA removal.Further analyses should be able to determine the actual depth of those pits and refine a CAA removal process.*

Finally, optical analyses were carried out on the crack surface of the SEN specimens in order to obtain data about the crack depth as a function of the crack length. The analyzed surfaces are shown in figure 8.14.

8.5   Discussions

The High Cycle Fatigue test results in both specimens show a tremendous improvement of the fatigue strength of the Laser Shock Peening treated samples compared to the unpeened samples and to specimens which were treated with other peening processes. It is possible to affirm that the reason for this improvement is

<div align="center">
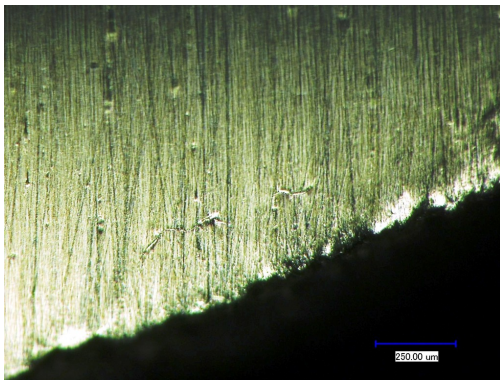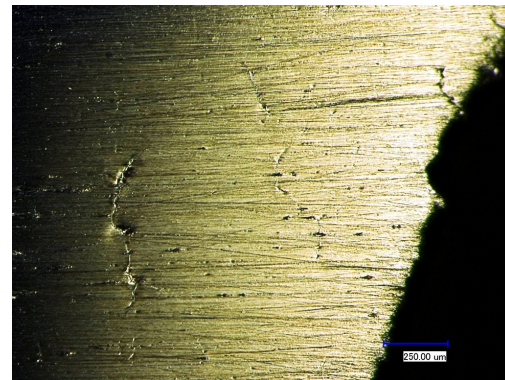
8.13.1   **8.13.2**

**Figure 8.13:** *Secondary flaws observed in SEN specimens.*

</div>

the deep compressive stress field on the surface that inhibits the nucleation and slows down the propagation of the cracks.

It is well known that, for low load levels, the small imperfections have a strong influence on the fatigue life. This explains the degrade of the fatigue strength of the CAA treated specimens compared to the bare samples. The effect of the peening technologies (and in particular the LSP) is to inhibit the nucleation from the small defects, behaving like a polishing. This is evident at the low load levels where the relative effectiveness of the peening procedures is typically much higher than for high load levels.

The Crack Propagation tests show that the crack is strongly slown down by the compressive residual stress field, especially for short cracks. For longer flaws, the crack tip reaches an area in which the stresses are tensile. Nonetheless the LSP is still able to provide enhancements to the crack growth behavior. As Clark and Sharp ("The effect of peening on the fatigue life of 7050 aluminium alloy") say, the retardation caused by a compressive stresses still operates when the crack tip has grown into the tensile stress field core, and is only gradually reduced by the tensile stress component, as the crack grows deeper into the core. The effect of the compressive residual stresses is always to retard the crack growth.

During the production of new components it is possible to increase fatigue strength applying CAA after other peening procedures, especially LSP. During repair and retrofit procedures it is possible to enhance the fatigue behavior remov-
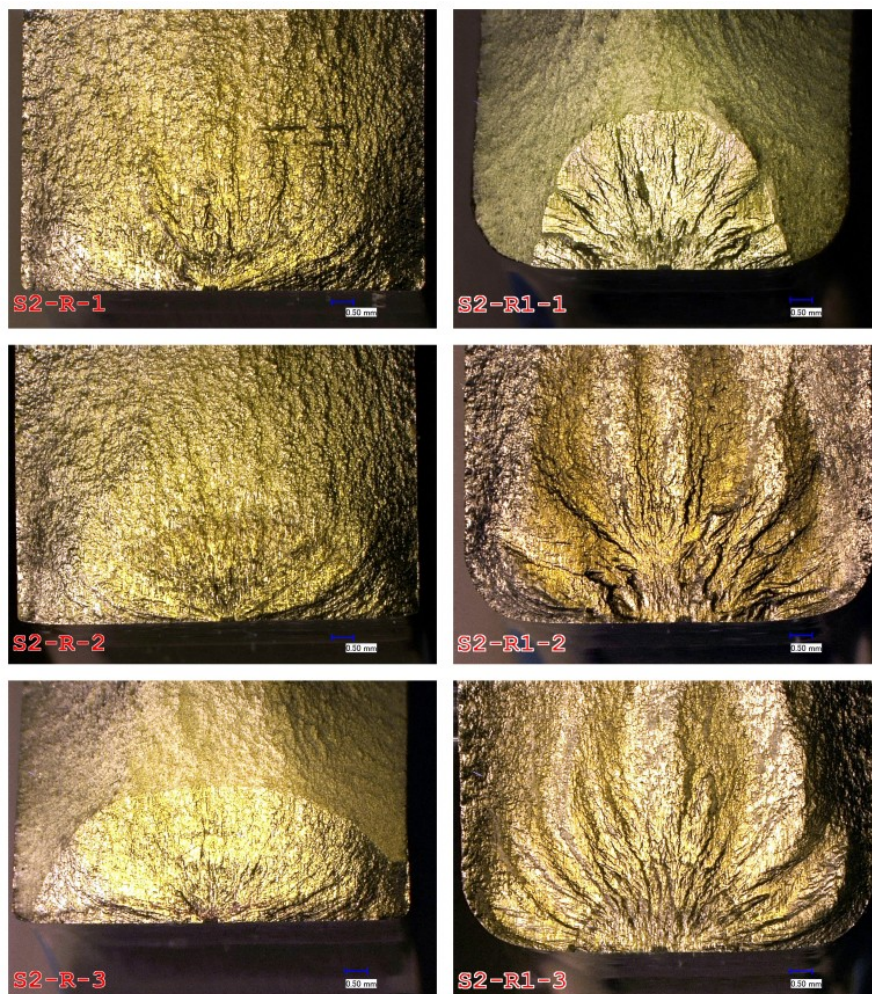
Figure 8.14: *Crack shapes in SEN specimens involved in Crack Propagation tests. The S2-R1-1 and the S2-R-3 specimens were statically broken at a given crack length; in the others a black ink was inserted during the test at the desired crack length.*

ing the CAA affected surface layer and applying peening. The LSP is the peening technology that provides the best results. Shot Peening and USP provide comparable enhancements to the fatigue strength; this small difference may not justify the additional costs of the USP compared to the SP.

It is shown in sec. 8.3 that in several LSP specimens, failure occurred on the back side of the thick section. Most probably, the reason of the failures in the thick sections is a combination of CAA pits and secondary bending, which introduces an extra tension in the back. The fact that only LSP treated samples had failures

away from the notch indicates that the LSP treatment made the notch ($K_t = 1.9$) to become a stronger (or at least less stressed) area compared to other ones such as the thick section pulling the failure away from the notch. The stress distributions in presence of LSP treatment are presented in part IV.

Previous studies carried out by EADS-IW stated that the maximum depth of the CAA pits was 60 μm, so a 100μm removal was considered to be enough to eliminate all risks associated to the CAA pits. Despite this, several pits were found after the 300μm removal (pfr. sec.8.4. This can be explained only if the pitting due to the CAA is able to proceed generating deeper pits even after the anodizing treatment and the washing phase. Further studies should be able to determine the actual depth of those pits and refine a CAA removal process.

The failures in the corner radii (see sec. 8.3) can be a symptom of a drop of the residual stress next to the corned, probably due to the edge effects. Moreover it is possible to state that the LSP generated stress field is more sensible to these edge effects. This is confirmed by Crudo (2012, p. 39-41).

The cause of the failures in the clamping holes in the SEN specimens can be identified in the inauspicious combination of CAA (applied in the holes also), tension concentration due to the load introduction in the holes and the fretting between the specimen and the pin.

8.5.1 Crack growth prediction models for the SEN specimens

The data collected in figure 8.14 about the crack shape in SEN specimens make it possible to create an empirical prediction model of the crack growth.
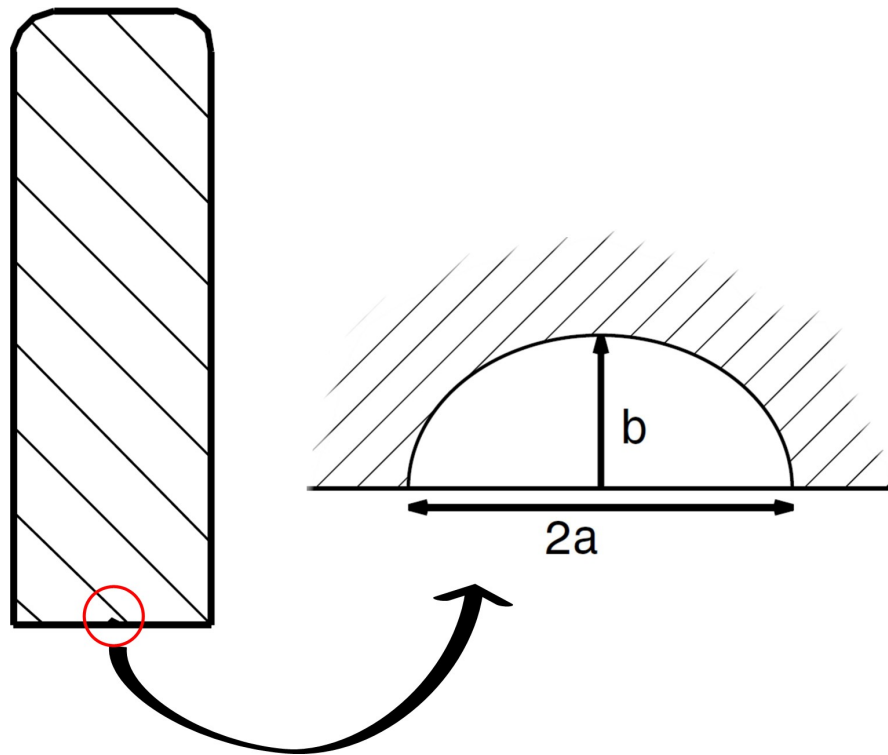
It is possible to define, for every crack length, an "aspect ratio" γ:

$$\gamma = \frac{b(\bar{N})}{a(\bar{N})}$$

where a and b are the dimensions of the crack, as shown in figure 8.15.

Hypotesis 8.5.1. Far enough from the edges (low edge effects) the crack shape has always the same aspect. Hence the aspect ratio does not change with the crack

Figure 8.15: *Characteristic dimensions in a lenticular crack.*

length ($2a$) neither with the crack depth (b) neither with the time or the number of cycles.

This hypothesis allows extending the previous formula also to a generic instant of time and consequently to a generic number of cycles of the fatigue life N. This way it is possible to define a new parameter globally valid (for this test conditions): the *growthratio*:

$$\zeta = \frac{b(N)}{a(N)} \Rightarrow b(N) = \zeta a(N) \quad \forall N \in [0, N_{\text{cr}}]$$

where N_{cr} is a suitable number of cycles from which the edge effects are not negligible. The data collected for the unpeened specimens is summarized in table 8.2 as well as the corresponding calculated aspect ratio.

Regarding the data coming from the unpeened samples only, the average value of the aspect ratio $\gamma(N)$ can be assumed as the growth ratio ζ:

Peened	$a(N)$ [mm]	$b(N)$ [mm]	$\gamma(N)$
no	1.388	1.174	0.846
no	3.175	2.667	0.840
no	4.680	3.609	0.771
no	4.742	3.477	0.733
yes	2.620	2.123	0.810
yes	3.323	4.002	1.204

Table 8.2: *Data collected from SEN specimens.*

$$\zeta_{\text{CAA}} = 0.798 \pm 7\%$$

The low scatter of the result ensures the validity of the hypothesis of independence of the crack depth on the crack length for unpeened specimens.

Regarding the peened samples, it is possible to notice that for a data point, the corresponding aspect ratio is bigger than 1, which means that the shape of the crack changes sensibly during the propagation and is influenced by the residual stresses. This information says that at a given depth, the crack can grow more in the depth than in the length, producing an important change of behavior. For this reason it is not possible to assume as valid the hypothesis of independence on the crack length also for peened specimens and further data are required in order to understand which correlation is there between ζ and a.

Part IV

Numerical simulations

In order to investigate on the stress distribution within the Step specimens, several Finite Element Method (FEM) analyses were carried out. The aims of these analyses were mainly two:

- reproduce the previous results obtained within EADS-IW;

- provide an explanation to the unexpected failures in the LSP treated specimens.

The model was drawn with CATIA V5R17 and the FEM analyses were carried out with Abaqus 6.10-1.

Chapter 9

Preprocessing

9.1   Model generation

The model was drawn with the software CATIA V5R17 according to the original EADS-IW drawings. (figure 9.1).

For simplicity's sake, the following modifications were made:

- the fillet in the thin section was removed;

- only half specimen has modeled using the symmetry plane as cutting plane.

9.2   Mesh and properties

In order to obtain a finer mesh in the notch region and a coarser one in the clamping region, the model was ideally divided in three parts: the central region (which includes the notch) and the two clamping regions; afterwards the three parts were linked with the command "Tie". The three parts are shown in figure 9.2

The regions to focus in are the notch and the back surface of the thick section, where the unexpected failures happened, so the mesh resulted much finer nearby those locations. The mesh of the center part is shown in fig. 9.3; details of the mesh near the notch and near the back surface are shown in figure 9.4.1 and 9.4.2 respectively.
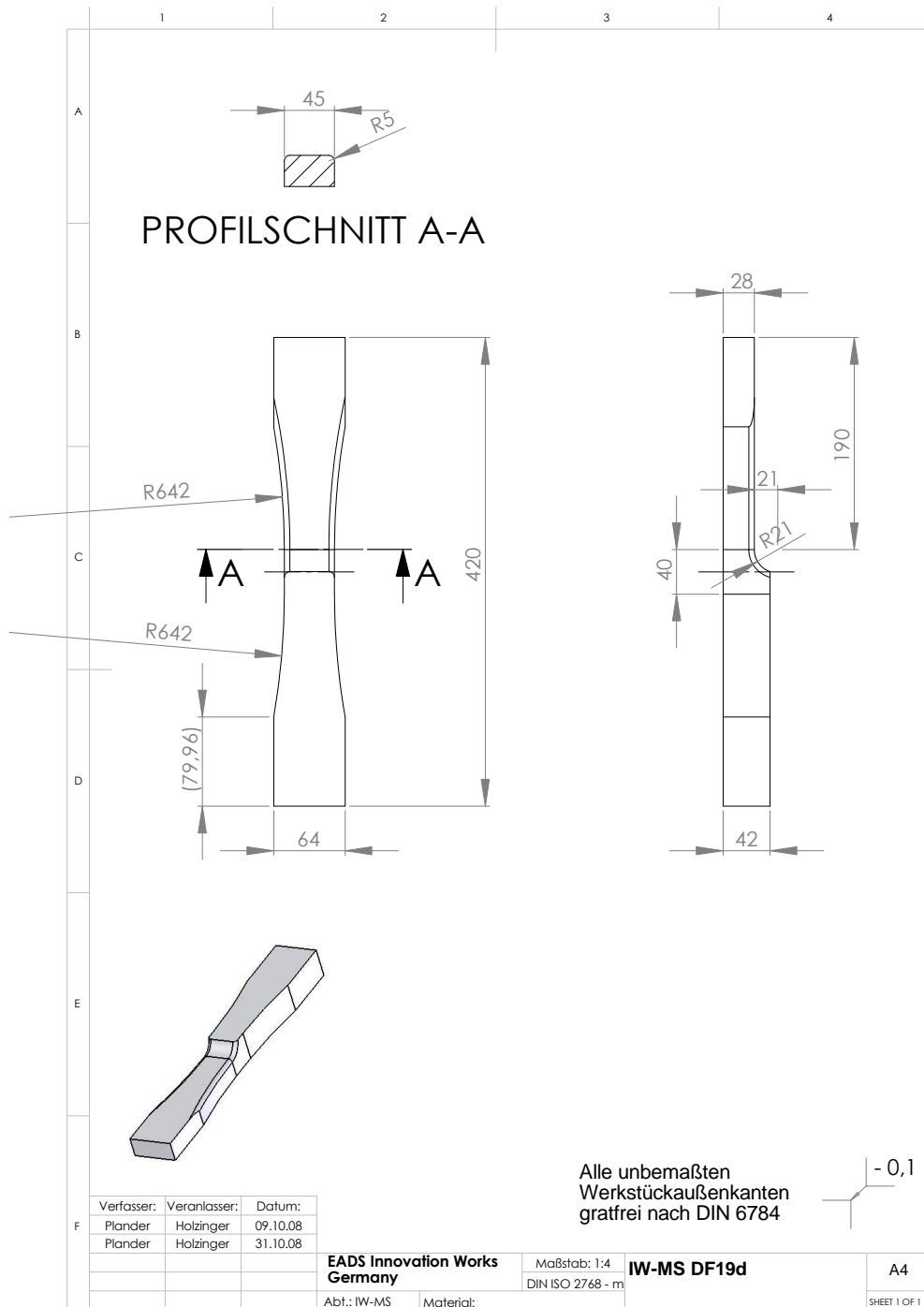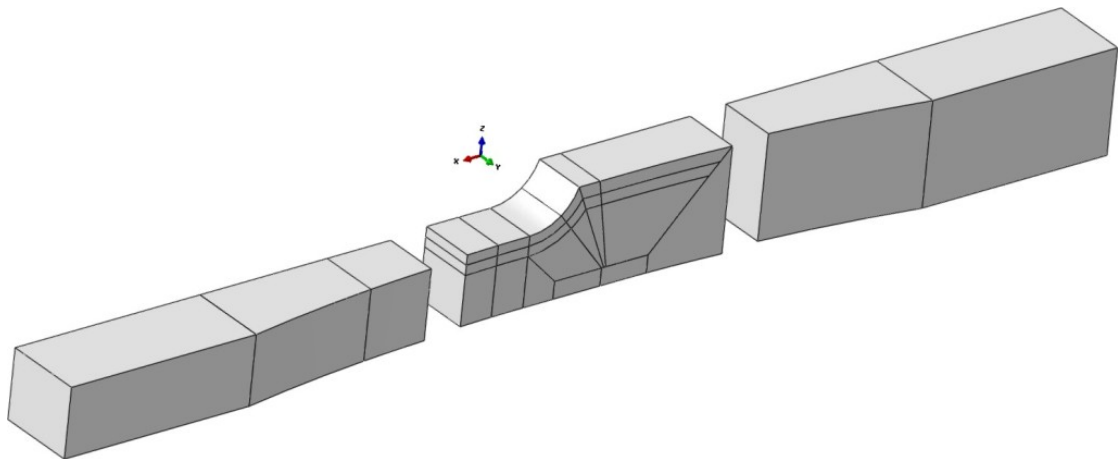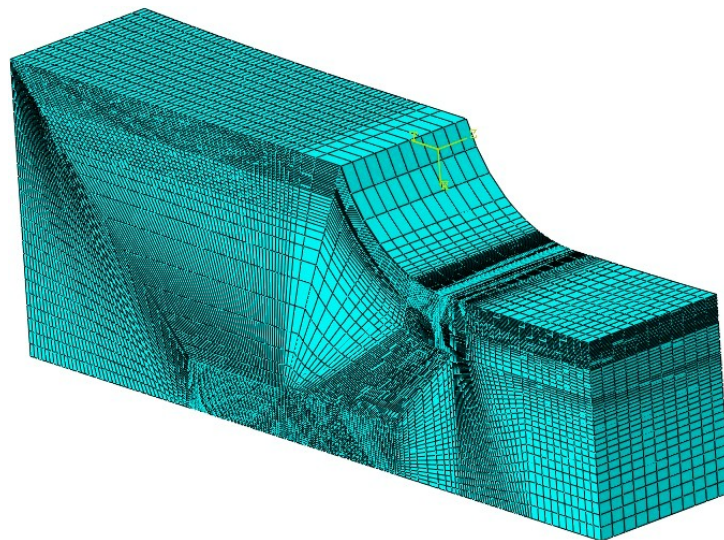
**Figure 9.1:** *Original EADS-IW design for the Step specimens.*

**Figure 9.2:** *The three parts virtually separated each other and merged again with the "Tie" command*

Figure 9.3: *Mesh of the center region of the Step specimen.*

The mesh generated has 138 504 elements and contains 123 956 C3D8 solid elements. The characteristic dimension of the elements in the interesting areas is 0.2 mm. The analyses took into account geometrical and material non-linearities.

Material   In order to simulate the elastic-plastic behavior of the aluminum alloy, a plasticity curve was used. The reference stress-strain curve is taken from the Military Handbook 5 (Defense 2001) and is shown in figure 9.5.
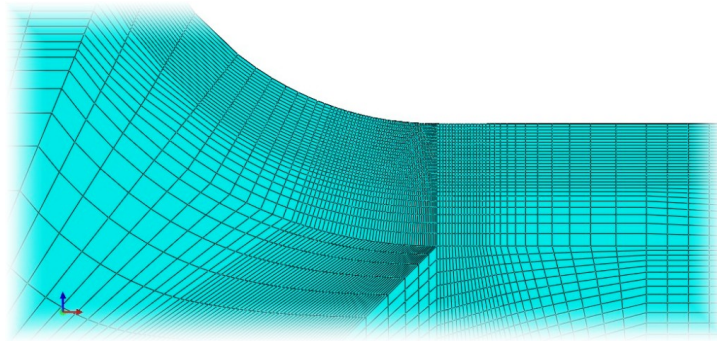
9.4.1
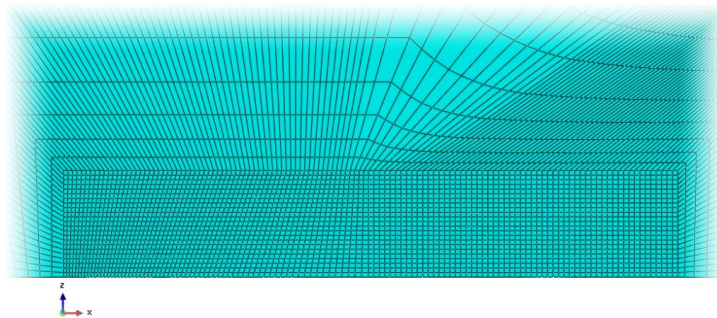
9.4.2

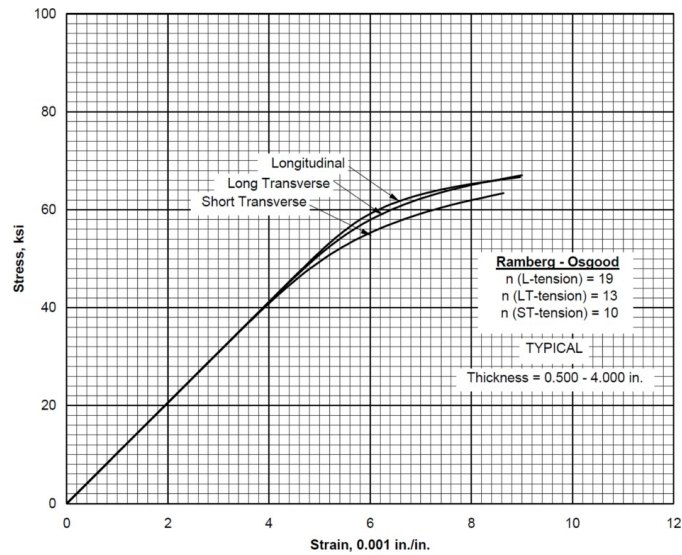**Figure 9.4:** *Details of the mesh near the interesting locations.*

**Figure 9.5:** *σ − ε curve for 7050-T7451 aluminum alloy. (Defense 2001)*

9.3   Boundary conditions

The constraints imposed are representative of the testing conditions: the surfaces indicated in figure 9.6.1 are completely clamped, the ones in figure 9.6.2 are free to slide in the longitudinal direction under the action of the external load (fig. 9.6.4). Moreover, a symmetry constraint was imposed on the symmetry plane (fig. 9.6.3).
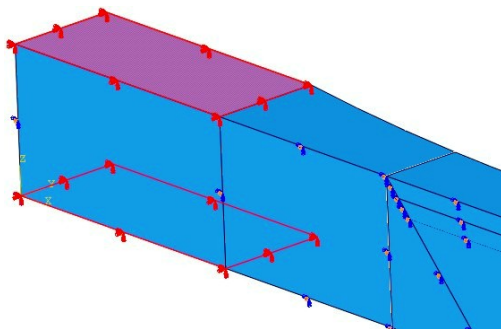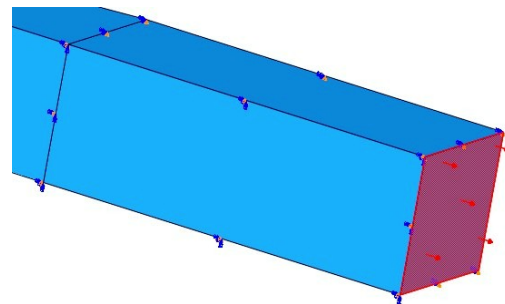

9.6.1: *Constraints: encastre on the thick clamping region.*
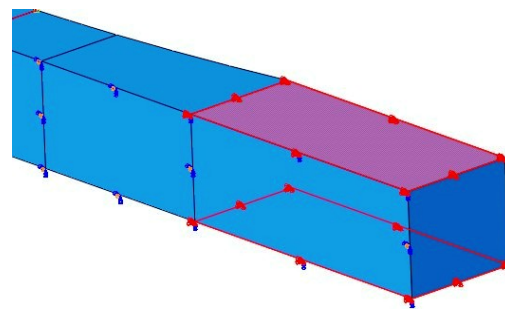
9.6.2: *Constraints: encastre on the thin clamping region.*
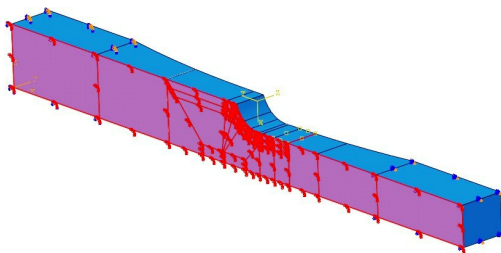
**9.6.3:** *Constraints: symmetry constraint on the symmetry plane.*

9.6.4: *Load on the thin clamping region.*

9.4   Compressive residual stresses simulation

In order to introduce the LSP effect in the model, compressive unbalanced stresses were inserted as a datum field. The input data were extrapolated from previous incremental center hole drilling measurements carried out by EADS-IW. These measurements show that the LSP affected depth in the Step specimens is about 35 mm.

To introduce the residual stress field in the most realistic way , a 34 mm thick layer near the notch was cut into 0.2 mm thick slices and at each element, the average residual stress measured value was assigned.

At the equilibrium at zero load, the stress distribution within the specimen is shown in figure 9.6: near the surface, the stress is highly compressive, then there is a tensed region; for equilibrium, near the back there is another tension region.
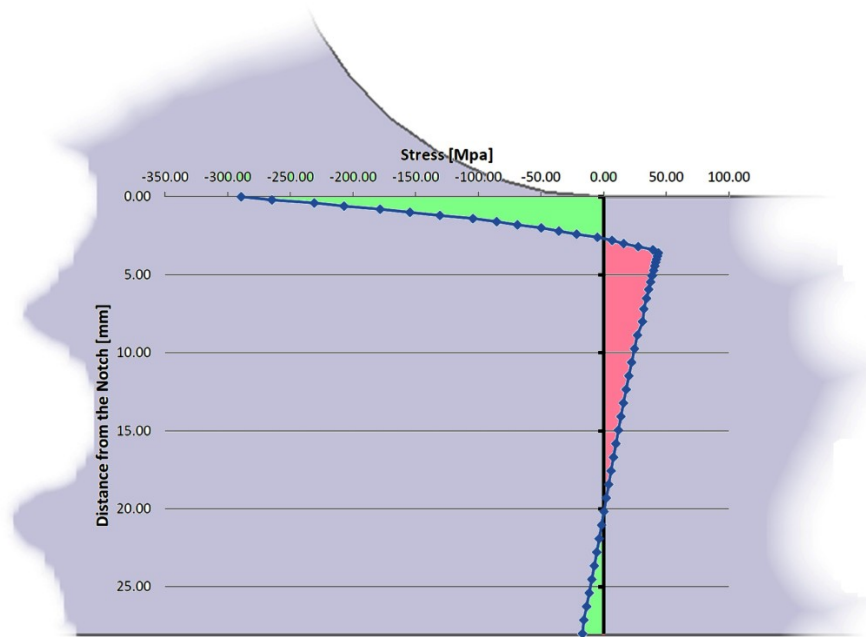
Figure 9.6: *In-depth stress profile within the specimens before the application of the external load.*

Chapter 10

Results and discussion

The simulations carried out aimed to evaluate the stress concentration factor in an unpeened specimen and then state the stress distribution in the LSP treated samples at different load levels.

10.1 Evaluation of the stress concentration factor

For the evaluation of the stress concentration factor K_t and in general the stress distribution per unit load, a linear elastic analysis was performed.

The stress concentration factor is defined as

$$K_t = \frac{\sigma_{\max}}{\bar{\sigma}}$$

where $\bar{\sigma}$ is the nominal stress in the notch section

$$\bar{\sigma} = \frac{F_{\text{ext}}}{A_{\text{notch}}} \Rightarrow F_{\text{ext}} = \bar{\sigma} A_{\text{notch}}$$

The external load, applied as a negative pressure in the surface showed in fig. 9.6.4, was chosen in order to obtain a suitable reference nominal stress in the notch section:

$$P_{\text{ext}} = \frac{F_{\text{ext}}}{A_{\text{clamp}}} = \frac{A_{\text{notch}}}{A_{\text{clamp}}} \cdot \bar{\sigma} \simeq 0.703 \cdot \bar{\sigma}$$
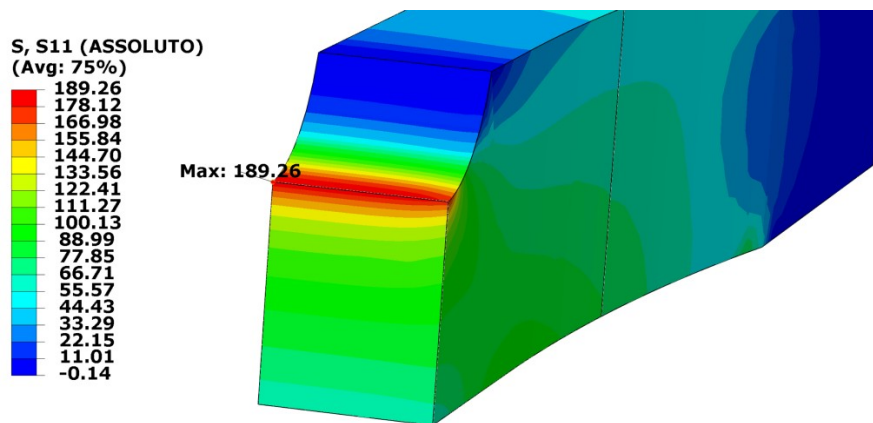
Figure 10.1: *FEM analysis on Step specimen, $\bar{\sigma} = 100$ MPa*
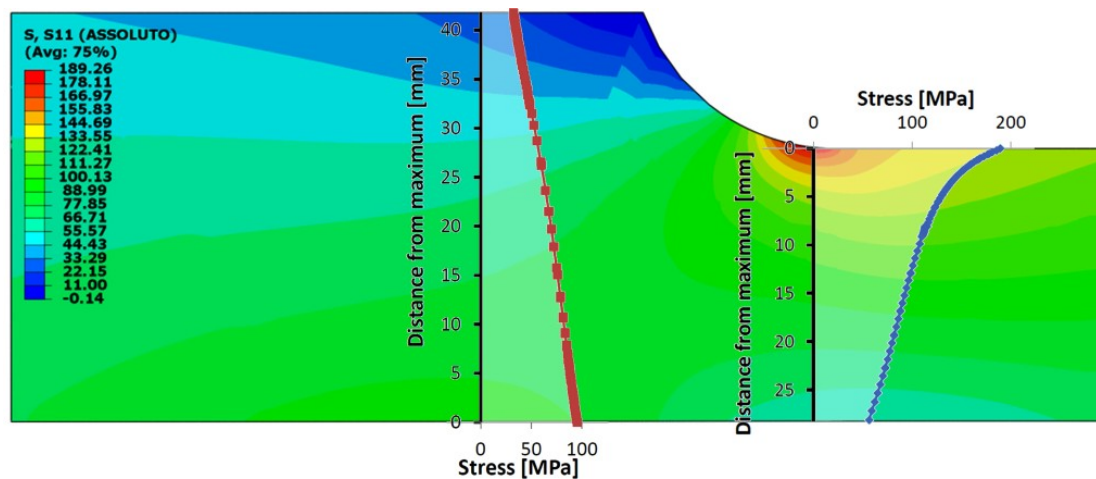

Figure 10.2: *Stress distribution in an unpeened specimen at $\bar{\sigma} = 100$ MPa.*

The chosen reference nominal stress was 100 MPa. The results are shown in figure 10.1: the maximum value of the longitudinal stress is 189.26 MPa, which confirms the approximate value of $K_t = 1.9$ used by EADS-IW. This value was confirmed by *Aramis* optical strain measurements.

10.2   Stress distribution in presence of residual stresses

Several FE analyses were performed at different stress levels after introducing the residual stress field. The analyses were divided in two steps: the first one aimed to balance the residual stress field, the second one applied the external load. The

stress levels used were:

- 100 MPa (fig. 10.4);

- 180 MPa (fig. 10.5);

- 250 MPa (fig. 10.6);

- 350 MPa (fig. 10.7);

- 450 MPa (fig. 10.8).

Analyses show that the absolute maximum of the stress acts underneath the surface at about 3.5 mm depth in the notch region. Given that the fatigue is a surface failure, the maximum on the surface was investigated: under a particular $\bar{\sigma}$ between 300 and 350 MPa, the maximum surface stress is in the back surface of the thick section. Some observations can be made:

1. for the lower stress levels, the LSP residual stress field is able to "pull" the maximum of the stress away from the notch, even for a $K_t = 1.9$;

2. the most highly stressed point on the surface is most probably the crack initiation location, this explains the unexpected failures from the back side;

3. for higher stress levels, the maximum of the tensile stress is again on the notch surface;

4. at the highest stress levels, the tensile stress in the core reaches the yielding stress and a massive region is yielded.

Indeed, the lowest load level[1] $\bar{\sigma}$ at which an LSP treated specimen involved in the experimental campaign had a failure in the notch is above 280 MPa, in accordance with the simulations. Figure 10.3 shows a fringe plot of an LSP treated specimen stressed at $\bar{\sigma} = 100$ MPa.

Figures 10.4, 10.5, 10.6, 10.7 and 10.8 show the stress distribution for the different load conditions above mentioned.
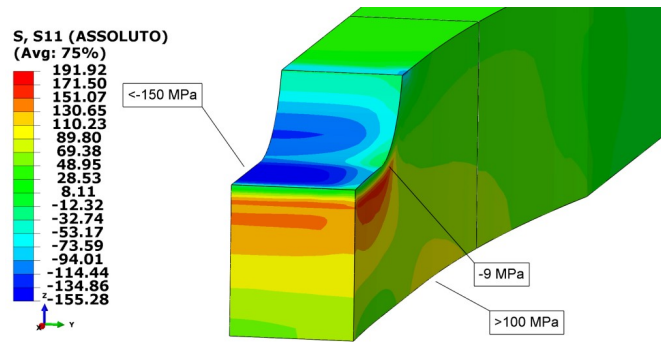
---

[1]For $R = 0.1$

Figure 10.3: *Stress distribution in an LSP treated specimen stressed at $\bar{\sigma} = 100$ MPa.*
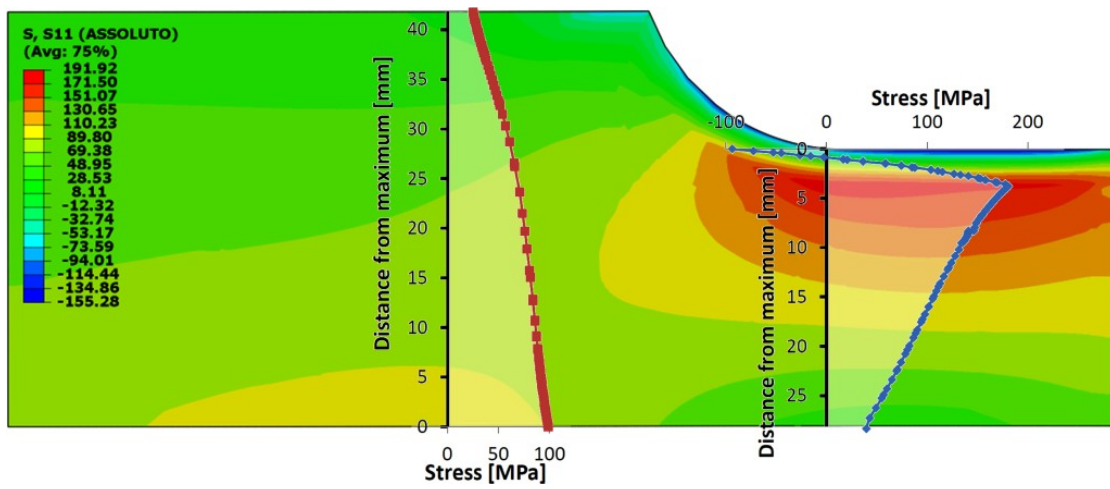

Figure 10.4: *Stress distribution in a LSP treated specimen for $\bar{\sigma} = 100$ MPa.*

Figure 10.5: *Stress distribution in a LSP treated specimen for $\bar{\sigma} = 180$ MPa.*

Figure 10.6: *Stress distribution in a LSP treated specimen for $\bar{\sigma} = 250$ MPa.*
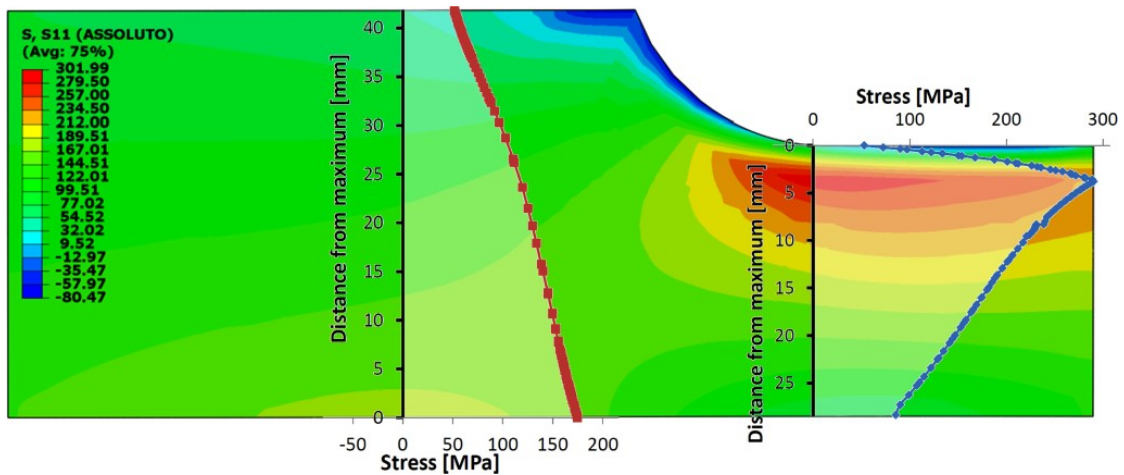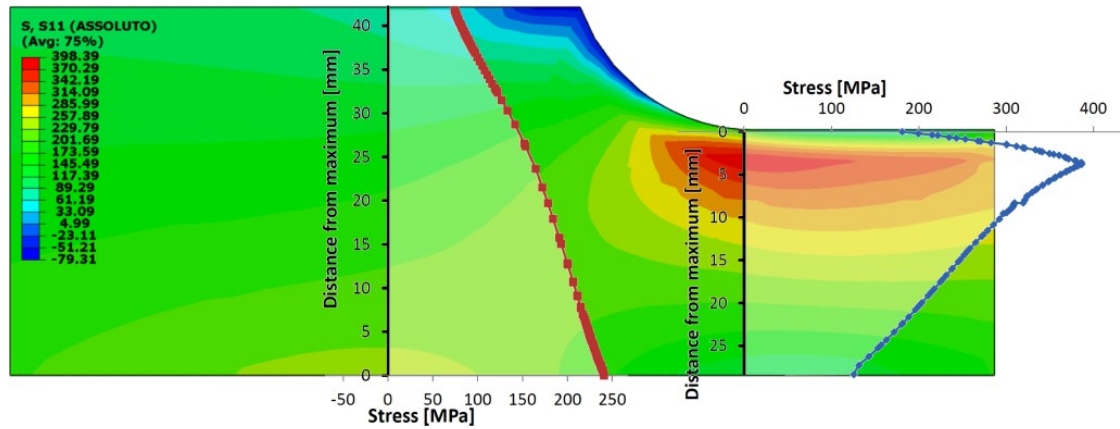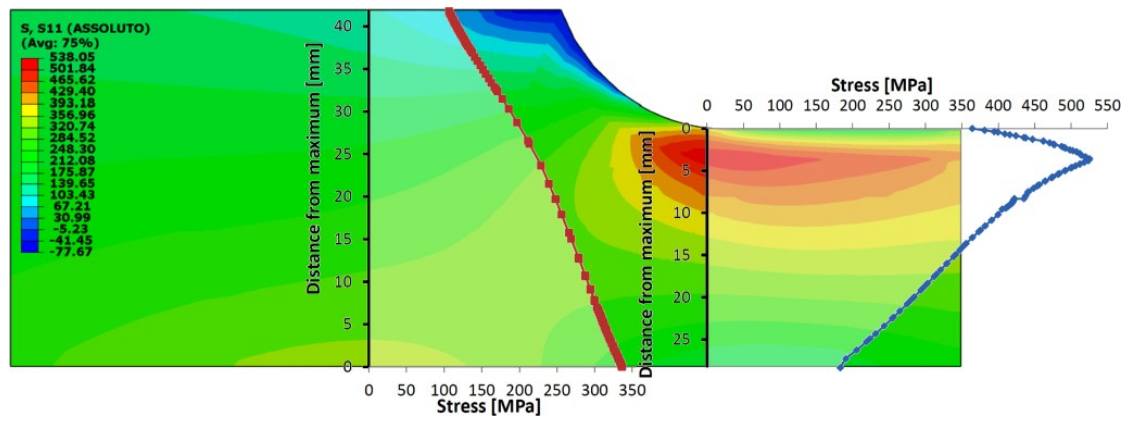

Figure 10.7: *Stress distribution in a LSP treated specimen for $\bar{\sigma} = 350$ MPa.*
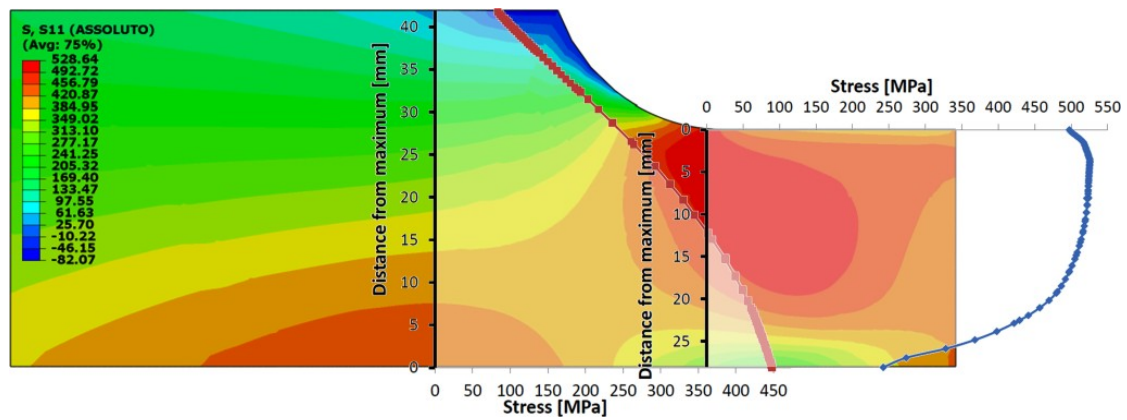

Figure 10.8: *Stress distribution in a LSP treated specimen for $\bar{\sigma} = 450$ MPa.*

Part V

Conclusion

Chapter 11

Conclusions

The physic phenomena regarding the plasma formation and the compressive residual stress generation by the propagation of shock waves in Laser Shock Peening treatments were reviewed.

After that, several surface treatments were analyzed and compared in order to investigate their effects on the fatigue behavior when applied on thick components. The Laser Shock Peening resulted the most effective treatment in extending the fatigue life of new and aged components; the Laser Shock Peening is able to counter the degrade due to anodizing processes. Retrofit solutions were analyzed and discussed.

The great advantages offered by the Laser Shock Peening are due to the low cold working, the reduced stress gradient after the treatment, the good surface finish and the exceptionally depth at which compressive residual stresses reach significant levels.

The decrease of effectiveness of Laser Shock Peening in presence of massive plastic cyclic deformation has been outlined.

About the Step specimens, the "Retro" group had a better fatigue behavior than the "Serial" one; that is probably due to the fact that the CAA has detrimental effects even though applied after Laser Shock Peening.

Combinations of Shot Peening and Laser Shock Peening proved to be possible and gave great improvements on SEN specimens' fatigue strength. This proves that combinations of different peening treatments can offer larger improvements

than the single treatments separately.

Evidences of a drop of the residual stresses after a service period were highlighted.

The unexpected failures occurred in the LSP treated specimens were explained by means of the results of FEM simulations: the surface treatment is able to reduce the local stress in the notch, thus the back of the thick section resulted the most stessed surface.
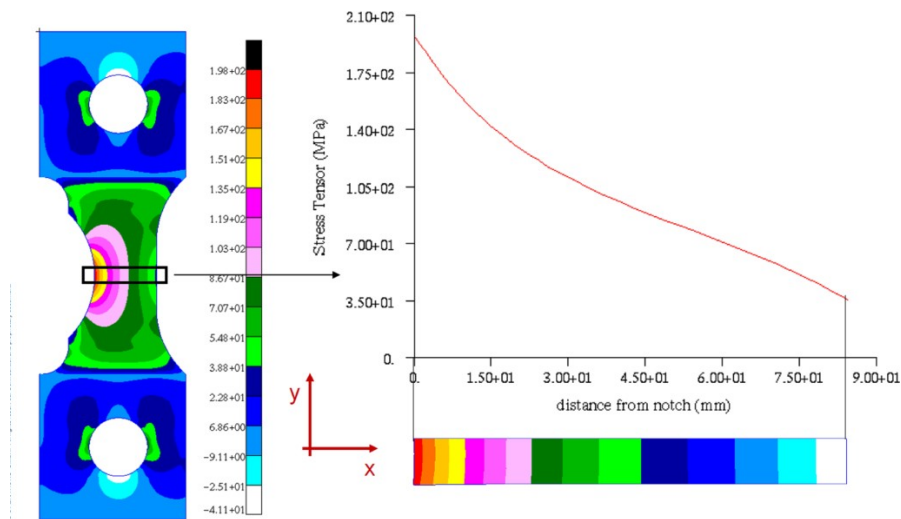
Chapter 12

Outlook

There is a huge potential for further optimization of the Laser Shock Peening treatment, thus further analyses that may be objectives for the future are:

- explicit simulation of the LSP effects on thick components, even combined with other surface treatments;

- Optimization of the LSP parameters based on the specific application (stress conditions, component's shape. . .);

- investigations on the sensitivity of the LSP to the edge effects (corners, edge radii. . .);

- deeper investigations on the residual stresses release process, that may allow defining rework procedures able to enlarge the fatigue life of the components virtually indefinitely;

- additional studies on the Crack Propagation in presence of residual stresses and developing of a Crack Propagation model for LSP treated components;

- Optimization of combinations of surface treatments by analyses on their mutual influence;

- developing of cheaper and easier processes and equipment;

- developing portable devices which can be easily handled.

Appendix A

Description of the stress field in the SEN specimen

A first approach analysis by the de Saint-Venant's theory is not adequate for the calculation of the stress distribution on a SEN specimen. The results of a FE analysis carried out by Coratella (1991) is presented. The in-depth stress in the notch section is shown in figure A.1: the external force introduced followed the criterion shown in section 10.1, thus a 100 MPa nominal stress was introduced. The peak stress is around 198 MPa, which confirms that approximately $K_t = 2$.

Figure A.1: *Stress profile in the notch section in a SEN specimen for $\bar{\sigma} = 100$ MPa. (Coratella 1991)*

Chapter A   Description of the stress field in the SEN specimen

Several failures during the test campaign started from the clamping hole. This is due to the usual combination of CAA, stress concentration in the clamping hole (fig. A.2) and fretting, which is unavoidable because of the high stress levels and because of the tension-compression nature of the test. The FE analysis associates a $K_t = 3.2$ to the hole, thus the local stresses are very high in a point in which no residual stress is introduced.
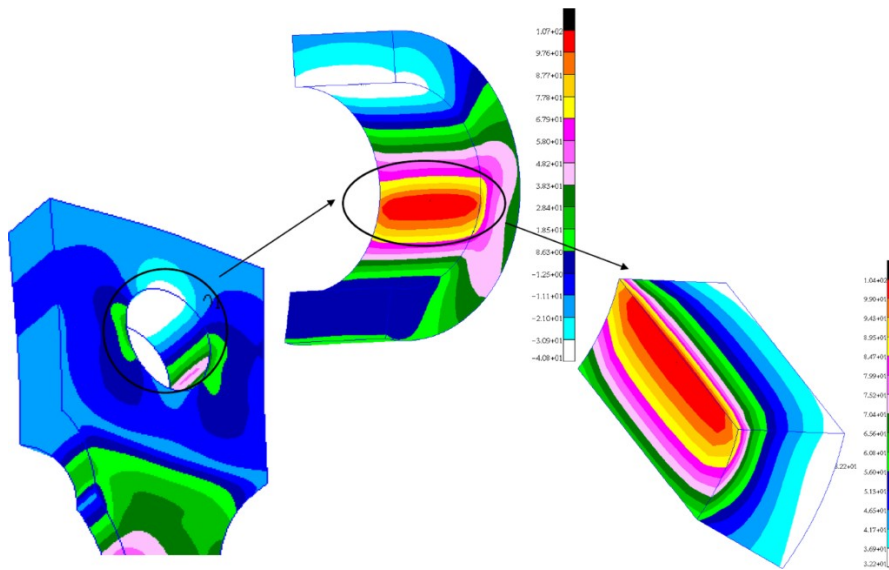
Figure A.2: *Stresses beside the clamping hole in a SEN specimen for $\bar{\sigma} = 100$ MPa. (Coratella 1991)*

Appendix B

Almen Intensity definition

Calibration of the impact energy or peening intensity of the shot stream is essential for controlled shot peening. The energy of the stream is a function of the media size, material, hardness, velocity and impingement angle. In order to specify measure and calibrate impact energy, J. O. Almen developed a method involving SAE 1070 spring steel specimens he called ALMEN strips.

Those strips are supported on 4 small balls and clamped by screws and are placed in the chamber in place of the item to be shot peened. Compressive stress introduced by the peening operation causes the strips to deform into an arch, which is measured using a gauge.

There are three standard Almen strips currently in use:

- "A" strip 0.051 inch (1.2954 mm) thick;

- "C" strip 0.094 inch (2.3876 mm) thick;

- "N" strip 0.031 inch (0.7874 mm) thick.

The approximate relationship between the three Almen strips types is 3N=A=0.3C. The usable range of curvature is 0.004 to 0.024 inch (0.1 to 0.61 mm).
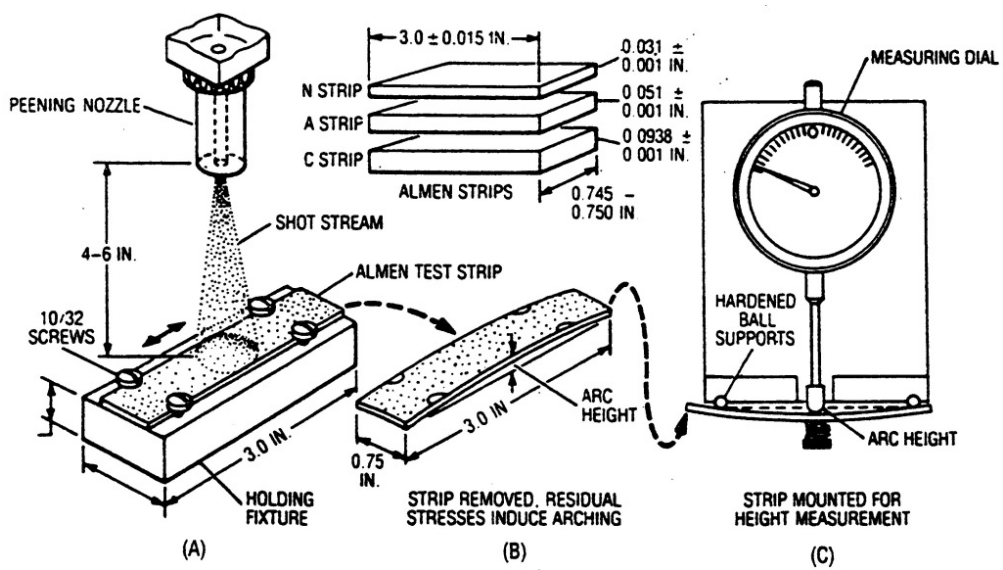
Figure B.1: *Schematic of the Almen test.*

Bibliography

Ballard, Patrick (1991). "Contraintes résiduelles induites par impact rapide. Application au choc-laser". PhD Thesis. Ecole Polytechnique.

Camargo, A. and H. Voorwald (2007). "Influence of anodization on the fatigue strength of 7050-T7451 aluminium alloy". In: *Fatigue & Fracture of Engineering Materials & Structures* 30.11, pp. 993–1007. URL: http://dx.doi.org/10.1111/j.1460-2695.2007.01169.x.

Clark, G. and P.K. Sharp. "The effect of peening on the fatigue life of 7050 aluminium alloy". In: ed. by DSTO Aeronautical and Marittime Research Laboratory.

Clauer, Allan H. (1996). "Laser shock peening for fatigue resistance". In: *Surface Performance of Titanium Alloys*. Ed. by Jean K. Gregory, Henry J. Rack, and Daniel Eylon. Minerals, Metals & Materials Society. Warrendale, PA, pp. 217–230.

Company, Metal Improvement (2001). *Shot-Peening Applications*. New Jersey, USA: Metal Improvement Company.

Coratella, Stefano (1991). "Laser Shock Peening Technology: design and optimization of a specimen and calibration of a model for the theory of eigenstrain". PhD Thesis. Open University.

Crudo, Cinzia (2012). "Optimization of FE analysis parameters for LSP modeling". In: *Final Review Meeting*. Ed. by Airbus.

Dane, C.B. et al. (2000). "High-Throughput Laser peening of metals using a high-average-power Nd:glass laser system". In: ed. by S. Nakai, L.A. Hackel, and W. Solomon.

Dane, C.B. et al. (2011a). "Commercial Applications of Laser Peening". In: *3ʳᵈ International Conference on Laser Peening, Osaka, Japan*. Ed. by Metal Improvement Company.

Dane, C.B. et al. (2011b). "On-Aircraft Laser Peening with a Mobile System". In: *3ʳᵈ International Conference on Laser Peening, Osaka, Japan*. Ed. by Metal Improvement Company.

Defense, U.S. Department of (2001). *Military Handbook - MIL-HDBK-5H: Metallic Materials and Elements for Aerospace Vehicle Structures*. Knovel Interactive Edition. URL: `http://www.knovel.com/web/portal/browse/display?_EXT_KNOVEL_DISPLAY_bookid=754&VerticalID=0`.

Devaux, D. et al. (1993). "Generation of shock waves by laser-induced plasma in confined geometry". In: *Journal of Applied Physics* 74.4, pp. 2268–2272.

Fabbro, R. et al. (1990). "Physical study of laser-produced plasma in confined geometry". In: *Journal of Applied Physics* 68.2, pp. 775–784. URL: `http://link.aip.org/link/?JAP/68/775/1`.

Heckenberger, Ulrike C. et al. (2010). "LSP to improve the fatigue resistance of highly stressed AA7050 components". In: *2ⁿᵈ International Conference on Laser Peening, San Francisco, USA*. Ed. by EADS Innovation Works.

Jensen, David (2010). "Adaptation of LSP Capability for Use on F-22 Raptor Primary Structure at an Aircraft Modification Depot". In: *2ⁿᵈ International Conference on Laser Peening, San Francisco, USA*. Ed. by Boeing, F-22 Air Vehicle Technology division.

Lee, Eungyeong, Yooin Jeong, and Sangshik Kim (2012). "S-N Fatigue Behavior of Anodized 7050-T7451 Produced in Different Electrolytes". In: *Metallurgical and Materials Transactions A* 43 (6), pp. 2002–2011. URL: `http://dx.doi.org/10.1007/s11661-011-1044-x`.

Liu, QianChu (2008). *An Effective life extension technology for 7xxx series aluminium alloys by laser shock peening*. Defence Science and Technology Organisation, Fishermans Bend, Victoria, Australia. URL: `http://pandora.nla.gov.au/tep/24592`.

Lykins, Chris, Paul Prevey, and Perry Mason (1995). *Laser shock peened compressive residual profile after exposure to temperature*. Aeropropulsion and power

directorate, Wright laboratory, Air Force Materiel Command, Wright-Patterson Air Force Base.

Mannava, Seetha Ramaiah et al. *Lower fluence boundary laser shock peening.* Patent 7097720.

Masse, Jean-Eric and Gérard Barreau (1995). "Laser generation of stress waves in metal". In: *Surface and Coatings Technology* 70.2-3, pp. 231–234. URL: `http://www.sciencedirect.com/science/article/pii/0257897295800204`.

Peyre, P. and R. Fabbro (1995). "Laser shock processing: a review of the physics and applications". In: *Optical and Quantum Electronics* 27, pp. 1213–1229.

Peyre, P. et al. (1996). "Laser shock processing of aluminium alloys. Application to high cycle fatigue behaviour". In: *Materials Science and Engineering* 210.1-2, pp. 102–113. URL: `http://www.sciencedirect.com/science/article/pii/0921509395100849`.

Peyre, P et al. (1998). "Laser-shock processing of aluminium-coated 55C1 steel in water-confinement regime, characterization and application to high-cycle fatigue behaviour". In: *Journal of Materials Science* 33 (6), pp. 1421–1429. ISSN: 0022-2461. URL: `http://dx.doi.org/10.1023/A:1004331205389`.

Peyre, P. et al. (2000). "Corrosion reactivity of laser-peened steel surfaces". In: *Journal of Materials Engineering and Performance* 9 (6), pp. 656–662.

Peyre, Patrice, L. Berthe, and R. Fabbro (2011). "Research activities during 25 years in France: from LALP to PIMM". In: *3rd International Conference on Laser Peening and related phenomena, Osaka, Japan.* Ed. by France LALS.

Prime, Michael B. (2008). "Everything engineers need to know to model shock behavior of metals". In: *1rd International Conference on Laser Peening, Houston, Texas, USA.* Ed. by Los Alamos National Laboratory NASA.

Sano, Yuji et al. (2010). "Applications of Laser Peening without Protective Coating to enhance Structural Integrity of Metallic Components". In: *The 2nd International Conference on Laser Peening, San Francisco, USA.* Ed. by Toshiba.

Shepard, M.J. "Applications and future trends in US Air Force Service". In: ed. by US Department of Defence Advanced component surface treatments: US Federal Aviation Administration.

Tenaglia, Richard D. and David F. Lahrman (2003). "Preventing fatigue failures with laser peening". In: *AMPTIAC Quarterly* 7.2, pp. 3–7.

116

Zel'dovich, Ya. B. and Yu. P. Raizer (1966). *Physics of shock waves and high temperature hydrodynamics phenomena*. Ed. by Academic Press. Vol. 1.